NASA TECHNICAL TRANSLATION NASA TT F-16899

THE OPTIMIZATION OF WIND TUNNEL CONTRACTIONS FOR THE SUBSONIC RANGE

G.G. Borger

Translation of "Optimierung von Windkanalduesen fur den Unterschallbereich, Ruhr-Universitat, Fakultat fur Maschinebau und Konstruktiven Ingenieurbau, Doctoral Dissertation, 1973, pp.1-151

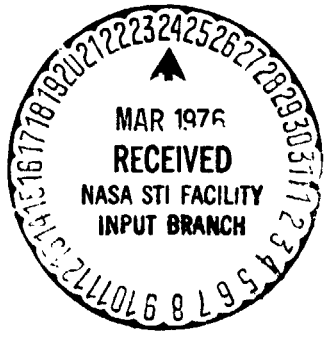

NATIONAL AERONAUTICS AND SPACE ADMINISTRATION
WASHINGTON,D.C. 20546 MARCH 1976

STANDARD TITLE PAGE

1. Report No. NASA TT F-16899	2. Government Accession No.	3. Recipient's Catalog No
4. Title and Subtitle THE OPTIMIZATION OF WIND TUNNEL CONTRACTIONS FOR THE SUBSONIC RANGE		5. Report Date March 1976 6. Performing Organization Code
7. Author(s) G.G. Borger		8. Performing Organization Report No. 10. Work Unit No.
9. Performing Organization Name and Address Leo Kanner Associates Redwood City, CA 94063		11. Contract or Grant No. NASw-2790 13. Type of Report and Period Covered Translation
12. Sponsoring Agency Name and Address National Aeronautics and Space Administration, Washington, D.C. 20546		14. Sponsoring Agency Code

15 Supplementary Notes

Translation of "Optimierung von Windkanalduesen fur den Unterschallbereich," Ruhr-Universitat, Fakultat fur Maschinebau und Konstruktiven Ingenieurbau, Doctoral Dissertaion, 1973, pp.1-151.

16. Abstract The reported investigation is concerned with the development of optimal contours for two-dimensional and axisymmetric subsonic wind-tunnel contractions. It is shown that the current approaches for the design of optimal contracting ducts are not satisfactory because of the absence of an adequate computational procedure for the flow characteristics. A description is given of a method for the calculation of frictionless flows in the case of two-dimensional and axisymmetric ducts of arbitrary contraction or extension characteristics. Fortran IV programs have been developed for the numerical computations involved. A method reported by Bradshaw et al. (1976) is used for the boundary-layer calculations. The developed mathmetical procedures are employed to optimize the design of the wind-tunnel contractions.

17. Key Words (Selected by Author(s))	18. Distribution Statement Unclassified-Unlimited		
19. Security Classif. (of this report) Unclassified	20. Security Classif. (of this page) Unclassified	21. No. of Pages 145	22. Price

NASA-HQ

THE OPTIMIZATION OF WIND-TUNNEL CONTRACTIONS FOR THE SUBSONIC RANGE

Summary /1*

The investigation deals with a theoretical analysis of two-dimensional and axi-symmetrical contractions for wind tunnels in the subsonic range, with a critical analysis of earlier research. For the calculation of frictionless flow in subsonic ducts a model is developed in which the walls are represented by vortex sheets, while the limits of the vortex sheets are formed by source and sink discs. The effects of friction are analyzed by means of the boundary layer calculation method by Bradshaw et al. The method for checking thus obtained for two dimensional and axi-symmetrical ducts with arbitrary contours is used to determine the optimal contours for subsonic wind tunnel contractions. Optimal contractions are defined as those having minimal length for a given contraction ratio and a given uniformity of velocity in the discharge while avoiding separation of the boundary layers.

*Numbers in the margin indicate pagination in the foreign text.

INDEX

Nomenclature

/2

Symbol	Units	Meaning
c_f	--	Friction factor, Eq. (3.1)
D	--	Relative diameter, relative to y_A
d	--	Displacement density factor, Eq.(4.19)
E	--	Complete elliptical integral of the second type
e_l, e_h, e_s	--	Correction parameter, Eqs. (4.8), (4.9), (4.10)
f	--	Relative error
G	--	Integral kernel function, Eq. (2.27)
I	--	Integral
K	--	Complete elliptical integral of the first type
k	--	Contraction ratio
k	--	Argument of the elliptical integrals E and K
L	--	Relative contraction, relative to y_A $\{L = \xi_E - \xi_A\}$
n	--	Number of
Re	--	Reynolds number
s	m	Local coordinates on the contraction contour
u	$\frac{m}{s}$	Component of w in x direction
v	$\frac{m}{s}$	Component of w in y direction
w	$\frac{m}{s}$	Flow velocity
w_l, w_h, w_s	--	Inversion point parameter, Eqs. (4.5), (4.6), (4.7)

Symbol	Units	Meaning
x	m	Local coordinate in primary flow direction
y	m	Local coordinates perpendicular to primary flow direction
α	--	Variable for parameter representation of ξ and η, Eq. (2.30)
Γ	$\frac{m^2}{s}$	Circulation /3
γ	$\frac{m}{s}$	Circulation over length of vortex sheet
Δ	--	Difference
δ^+	m	Displacement density
η	--	Dimensionless y-coordinate, Eq. (2.24)
Θ	m	Impulse loss density
ν	$\frac{m^2}{s}$	Kinematic viscosity
ξ	--	Dimensionless x-coordinate Eq.(2.23)
ρ	$\frac{kg}{m^3}$	Density
τ_w	$\frac{kg}{m\ s^2}$	Tangential stress
ϕ	$\frac{m^2}{s}$	Velocity potential
d_ϕ	$\frac{m^2}{s}$	Difference between velocity potentials of two points
ω	--	Dimensionless γ value, Eq. (2.25)

Subscripts

Index	Meaning
A	Initial contour point (see Fig.1)
B	Reference value, Eq. (4.19)
E	Final contour point (see Fig.1)
e	Two-dimensional
i	Induced
korr	Corrected
max	Maximum value of the induced unit
min	Minimal value of the induced unit
q	Caused by source and sink
r	Axi-symmetrical
uk	Uncorrected
δ	Relative to the outside of the boundary layer
θ	Relative to the impulse loss density

/4

Superscripts

Index	Meaning
$\rightarrow$	Vector
'	Point with a singularity
+	Defined in Eq. (2.5) and (2.7), exception δ^+ (see there)
$\cdot$	First derivative with respect to α
$\cdot\cdot$	Second derivative with respect to α
^	Multiplied by $\dot{\xi}$, Eq. (2.32)
-	Mean value

1. Literature

/6

About two dozen works have been published in the last 50 years about the design of subsonic wind tunnel contractions. The distribution of the works over so long a period of time indicates that this problem has never been the core problem of flow mechanics. The consequence was that a continuous body of work has nowhere been prepared about this problem. The authors (including the author of the present work) generally took up this subject because they were faced with a concrete case in which wind tunnel contractions had to be designed, and none of the methods discussed in the literature were satisfactory. Generally a new method was then developed and published based on a full development of one of the previous works (see e.g. Whitehead, Wu and Waters [1], Szczeniowski [2], Jordinson [3], Cohen and Ritchie [4], and others).

Figure 1 is a schematic representation of a wind tunnel contraction for the incompressible velocity range as well as the appropriate velocities along the axes and along the contour. The works about wind tunnel contraction can be divided into three groups.

Group 1: An arbitrary velocity curve is analytically specified for a flow line in the flow from the low entry velocity to a high test velocity. With the differential equation for incompressible flow lines the curves for additional flow lines and their velocity distribution is calculated. One of these flow lines is selected on the basis of several criteria, and chosen as the contour flow line for a wind tunnel contraction.

This group includes the works by Witoszynski [5] (1922), /7
Szczeniowski [2] (1942), Tsien [6] (1944), Thwaites [7] (1946), Cohen and Ritchie [4] (1962), and Mills [8] (1968).

The method by Witoszynski [5] is based on an axi-symmetrical flow, with flow lines parallel to the axis in the initial and final sections of the contractions. The initial and final sections are therefore equipotential plane surfaces. To achieve this, a velocity distribution is assumed which decreases and increases in wave form along the axis of symmetry. The stream tube, calculated according to the LaPlace equation, a section of which will serve as the contraction contour, correspondingly contracts and expands. In this application the flow upstream and downstream of the contraction is led in parallel tubes or as a free jet. Therefore the flow in such a contraction certainly deviates markedly from the calculated flow. An additional source of error is an approximation in the calculation, increasing with the contraction ratio. Witoszynski suggested his method may be used for contour determination of diffusers, where the deviations can be ignored due to a relatively minor change in cross section. The length of the contraction is a free parameter in Wytoszynski's work.

It is interesting to note that up to this date, satisfactory wind tunnel contractions are being designed with the use of Witoszynski's formula: using a ratio of maximum diameter to contraction length:

$$\frac{D_{max}}{L} \approx 1 \qquad (1.1)$$

In line with a proposal by Prandtl [9] (1932) the contractions are expanded somewhat at the exit. The flow in such contractions is certain to deviate somewhat from that calculated by Witoszynski. The application of such contractions can therefore only be justified by the satisfactory results obtained.

/8

A further development of Witoszynski's idea is represented by the works by Thwaites [7] and Mills [8], although Thwaites does not seem to be familiar with Witoszynski's work. Thwaites represents the contraction contour in the form of a suitably chosen series of

harmonic functions, whereby the initial and final sections of his contraction become equipotential planes, the velocity increasing monotonically between these points.

A disadvantage of such contours, as is the case with Witoszynski, is the fact that the calculation is based on a contour stream tube, deviating from the actual flow upstream and downstream of the contraction. It can therefore be expected that exactly in the areas sensitive to pressure increase, at the entry and exit cross section, deviations from the calculated velocities occur.

The methods of Szczeniowski [2], Tsien [6] and Cohen and Ritchie [4] are of a somewhat different nature. In this case the velocity is specified monotonically increasing along the symmetry axis, with external stream tubes calculated with the Laplace equation. All stream tubes approximate asymptotic cylindrical tubes upstream and downstream. In the practical application the contour flows selected are transfered to the cylindrical tubes via slightly rounded sections. Such contractions therefore have the same problems as the previously described ones: the effect of the rounded sections on the velocity curves at the end of the contractions cannot be exactly determined.

Group 2: A two dimensional non-compressible flow field with /9 singularities (expansions and contractions) is assumed. Position and size of the singularities are chosen to cause appropriate contour flow lines. Especially suitable is the representation of such flow lines and the choice of a contour flow line in the hodograph-plane. It is thus possible to choose a velocity distribution along the contour, before the geometry of the contour is determined.

This group includes the works by Hughes [10] (1944), Cheers [11] (1945), Libby and Reiss [12] (1951), Whitehead, Wu and Waters [1] (1951), Gibbings [13] (1964) and [14] (1966), Jordinson [3] (1961) and Lau [15] (1964) and [16] (1966).

Whitehead, Wu and Waters indicate how the results of this method can be translated to a system of axi-symmetrical flows.

The work by Hughes [10, published in 1944] is the most eccentric of this group. A contour flow line is proposed in this work, which incorporates a velocity jump, making this work only useful by approximation.

The works by Cheers [11], Libby and Reiss [12], Lau [15], [16] and Gibbins [13], [14] are based on a line in the two dimensional flow field, determined by equi-spaced source points, perpendicularly approached with constant velocity. Appropriate contour flow lines are selected from the flow lines thus resulting. The resulting contours approach the infinite parallel walls asymptotically. They must therefore be adapted to the parallel duct walls by rounding off at the contraction ends. This again causes a deviation of the real flow relative to the theoretical flow. Gibbings [14] and Lau [16] /10 discuss several possibilities to estimate the uniformity of the test section velocity, relating it to the length of the contraction.

A very adaptable method, also computationally relatively simple, is that by Whitehead, Wu and Waters [1]. This method was expanded by Jordinson [3] to extremely large contraction ratios. Several expansions and contractions are assumed in the flow field, creating contour flow lines with walls running parallel to the center line upstream and downstream of the contraction. Areas of increasing pressures occur near the entry cross section and near the exit cross section. The equation for the contour flow line contains an

independent variable, represented in Fig.1 with a and b, representing the velocity differences corresponding to the pressure increase. This makes it possible to choose the pressure increase arbitrarily low, although increasing the length of the contraction. It also makes it possible to minimize the deviation of the contour velocity from the average velocity in the exit cross section, again resulting in greater length. A disadvantage of this method is that the velocity curve is predetermined by the given singularities, making optimization impossible.

Group 3: An arbitrary contraction contour is specified and an appropriate non-compressible flow is calculated. The contour is varied until it results in an appropriate contraction flow.

The checking procedure developed by Batchelor and Shaw [17] (1944), is based on a contour, obtained when assuming a harmonic curve for the velocities averaged over the cross section. In the case of greater contraction ratios an average velocity, /11 so defined, deviates significantly from the actual velocities along the contour. Batchelor and Shaw calculate the actual non-compressible flow to such a contour with the aid of the relaxation method, choosing the flow line and the interior of the original contour, in which the maximum pressure increase does not exceed the value for a diffuser with 3.5° one-sided opening angle.

As mentioned in Cheers' [11] critical analysis of the method by Batchelor and Shaw [17], the shape of the contour eventually chosen necessarily depends on the original contraction. The shape of this contraction was based on the incorrect assumption of a constant velocity distribution through the cross sections. Therefore it probably does not represent the optimal shape. Furthermore it does not allow an exact indication of the boundary layer immediately upstream of the contraction. This boundary layer, however,

determines how great the pressure increase at the entry to the contraction may be, without causing separation. To use a standard 3.5° diffuser as a basis apparantly is not adequate to ascertain universally fitting boundary layers.

Batchelor and Shaw [17] did not fully exhaust the advantage of a checking method for the determination of an optimal contraction contour. The advantage is the possibility to study all possible contraction contours, after which the most suitable contour is selected. This is the purpose of the present work. It does not use the relaxation method, used by Batchelor and Shaw, but the /12 singularity method developed in Chapter 2. Boundary layer calculations are carried out instead of a comparison with a diffuser, in order to determine the allowable pressure increase. The problems caused by this method are covered in Chapter 3. Chapter 4 develops a method for the determination of optimal contraction contours.

This method results in two dimensional and axi-symmetrical contraction contours, shorter than all previously suggested methods. It also allows a definition of the effect of the pressure increase areas and makes it possible to avoid boundary layer separation. The discontinuity in the test section velocity is only a fraction of the unavoidable discontinuity caused by flow disturbances. Also the displacement effect of the boundary layer is integrated into the method.

2. Frictionless Flow

This section represents a method to calculate frictionless /13
flow through two dimensional and axi-symmetrical ducts with arbitrary expansions or contractions. The method is based on Küchemann and Weber [18], Vandrey [19] and Hucho [20], however, incorporates significant improvements, making it possible to achieve a high degree of accuracy with a moderate number of plotting points. It is preferable to carry out the derivation of the basic relationships, as in the present case, contrary to the previously mentioned works; the calculations are made for ducts with internal flows, instead of solid bodies surrounded by flow. This causes several modifications to the equations.

2.1 Explanation of the Vortex Sheet Model

Fundamental to this method is the representation of solid walls by the flow-through vortex sheets (Fig.2). A vortex sheet consists of a continuous system of potential vortexes of infinitesimally small circulation. The axes of these potential vortexes run perpendicular to the plane of the flow for a two dimensional flow, and surround the flow in the form of a ring in the case of axi-symmetrical flow. The combined currents over a section ds result in a circulation $d\Gamma$: /14

$$d\Gamma = \gamma(s)\, ds \qquad (2.1)$$

In Eq. (2.1) $\gamma(s)$ represents the circulation relative to length, here defined as the density of the vortex sheet. The density $\gamma(s)$ varies along the contour. Küchemann and Weber [18] show on page 48 that the intensity $\gamma(s)$ is equal to the difference between the velocity components parallel to the layer on both sides of the layer. If the layer must represent a solid wall, intensity $\gamma(s)$ must be chosen in such a way that everywhere along the layer the kinematic flow conditions are satisfied. If it is furthermore

required that at the outside of the contraction contour the velocity equals 0, the local intensity of the layer must be equal to the local velocity $\vec{w}$ at the inside of the layer:

$$\gamma(s) = |\vec{w}(s)| \tag{2.2}$$

If the layer is in a stationary location, it develops a velocity $+\frac{\gamma}{2}$ on the one side, and $-\frac{\gamma}{2}$ at the other side. For the requirement that on the one side of the system the velocity must be zero, and $\vec{w}$ on the other side, the local velocity created must be superimposed on the velocity induced by the entire singularity system: /15

$$\vec{w}_i = \frac{\vec{w}}{2} \tag{2.3}$$

2.2 Biot-Savart Law

According to the potential theory all singularities in the flow field produce a velocity $\vec{w}_i(x,y)$ at each point of the flow field. Where the singularities of the flow field are eddies, as in the present case, the induced velocity at a point P(x,y) can be calculated with the Biot-Savart Law. For axi-symmetrical and two dimensional flows the corresponding equations by Küchemann and Weber [18] (p.304) can be used.

A circular vortex sheet ring with circulation Γ and radius y', centered at point x', induces a velocity vector $d\vec{w}_i$ at point P(x,y). With Eq. (2.1) and the elliptical integrals K(k) and E(k), as defined e.g. by Abramowitz and Stegun [21] (p.589), in the form of tables and given by approximation equations for practical application, the components for $d\vec{w}_i$ are obtained:

$$du_i = \frac{\gamma(s')\,ds'}{2\pi}\,\frac{1}{\sqrt{(x-x')^2+(y+y')^2}}\left\{K(k) - \left\{1+\frac{2(y-y')\,y'}{(x-x')^2+(y-y')^2}\right\}E(k)\right\} \tag{2.4}$$

$$= \frac{\gamma(s')\,ds'}{2\pi}\,u_r^+ \tag{2.5}$$

and:

$$dv_i = \frac{\gamma(s')\,ds'}{2\pi}\,\frac{\{-(x-x')\}}{y\sqrt{(x-x')^2+(y+y')^2}}\left\{K(k) - \left\{1+\frac{2\,y\,y'}{(x-x')^2+(y-y')^2}\right\}E(k)\right\} \tag{2.6}$$

$$= \frac{\gamma(s')\,ds'}{2\pi}\,v_r^+ \tag{2.7}$$

/16

The argument k of the elliptical integral is:

$$k = \sqrt{\frac{4\,y\,y'}{(x-x')^2+(y+y')^2}} \tag{2.8}$$

In the case of two dimensional flow the circular vortex sheet ring is replaced by two infinitely long, parallel eddy lines of opposing circulation, perpendicular to the plane of flow. With the abbreviations introduced above the components of $\vec{w}$ can be obtained:

$$du_i = \frac{\gamma(s')\,ds'}{2\pi}\left\{\frac{-(y-y')}{(x-x')^2+(y-y')^2} + \frac{(y+y')}{(x-x')^2+(y+y')^2}\right\} \tag{2.9}$$

$$= \frac{\gamma(s')\,ds'}{2\pi}\,u_e^+ \tag{2.10}$$

and:

$$dv_i = \frac{\gamma(s')\,ds'}{2\pi}\left\{\frac{(x-x')}{(x-x')^2+(y-y')^2} - \frac{(x-x')}{(x-x')^2+(y+y')^2}\right\} \qquad (2.11)$$

$$= \frac{\gamma(s')\,ds'}{2\pi}\,v_e^+ \qquad (2.12)$$

The components of the velocity $\vec{w}_i$, induced by the entire layer /17 at point P(x.y) thus are:

$$u(x,y) = \frac{1}{2\pi}\int_{s_A}^{s_E}\gamma(s')\,u^+\,ds' \qquad (2.13)$$

$$v(x,y) = \frac{1}{2\pi}\int_{s_A}^{s_E}\gamma(s')\,v^+\,ds' \qquad (2.14)$$

2.3 Formulation of an Integral Equation for $\gamma(s)$

In this section an equation for the calculation of the circulation distribution $\gamma(s)$ shall be derived. The derivation of this equation is carried out as shown by Vandrey [19]. Given two points $P_1(x_1,y_1)$ and $P_2(x_2,y_2)$ at a distance ds apart on the vortex

sheet (see Fig.2). Both points are on a longitudinal cross section plane. An equation must now be derived for the variation of the flow potential $\phi(x,y)$ along the outside of the vortex sheet, between P_1 and P_2. Corresponding to the considerations of section 2.1 the flow at that point must be stationary. This condition is extensively discussed in section 2.5. Therefore:

$$d\phi = u\,dx + v\,dy = \vec{w}\,d\vec{s} = 0 \qquad (2.15)$$

The curve for the potential function $\phi(x,y)$ can then be determined from the singularities available in this field. Three components contribute to the potential difference $d\phi$ between points P_1 and P_2:

1. Components $d\phi_1$ of the eddy layer between P_1 and P_2 /18
2. Components $d\phi_2$ of the entire remaining portion of the vortex sheet
3. Component $d\phi_3$ of other singularities in the field.

The vortex sheet between points P_1 and P_2 induces a velocity $-\frac{\gamma}{2}$ in the direction of the surface. Therefore:

$$d\phi_1 = -\frac{\gamma(s)}{2}\,ds \qquad (2.16)$$

The entire remaining vortex sheet induces a velocity corresponding to Eqs. (2.13) and (2.14):

$$d\phi_2 = u\,dx + v\,dy \qquad (2.17)$$

$$= \frac{1}{2\pi}\int_{s_A}^{s_E} \gamma(s')\,(u^+\,dx + v^+\,dy)\,ds' \qquad (2.18)$$

It is assumed that outside the vortex sheet additional singularities are present. The velocity components induced by these are represented by u_q, v_q. They cause potential differences between P_1 and P_2:

$$d\phi_3 = u_q\, dx + v_q\, dy \tag{2.19}$$

Substituting Eqs. (2.16), (2.18), and (2.19) in Eq. (2.15) /19 the following is obtained:

$$d\phi = 0 = -\frac{\gamma(s)}{2}\, ds + \frac{1}{2\pi}\int_{s_A}^{s_E} \gamma(s')\,(u^+dx + v^+dy)\, ds' + u_q dx + v_q dy \tag{2.20}$$

The independent variable x can now be introduced instead of s, so that:

$$ds = \sqrt{dx^2 + dy^2} \tag{2.21}$$

Dividing Eq. (2.20) by $\frac{ds}{2}$, the following is obtained:

$$0 = -\gamma(x) + \frac{1}{\pi}\int_{x_A}^{x_E} \frac{\gamma(x')}{\sqrt{dx^2 + dy^2}}\,(u^+dx + v^+dy)\,\sqrt{dx'^2 + dy'^2} + 2\,\frac{u_q dx + v_q dy}{\sqrt{dx^2 + dy^2}}$$

$$\gamma(x) = \frac{1}{\pi}\int_{x_A}^{x_E} \frac{\gamma(x')}{\sqrt{dx^2 + dy^2}}\,(u^+dx + v^+dy)\,\sqrt{dx'^2 + dy'^2} + 2\,\frac{u_q dx + v_q dy}{\sqrt{dx^2 + dy^2}} \tag{2.22}$$

Eq. (2.22) is normalized, by expressing all lengths relative to the center line distance y_A of point A (see Fig.2). The vortex /20 sheet intensity $\gamma(s)$ is referred to the intensity $\gamma(-\infty)$, being the velocity for the layer infinitely far upstream from the contraction,

if the contour were continued with constant cross section up to that point. Intensity $\gamma(-\infty)$ is equal to the flow in cross section $x = x_A$, for reasons of continuity. Thus the following new values are defined:

$$\xi = \frac{x}{y_A} \tag{2.23}$$

$$\eta = \frac{y}{y_A} \tag{2.24}$$

$$\omega(\xi) = \frac{\gamma(\xi)}{\gamma(-\infty)} \sqrt{1 + \left(\frac{d\eta}{d\xi}\right)^2} \tag{2.25}$$

The Fredholm integral equation of the second order thereby becomes:

$$\omega(\xi) = \frac{1}{\pi} \int_{\xi_A}^{\xi_E} \omega(\xi') \left\{u^+(\xi,\xi') + v^+(\xi,\xi') \frac{d\eta}{d\xi}\right\} y_A d\xi' + \left\{u_q + v_q \frac{d\eta}{d\xi}\right\} \frac{2}{\gamma(-\infty)}$$

(2.26)

Introducing the abbreviated forms:

$$G(\xi,\xi') = \{u^+(\xi,\xi') + v^+(\xi,\xi') \frac{d\eta}{d\xi}\} Y_A \qquad (2.27)$$

and /21

$$\omega_q(\xi) = 2 \left\{\frac{u_q}{\gamma(-\infty)} + \frac{v_q}{\gamma(-\infty)} \frac{d\eta}{d\xi}\right\} = 2 \left\{u_q^+ + v_q^+ \frac{d\eta}{d\xi}\right\} \qquad (2.28)$$

the following is obtained for the integral equation:

$$\omega(\xi) = \frac{1}{\pi} \int_{\xi_A}^{\xi_E} \omega(\xi')\, G(\xi,\xi')\, d\xi' + \omega_q(\xi) \qquad (2.29)$$

Appendix 1 shows that $G(\xi,\xi')$ results in a singular location for $\xi = \xi'$ in the axi-symmetrical case. In the case of a two dimensional flow a finite limiting value of $G(\xi,\xi')$ exists for $\xi = \xi'$, which is also calculated in Appendix 1.

2.4 Translation of the Integral Equation into a System of Linear Equations

The translation of the integral equation (2.29) basically follows the works by Vandrey [19] and Hucho [20]. For the later numerical treatment of the integral equation it is advantageous to introduce a new independent variable α. This allows for the accumulation of plotting points in a certain ξ range (see Fig.4). This results in:

$$\left.\begin{aligned} &\xi = \xi(\alpha) \\ \text{and} \quad &\\ &\eta = \eta(\alpha) \end{aligned}\right\} \qquad (2.30)$$

Derivations with respect to α are represented by a point.

/22

$$\left.\begin{aligned} \frac{d\xi}{d\alpha} &= \dot{\xi} & \frac{d^2\xi}{d\alpha^2} &= \ddot{\xi} \\ \frac{d\eta}{d\alpha} &= \dot{\eta} & \frac{d^2\eta}{d\alpha^2} &= \ddot{\eta} \end{aligned}\right\} \qquad (2.31)$$

The following are now introduced:

$$\left.\begin{aligned} \hat{\omega}(\alpha) &= \omega(\xi) \cdot \dot{\xi} \\ \hat{\omega}_q(\alpha) &= \omega_q(\xi) \cdot \dot{\xi} \\ \hat{G}(\alpha,\alpha') &= G(\xi,\xi') \cdot \dot{\xi} \end{aligned}\right\} \qquad (2.32)$$

Also:

$$d\xi' = \frac{d\xi'}{d\alpha'} d\alpha' = \dot{\xi}' \, d\alpha' \qquad (2.33)$$

Thus the integral equation (2.29) becomes:

$$\hat{\omega}(\alpha) = \frac{1}{\pi} \int_{\alpha_A}^{\alpha_E} \hat{\omega}(\alpha') \, \hat{G}(\alpha,\alpha') \, d\alpha' + \hat{\omega}_q(\alpha) \qquad (2.34)$$

This integral equation must be solved numerically; it is therefore translated into a system of linear equations. The entire length of the layer $\alpha_E - \alpha_A$ is initially divided into n = sections with the width $\Delta\alpha$. Subsequently n equations for the n values of $\hat{\omega}$ are derived from Eq.(2.34) at the interval centers.

Thus the following system of equations is obtained from Eq.(2.34):

$$\hat{\omega}_\mu = \frac{1}{\pi} \sum_{\nu=1}^{n} \int_{\alpha_\nu - \frac{\Delta\alpha}{2}}^{\alpha_\nu + \frac{\Delta\alpha}{2}} \hat{\omega}(\hat{\omega}_{\nu-1}, \hat{\omega}_\nu, \hat{\omega}_{\nu+1}, \alpha') \, \hat{G}(\alpha_\mu, \alpha') \, d\alpha' + \hat{\omega}_q(\alpha_\mu) \qquad /23$$

$$\mu = 1, 2, \cdots, n \qquad (2.35)$$

The kernel function $\hat{G}(\alpha_\mu, \alpha')$ is calculated for each interval $\Delta\alpha$ at several points (nine points were chosen in the application). The circulation intensity $\hat{\omega}(\alpha')$ is calculated at the same points by means of quadratic interpolation of the $\hat{\omega}$ values of the interval centers from the three nearest intervals ν-1, ν, and ν+1. The integration of the integral occuring in Eq.(2.35) is then carried out with the aid of the Simpson rule. The only deviation from this rule occurs at the point $\mu = \nu$ in the axi-symmetrical case. There $\hat{\omega}$ is assumed constant, while the solution from Appendix 2 is used for the residual integral.

Eq.(2.35) results in a system of linear equations, derived in Appendix 3.

The improvement of this system of equations relative to the system by Hucho [20] is explained in Fig.3. Whereas Hucho retains $\hat{\omega}$ constant at each interval $\Delta\alpha$, resulting in a stepped shape for the resulting $\hat{\omega}(\alpha)$ curve, the presently used system of equations allows for a continuous $\hat{\omega}(\alpha)$ curve (Fig.3.b). The deviation

of a stepped curve from the actual curve increases with the differential coefficient $\frac{d\Omega}{d\alpha}$. Quadratic interpolation and the Simpson rule, on the other hand take into account the slope and the curve of the $\Omega(\alpha)$ curve, whereby the error only amounts to the third derivative $\frac{d3\Omega}{d\alpha 3}$. When an appropriate parameter interpretation $\xi(\alpha)$ of the coordinate in the centerline direction is used as well as the previously mentioned improvement, it results in adequate accuracy at a number of plotted points n ≈ 30-60. The accuracy of the results for the $\Omega(\alpha)$ curve is discussed fully in Section 2.6. /24

2.5 Source and Sink Discs

A system of linear equations was developed in the previous section and in Appendix 3, for the calculation of the circulation distribution of the turbulent boundary layer, and the velocity distribution at the inside. Each line of this equation contains the expression $\Omega_q(\alpha_\mu)$. According to Eq.(2.28) and (2.32):

$$\hat{\omega}_q(\alpha_\mu) = \left(2 \dot{\xi} (u_q^+ + v_q^+ \frac{\dot{\eta}}{\dot{\xi}}) \right)_\mu \qquad (2.36)$$

In Eq.(2.36) u_q^+ and v_q^+ are the dimensionless components of a velocity, induced by the singularities outside the turbulent layer at point (ξ_μ, η_μ). /25

In the present case the turbulent layer represents the contour of a wind tunnel contraction, and possibly the contour of the steady flow region and the test length immediately downstream. A flow shall be generated inside these contours, with the properties calculated with the aid of the system of equations (2.35). However, steady flow section, contraction, and test length are not isolated; rather there is a transition to the steady flow section and a transition

behind the test section. For the experimental analysis of wind tunnel contractions it would be ideal to use straight ducts for the transition sections with homogeneous velocity distributions, which cannot disturb the accuracy of the tests. Such a system corresponds to the approach of two semi-infinitely long turbulent boundary layer cylinders, or in the case of two dimensional flow, two dimensional turbulent boundary layers with constant circulation. These turbulent boundary layers can be connected to the turbulent layers of variable circulation density which have been calculated according to Eq.(2.35). The transition takes place so far away from the contraction, that the deviation from homogeneous flow, resulting from flow contraction, is virtually eliminated. For inhomogeneous flow between turbulent layers with /26
constant circulation, the kinematic flow conditions are not fulfilled along the turbulent layer.

For numerical-mathematical reasons the cylindrical or two dimensional turbulent layers with constant circulation density are represented in the present work by a source and sink disc with constant intensity, perpendicular to the center line of the arrangement. The discs represent the boundaries of the turbulent layer with variable circulation at the beginning and the end, as shown in Fig.2. Küchemann and Weber [18] have shown that such contraction and expansion discs induce the same flow field as semi-infinitely long turbulent cylinders of constant circulation density (except for a constant velocity in the interior of the semi infinitely long cylinders).

When a semi-infinitely long cylindrical turbulent layer with constant circulation distribution is enclosed by means of a source disc with the same intensity, all velocities outside the cylinder must be zero. The expansion is then supplied only from the turbulent cylinder.

Something similar occurs when an expansion and contraction disc are connected to the turbulent layers of varying circulation density, the section of steady flow, the contraction, and the test lengths. The entire flow volume given off by the source disc is transported through the ducts and taken up by the sink disc at the end of the test section. External to this arrangement there is no disturbance, providing the following two conditions are complied with: /27

(a) The entire flow volume given off by the source disc must be identical to the flow volume received at the sink disc.

(b) Steady flow section and test section must be long enough to adequately dampen the velocity changes due to the contraction.

If these conditions are not satisfied, flows will occur in the vicinity of the discs, outside the contraction.

The first condition can be satisfied easily with the choice of the intensities. Test calculations have shown that the errors caused by non-compliance with the second condition are very minor. If e.g. the source disc is connected immediately to the wide end of the contraction, the error resulting from non-compliance with the second condition in the downstream portion of the contraction is not arithmetically significant (compare also Section 2.6).

In Appendix 4 the equations for components u_q^+ and v_q^+, induced on the contour by the source and sink discs, are derived. These equations can be entered into Eq.(2.35) and (2.36), allowing the system of equations to be solved.

For the numerical computation, Fortran-IV computer programs /28
were developed for the two dimensional and the axi-symmetrical cases. These programs, together with a short instruction, are available at the Institute for Thermodynamics and Fluid Dynamics at the Ruhr-University, Bochum.

2.6 Accuracy of the Computations

The numerical computation of the potential flows causes inaccuracy of the results. Sources of these inaccuracies, in the order of their probable importance are:

(a) The kinematic flow condition is only satisfied in a limited number of plotting points.

(b) The calculated turbulent layer of variable circulation has only a finite length. Outside this length the cylindrical ducts are simulated less accurately with increasing inhomogeneity of the velocity profile in the exit cross section.

(c) A linear system of equations with up to 70 equations is numerically not fully solved. For the solution the modified subroutine GLD 4 of the German computer center, Darmstadt, is used.

(d) In calculating the thickness of the vortex sheet, individual points occur whose effect are only taken into consideration by approximation. /29

(e) The integral obtained in Eq.(2.35) is only computed by approximation with the Simpson rule.

(f) The contour curve $\eta(\alpha)$ and $\xi(\alpha)$, as well as the derivatives $\dot{\eta}$, $\ddot{\eta}$, $\dot{\xi}$, $\ddot{\xi}$ are determined on the contour created by points, with the aid of the Newton interpolation method.

(g) The elliptical integrals are calculated only by approximation equations to an accuracy $\pm 2 \cdot 10^{-8}$.

The aggregate of these inaccuracies must be kept small enough, not to essentially affect the accuracy of the contour optimation process described in the following chapters.

The curve for the contour velocity $w(\xi)$ shall serve as the basis for the boundary layer calculation. The maximum allowable error, therefore, is:

$$f_{k,max} = \left.\frac{\Delta w}{w}\right|_{max} < 5 \cdot 10^{-3} . \qquad (2.37)$$

The maximum allowble error for the velocity profile $u(\eta)$ at the exit cross section of the contractions amounts to:

$$f_{p,max} = \left.\frac{\Delta u}{u}\right|_{max} < 0{,}3 \cdot 10^{-3} \qquad (2.38)$$

Comparative computations with essentially more accurate potential flows were carried out in order to test whether these tolerance limits can be adhered to. A single vortex ring or two parallel vortex filaments are made to flow uniformly, perpendicular /30 to the plane. In each case one of the flow lines thus caused was used as the contour flow line (Fig.6). The curve for these flow lines at the velocities along them (Fig.7) can be computed numerically as accurately as desired. The flow line curve of Fig.6, thus obtained, was stated for the vortex sheet-computer program between the limits $-2 < \xi < 2$. The flows cannot be compared close to the limits, since the program simulates semi-infinitely long two dimensional layers or semi-infinitely long circular-cylinderical ducts, whereas the flow simulated by the vortex ring only has symmetry-parallel flow lines in the infinite dimension. Outside this initial area, the flow lines never deviated more than

$$\left.\frac{\Delta w}{w}\right|_{max,e} < 2{,}5 \cdot 10^{-3} \qquad \left.\frac{\Delta w}{w}\right|_{max,r} < 3 \cdot 10^{-3}$$

with an average area of:

$$\left.\frac{\Delta w}{w}\right|_{mittel,e} < 0{,}5 \cdot 10^{-3} \qquad \left.\frac{\Delta w}{w}\right|_{mittel,r} < 1 \cdot 10^{-3}$$

between the results of the two methods. In this case only 70 plotting points were used, the range $-2 < \xi < 0$, approximately corresponding /31 to the wind tunnel contraction, only is covered by 35 plotting points. Furthermore, no accumulation of plotting points in areas of greater velocity variations were used, a method by which the accuracy could have been further increased.

Also the velocity profiles at the point $\xi = 0$ remained within the tolerance limits (2.38). It can be assumed that in the case of contraction calculation described in Chapter 4, the errors will be even less than in the test calculations, since a greater plotting point density is used for the profile in the areas with greater variation in contour velocity.

3. Boundary Layer

/32

3.1 Literature Pertaining to Boundary Layers in Wind Tunnel Contractions

The works about wind tunnel contractions, cited in Chapter 1, either do not concern themselves with boundary layers, or only marginally. In most cases this is justified with a reference to monotonically increasing velocities along the contour, retaining the integrity of the boundary layers.

Batchelor and Shaw [17] report a calculation of the boundary layer, however, no reliable results could be obtained with this method. For this reason, Batchelor and Shaw [17] selected a contraction, in which the maximum pressure increase is equal to that in a diffuser with 3.5° half-opening angle (see Chapter 1). As in such diffusers the boundary layer is known not to separate, an equal pressure gradient was also considered to be harmless in the case of wind tunnel contraction boundary layers. Batchelor and Shaw interpreted an area of pressure increase at the downstream section of the contraction as a calculation error.

Whitehead, Wu and Waters [1] allowed two areas of pressure increase in their method, as can be seen in Fig.1 for the basic velocity curve. Although in many contractions close to the entry cross section boundary layer separation and subsequent variations in the flow velocity occur, this danger was avoided by Whitehead, Wu and Waters, by selecting a very gradual transition of the cross section at the beginning of the contraction. Also in this case no boundary layer computation was attempted. The authors solely recommended to compensate for the displacement effect of the boundary layer by a slight outward deviation of the contraction walls.

3.2 Properties of Wind Tunnel Boundary Layers /33

The boundary layers of all wind tunnel contractions have several properties in common. These properties shall be described in the following. This will result in conclusions pertaining to the choice of an appropriate boundary layer computational method, as well as the choice of realistic initial and additional conditions, and a critical analysis of the results of the computation.

3.2.1 Structure of the Boundary Layer Downstream from a Screen

The boundary layer in a wind tunnel contraction differs from solid bodies surrounded by flow, or tunnel flows from a reservoir, in that there is no defined initial point.

All closed circuit wind tunnels have a cylindrical steady flow section upstream of the contraction, of lesser or greater length, preceded by a number of screens and a rectifier for the homogenization of the flow velocity with respect to quantity and direction. Downstream of the last screen the flow is highly turbulent, with vortexes with diameters in the range of magnitude between the diameter of the screen wire diameter, and the mesh /34
size. The vortexes of the Karman vortex street increase downstream of the screen wires as they are carried downstream, until they overlap the neighboring vortexes, causing them to cancel one another out. This process represents the desired impulse-homogenization effect. According to this effect, no vortexes can be created independent from neighboring vortexes whose magnitude is in excess of those created by the screen mesh (compare Bradshaw [22]).

A boundary layer, located along the wall under such a flow, is involved in the homogenization process. The screen vortexes

affect an impulse transport from the center of the flow into the boundary layer. The boundary layer therefore becomes very thin. The wall can attenuate the turbulent flow in its vicinity to such an extent, that it can be said a wall-parallel flow results. Only when the vortexes in the center of the flow decrease as they are carried through the steady flow section, a boundary layer can develop again. Due to its origin this boundary layer is certainly turbulent. A normal turbulent boundary layer, is defined here as one, consisting of a laminar lower layer close to the wall, followed by a layer of increasing turbulence (applicability area of the universal boundary effect), a layer of turbulence of the same magnitude as the boundary layer thickness, and finally an interrupted zone, bounding a constant core-flow. /35

3.2.2 Initial Conditions for a Boundary Layer Computation

Under the circumstances just described, it is certainly impossible to indicate a point, at which the boundary layer parameters are adequately known to be used as a basis for a boundary layer computation. However, there are also situations where the boundary layer downstream of the screen is very thin. Very thin is understood to mean: their dimensions are small relative to the length of the path, required for the core-flow to be significantly modified. Contrary to thick boundary layers, such thin boundary layers are practically solely dependent on local conditions (pressure-gradient, core velocity, and, in the case of axi-symmetrical flow, also the local contraction). Disturbances or other effects, located upstream of the boundary layer, affect it only insignificantly downstream.

This phenomenon can be well explained with the vortex-model introduced by Bradshaw [23]. According to this model, boundary layer turbulence originate as small vortexes at the extremities

of the laminar lower layer. Due to the cumulative effect of lateral velocity, viscosity, and the wall, certain vortex frequencies are attenuated less than others. Vortexes of these frequencies increase and absorb the energy of other vortexes. During this /36
increase in magnitude they are repulsed from the vicinity of the wall. Frequency and increase are affected by the local pressure gradients, and the external velocity (or the velocity of neighboring vortexes). When the vortexes have reached the outer zone of the boundary layer, and have reached the size of the boundary layer thickness, the disintegration sets in. The vortexes dissolve in many smaller mixed air particles, which partly dissipate, and partly add their energy to other vortexes. As the vortex growth is limited by the boundary layer thickness, vortex creation and disintegration follow one another more rapidly as the boundary layer decreases in thickness. Since, on the other hand, these vortexes carry the boundary layer properties, which they have absorbed during their growth (frequency, energy) downstream; this transport decreases with decreasing life of the vortexes. Several independent boundary layer-thickness computation methods have shown that the effect of initial conditions on the path of the boundary layer in a wind tunnel contraction is insignificant, providing the initial boundary layer-thickness is selected small. From this it can be concluded, that a realistic boundary layer path results for a wind tunnel contraction, if a suitable computational method with arbitrary initial parameters, but very small initial boundary layer-thickness is initiated local to the last homogenization screen.

3.2.3 Zones of Varying Boundary Layer Behavior /37

Figure 8 shows a typical pressure, and boundary layer curve for a wind tunnel contraction. At the entry point of the flow into the contraction a weak pressure increase exists. This pressure increase also occurs upstream of the contraction along the cylindrical or straight walls of the steady flow section. There the flow is initially slowed, whereas it is increased in velocity near the centerline of the steady flow section and the entry to the contraction. The pressure gradient along the wall decreases, with increasing length of the steady flow section. At any rate, the boundary layer-thickness increases significantly in this area. In the case of contractions which contract close to the entry point, the boundary layer can be separated completely.

Shortly before the contour-inversion point WP is reached, the acceleration of the entire flow also affects the zone close to the wall, subject to a strong pressure decrease. The boundary layer again decreases in thickness and becomes less subject to separation. This can be recognized in Fig.8 by the great contour-velocity gradients. At strong acceleration of the flow close to the wall, it is even possible that the boundary layer becomes laminar again. The problems caused by this effect on the calculation of such boundary layer thicknesses will be discussed extensively in Section 3.3.

It has been described above, how the turbulent boundary /38
layers carry the boundary layer properties downstream. During the acceleration near the midpoint of the contraction contour, the boundary layer becomes very thin. Correspondingly, this part of the boundary layer partly transmits any properties of the velocity-profile, the friction profile, or the turbulence-structure. The history of the boundary layer is largely neutralized by this

acceleration area. This property of the boundary layer is especially important for the dimensional method of the present work, because it enables us to make statements about the behavior of the boundary layer in the exit flow of a wind tunnel contraction, although the behavior of the boundary layer in the supply area is not known.

Whereas, as the acceleration decreases towards the exit of the contraction (i.e., the absolute value of the negative pressure gradient), the boundary layer thickness increases again. Thus the acceleration of the flow is generally not associated with an increasing boundary layer thickness. Rather it only occurs with a decreasing boundary layer thickness, when the acceleration exceeds a certain value. This value increases with higher intensity and lesser thickness of the boundary layer. /39

At the contraction exit there is a short section where the pressure again increases significantly. Correspondingly the boundary layer there thickens considerably and again the danger of boundary layer separation occurs.

3.3 Requirements of the Boundary Layer Separation

In connection with the dimensional determination of a wind tunnel contraction it is not necessary to know all properties of the boundary layer. Boundary layer separations must solely supply answers to the following questions:

(1) How safe against separation in the pressure-increase zone is the boundary layer?

(2) To what extent is the core-flow displaced by the boundary layer?

3.3.1 Freedom from Separation

An indication of the extent to which a boundary layer is protected from separation, is the wall-friction force τ_w. It is common to indicate it in the form of a dimensionless wall-friction coefficient c_f:

$$c_f = \frac{\tau_w}{\frac{\rho}{2} u_\delta^2} \qquad (3.1)$$

The wall-friction coefficient c_f is a function of the geometry and the Reynolds-number. The calculations have shown that the affect on c_f of the Reynolds-number can be ignored. Only a relatively narrow range of Reynolds-numbers applies to wind tunnel contractions. In this range c_f varies very little. /40

Boundary layer separation sets in when c_f equals zero. In wind tunnel contractions maximal c_f-values of

$$c_{f_{max}} \approx 0.007 \qquad (3.2)$$

occur in the area of the greatest flow acceleration. As outlined in the description of the previous section, the separation must be avoided in the first area of increasing pressure. Therefore, minimum values for c_f of

$$c_{f_1} > 0.002 \qquad (3.3)$$

should be adhered to in this area for the dimensional determinations described in Chapter 4. This relatively high limiting value takes into consideration the inaccuracy, still inherent in all boundary layer calculations (compare e.g., Kline et al [24] and Coles and Hirst [25]).

Calculations have demonstrated, that the freedom from separation increases, with a shorter constant flow section upstream of the contraction. To avoid separation even in the least favorable cases, all contraction boundary layers of the supply flows are calculated for the constant flow section $L_B = \eta_A$ (η_A, see Fig.2), as recommended by Pope and Harper [34] (p.66).

The second area of increasing pressure has much steeper pressure gradients than the first one. From [24] and [25] it can be seen that this also increases the inaccuracy of the boundary layer calculations. An additional reason for the inaccuracy of the /41
boundary layer determination in this area is the possibility that in the previous acceleration area lamination of the boundary layer may have taken place again. There are several criteria for the return to a laminar pattern. Bradshaw [26] summarizes these criteria. For the initiation of the return to a laminar pattern the condition:

$$Re_{\theta} = \frac{u_\delta \theta}{\nu} \leq 320 . \qquad (3.4)$$

applies.

It is not yet fully known how laminar boundary layers behave. Research is underway to accurately analyze such boundary layers. Results are presently available, e.g. by Brinich and Neumann [27], and Narasimha et al. [28]. It can be assumed that boundary layers returned to a laminar pattern, as laminar boundary layers in general, which have previously been accelerated considerably, return to the turbulent pattern very rapidly, as soon as pressure decrease is eliminated (see e.g. Walz [29], p.158, and an oral report by Prof. Narasimha).

No reliable results can therefore be expected from calculations of the contraction boundary layers, whenever a value less than the limiting value (3.4) is reached. When pressure increase sets in again, the boundary layer certainly is very thin. Corresponding to the considerations in Section 3.2 the curve for a thin boundary layer is largely independent from the initial conditions chosen. It is therefore possible to re-initiate the calculation for the turbulent boundary layer with very minor boundary layer thickness at the point of renewed pressure increase downstream of the acceleration area. Due to the relatively considerable uncertainty /42 of the results so calculated, an even higher minimal value for the wall friction coefficient c_f should be selected than is the case in the first area:

$$c_{f_2} > 0.0025 \qquad (3.5)$$

When comparing the maximum wall friction coefficient $c_{f_{max}}$ from Eq.(3.2) with the lower limiting values c_{f_1} and c_{f_2} from Eq.(3.3) and (3.5), it will be noticed that at a relatively inaccurate determination of c_f a great degree of freedom from separation of the boundary layer ($c_{f_{Ab}} = 0$) is present.

3.3.2 Displacement

The dimensional computation method for wind tunnel contractions, described in Chapter 4, is based on the calculation of the potential-flow in specified contraction contours. With the results boundary layer calculations are carried out subsequently. The boundary layer displaces the frictionless core-flow away from the wall to the extent of its displacement thickness. As a result the contour of the potential-flow calculation differs from a

contour, causing the identical core-flow with the influence of a boundary layer, by the amount of the displacement density. This error is generally so small relative to the contour-dimensions, /43 that it can be ignored. At the end of Chapter 4 an example-calculation is discussed, from which it is obvious that ignoring this displacement is practically without effect on the value for the wall-friction coefficient c_f, and therefore on the sensitivity to boundary layer-separation.

As will be shown in Chapter 4, the velocity distribution over the exit-cross section of a contour is practically only determined by the contour in the area of the second flow decrease. The velocity distribution over the exit-cross section of the contraction must be constant with great accuracy. The error resulting from a boundary layer displacement represents a significant disturbance for this degree of accuracy. Therefore the boundary layer displacement is taken into account in the area of the second pressure increase. Section 4.7 describes the details of this process. There it will also be shown in an example, how the method of accounting for the boundary layer-displacement in the vicinity of the exit-cross section is fully adequate for the present case.

Since the affect of the boundary layer-displacement on the velocity-profile in the exit cross section is, though noticeable, still relatively small, an error of up to approximately 30% in the calculation of the displacement-thickness does not have any significant affect on the result.

3.4 Selection of a Boundary Layer Computation Method /44

For the selection of an appropriate boundary layer computation method the results of the 1968 conference on the calculation of turbulent boundary layers at Stanford are used as a basis (see Kline et al. [24] and Coles and Hirst [25]). Since tne contraction boundary layers described in Section 3.2 are subject to very strong variations of pressure and velocity in their course, a computational method must be selected which takes into consideration this turbulent origin of the boundary layer. It is not sufficient to compensate for the history of the average velocity profile. As explained above, the boundary layer properties are largely determined by the turbulent fluctuations. A boundary layer computation method, which compensates for the turbulence, has been developed by Bradshaw et al. [30]. More detailed information about the application of this method is contained in a series of reports by the National Physical Laboratory. Bradshaw [31] gives a summary of these reports. In this method the turbulence energy equation is transformed into a differential equation for the turbulent friction forces. This is done with the definition of three empirical functions, associating the local turbulence energy and their diffusion and dissipation with the friction force profile. The turbulent energy equation, the mean time equation for the impulse flow, and the equation for the mean mass discontinuity form a system of hyperbolical differential equations. /45 This system can be solved numerically with the characteristic value method.

The Fortran computer program by Ferris and Bradshaw [32] was modified slightly for the calculations of contraction boundary layers. The modifications mainly apply to the computation of the intervals between the reference points, which are perpendicular to the walls. In highly accelerated flows the boundary layers become thinner, and an automatic reduction of the interval width must be provided.

4. Contraction Sizing /46

4.1 Requirements of a Wind Tunnel Contraction

Both preceding chapters described how the flow processes in a wind tunnel contraction can be calculated. The expedients developed there shall now be used in a method to determine the optimal wind tunnel contractions.

A given contraction ratio k for the contraction shall be assumed as the basis for the contraction in a planned wind tunnel. The contraction ratio is defined as the quotient of the average exit velocity and the average entry velocity at the contraction. It is therefore always greater than unity.

As described by Prandtl [9], Gersten [33] and Pope and Harper [34], a contraction decreases the velocity differences in a flow. This phenomenon applies to the velocity differences caused by different specific energy levels of adjacent air layers in the flow. Such energy differences can be caused e.g. by the friction of a certain air layer relative to the deflection baffles in the wind tunnel corners, or other internals, whereas the adjacent air layers do not experience this deceleration. The equalizing effect of a contraction is caused by the fact that the pressure in all adjacent air flows decreases, while the kinetic energy, corresponding to the Bernouill equation increases with constant total energy. At the end of the contraction the kinetic energy of the flow has then increased to such an extent, that the remaining energy difference in the flow only causes minor velocity /47
differences. The degree of homogenization of the flow velocities is therefore dependent on the contraction ratio k and not on the shape of the contraction contour.

The impulse exchange between air layers of differing velocities also causes a, though lesser, homogenization of the flow. This phenomenon is covered by Schlichting [35] in Chapter 24: leeward of a body the wind velocity U_∞ is decelerated by u_1. The width b of the section sheltered against the air flow increases with path length x of the flow, as a function of the mixing path ℓ of the local turbulence. The velocity deviation u_1 therefore decreases correspondingly. Schlichting gives a relationship Eq.(24.12):

$$\frac{db}{dx} \sim \frac{\ell}{b} \frac{U_1}{U_\infty}$$

The capacity balance of the velocity in the sheltered area is therefore more effective e.g. along the path between a flow screen upstream of the contraction and the test length, with decreasing velocity U_∞. It follows that it is desirable to have long constant flow sections and short high velocity sections upstream of a contraction. The procedures just described indicate that it is impossible to remove all irregularities from the flow, even with an ideal contraction contour. However, with an appropriate contraction contour it is possible to have the specific kinetic energy increase by the same amount along all flow lines of the contraction flow. Only under that condition is it possible to achieve a constant velocity in the test section at large contraction ratios of k.

There is a general correspondence between the contraction length and the homogeneity of the test section velocity. The deviation from constant test section velocity, caused by the contraction, can be minimized with decreasing the length of the contraction. However, we have previously explained that it is desirable to select the contraction as short as possible. In order to establish a compromise between these two requirements it is necessary to estimate the disturbing flows in the test section. /48

Pope and Harper [34] suggest a maximum deviation of the test section velocity of 0.25% for good wind tunnels. Disturbances of this order of magnitude cannot be avoided with the choice of contour, since they are present in the flow before it reaches the contraction. The discontinuities of the flow velocity in the test section caused by the contour, should be of a lesser magnitude than the remaining disturbances. However, it appears to be useless to keep these disturbances essentially smaller than the other disturbances. For this reason a maximum deviation of $\pm 0.1\%$ of the average test section velocity was chosen for the velocity irregularity resulting from the contour. Since the method for the calculation of the velocity distribution in the exit cross section of the contraction, described in Section 2.6, does not exceed an accuracy of $\pm 0.03\%$ of the average velocity, the calculated deviation of the test section velocity should not exceed $\pm 0.07\%$.

Flows in wind tunnel contractions basically behave like frictionless flows. The effect of wall-friction can be compensated by means of boundary layer calculations. The requirements /49
for wind tunnel contractions thus obtained, are represented in Section 3.3.

The dimensional determination of a wind tunnel contraction now represents the following optimization problem:

The contour curve $y(x)$ must be so determined that the relative total length L of the contraction is at a minimum. The following auxiliary conditions are to be maintained:

a) The contraction must have the contraction ratio k (4.1)

b) The arithmetic irregularity of the test section velocity must satisfy the condition

$$\left.\frac{\Delta u}{\bar{u}}\right|_{\text{Test section}} \leqq \pm 0.07 \quad \S \qquad (4.2)$$

c) The wall friction coefficient c_{f1} must satisfy the condition

$$c_{f1} \geq 0.002 \tag{4.3}$$

at the entry zone of the contraction, corresponding to section 3.3.1.

d) The wall friction coefficient c_{f2} must satisfy the condition

$$c_{f2} \geq 0.0025 \tag{4.4}$$

in the exit zone of the contraction, corresponding to section 3.3.1.

4.2 Geometrical Parameters of a Wind Tunnel Contraction /50

The optimization problem just formulated, unfortunately cannot be solved in its general form. In theory it could be used with the variation method as developed by Rechenberg [36] for experimental optimization. In the present case, however, the auxiliary conditions cannot be represented as simple functions of the contour curve. Only after a complicated computational program has been carried out, is it possible to determine whether it is possible to satisfy these conditions. For this reason an attempt must be made to find another possibility to approximate the optimum. A first step in this direction is the reduction of the general contour curve y(x), to the minimum number of parameters, determining its curve. In order to avoid separation of flow, the flow must follow the contour smoothly, without breaks or jumps. Since the flow is carried to the contraction in a cylindrical duct without curves in the direction of the flow, and must also leave the contraction in the form of a straight, bundled flow, slope and

curvature of the contour curve y(x) at the initial point A (compare Fig.2) and exit point E must be zero. The contour then initially curves in, goes through an inversion point, after which it curves outward, up to point E where slope and curvature again become zero. This curve can essentially be described by the location (x_{WP}, y_{WP}) of the inversion point WP and by the slope $\left.\frac{dy}{dx}\right|_{WP}$ of the function y(x) at the inversion point (Fig.2). For these three parameters dimensionless constants are defined as follows: /51

$$w_\ell = \xi_{WP} - \xi_A \qquad (4.5)$$

$$w_h = 1 - \eta_{WP} \qquad (4.6)$$

$$w_s = \left.\frac{d\eta}{d\xi}\right|_{WP} \frac{w_\ell}{w_h} \qquad (4.7)$$

When the three parameters w_ℓ, w_h, and w_s are determined, and when furthermore the slope and curvature of the contour curve y(x) at points A and E are zero, and y(x) should have a minimum curvature at all points, the contour curve is determined except for some minor deviations. The computer program developed for the potential flow includes the computation of a contour curve, which satisfies all conditions mentioned at points A and E as well as the stated parameters w_ℓ, w_h and w_s. Details about this computer program can be found in Appendix 7.

A set of contours is defined by the reduction of the general contour curve y(x) to one determined by the five parameters w_ℓ, w_h and w_s, η_E (corresponding to k) and L. This set probably does not include the required optimum curve. As early as 1932, Prandtl [9] (p.77) indicated that the homogeneity of the test section velocity can be improved, when the cross section opens up somewhat close to the contour exit point E. Whereas Prandtl suggested determining the dimensions of this expansion in model tests, the /52

computer program suggested in Chapter 2, with the aid of a boundary layer computation as described in Chapter 3, enables the computation of the effect of such an expansion. The general curve for such a contour correction is represented in Fig.5. The same conditions which were associated with the requirements for the contour curve are associated with the contour correction. Slope and curvature at the entry and exit points of the correction must be equal to zero, and the correction may be characterized only by the conditions at the inversion point WPK. Thus three additional parameters e_ℓ, e_h, and e_s, defined in Fig.5, must be considered in the contour curve. The following applies:

$$e_\ell = \frac{\Delta\xi_e}{\eta_E} \qquad (4.8)$$

$$e_h = \frac{\Delta\eta_e}{\eta_E} \qquad (4.9)$$

$$e_s = \left.\frac{d\eta}{d\xi}\right|_{WPK} \frac{e_\ell}{e_h} \qquad (4.10)$$

The optimization problem introduced at the end of Section 4.1 therefore becomes:

Six parameters w_ℓ, w_h, w_s, e_ℓ, e_h, e_s must be determined in such a way as to minimize the total length L of the contraction, still satisfying the auxiliary conditions (4.1) through (4.4).

4.3 Flow in the Entry Zone to the Contraction /53

Also after the introduction of the six parameters mentioned above, the optimization problem cannot be directly solved, due to the impossibility of analytically associating the parameters and the auxiliary conditions. For this reason it was attempted, with the aid of test calculations, to establish relationships between

the contour parameters and the auxiliary conditions. One of the major conclusions is the possibility, described in Chapter 3, of a division of the contour into an entry flow zone and an exit flow zone (Fig.2). The shape of the contour curve in the entry zone is practically free from any effect on the flow in the exit flow, and vice versa. The transition area between the two zones is close to the contour inversion point WP.

The auxiliary condition (4.3) is: the wall friction coefficient c_{fl} must satisfy the condition $c_{fl} \geqq 0.002$, as shown in Section 3.3.1. The contour in this zone is made dimensionless with the y-value y_A at point A per Eqs.(2.23) and (2.24); it now only depends on three parameters w_ℓ, w_h and w_s. It is thus possible to determine lines with a constant w_h-value for a $w_\ell(w_s)$-diagram (Fig.9), where c_{fl} just reaches the limiting value

$$c_{fl,Gr} = 0.002 \qquad (4.11)$$

Outside the boundaries are parameter values which lead to c_{fl}-values greater or smaller than $c_{fl,Gr}$. The boundary lines have minimum points in the represented range. This indicates that the shorter entry zones occur when the contour curve has even curvature over as great an area as possible. Excessive contour slope at inversion point WP results in a significant curvature of the contour close to the inversion point. Excessively small inversion point slope results in a significant contour curvature close to point A.

The calculation of the c_{fl}-values accompanying a certain set /54 of values for w_ℓ, w_h and w_s, is carried out by initially calculating a potential flow with the computer program from Chapter 2. The velocity curve along the contour, thus obtained, is used to calculate the appropriate boundary layer with the computer program selected in Section 3.4. The boundary layer calculation starts

with arbitrary initial values and a very thin boundary layer at the entry to the section of constant flow, i.e. at a location upstream of point A by η_A. It results in the smallest value for c_f occurring in the entry zone, represented by c_{fl} in accordance with Section 3.3.1.

4.4 Flow in the Exit Zone of Uncorrected Contractions

Calculations of the potential flow in contractions were carried out, in which the three correction parameters e_ℓ, e_h and e_s were made equal to zero. Thus the contour basically coincided in all cases with the dashed curve shown in Fig.5.

The calculations resulted in velocity profiles $u(\xi_E,\eta)$ in the exit cross section of the contraction. The lowest velocity u_{min} at the centerline, and the greated velocity u_{max} at the contour, all occured at these profiles (at point E according to Fig.2). From the results the curves $\frac{u - u_{min}}{u_{max} - u_{min}}(\frac{\eta}{\eta_E})$ could be determined. Some of these curves are shown in Fig.10. It can be seen from this that all $u(\xi_E,\eta)$-profiles with the same [illegible]

$$\left.\frac{\Delta u}{\bar{u}}\right|_{uk} = \left.\frac{u_{max} - u_{min}}{\bar{u}}\right|_{uk} \qquad (4.12)$$

/55

very accurately with one another. Consequently $\left.\frac{\Delta u}{\bar{u}}\right|_{uk}$ can be used as unbiased parameters for the velocity profiles of uncorrected contractions (i.e., contractions with e_ℓ, e_h and e_s equals zero) at the exit cross section.

4.5 Contour Corrections in the Exit Zone

An attempt has been made, with the aid of parameters e_ℓ, e_h and e_s, to correct the contour curve to minimize the difference $\frac{\Delta u}{\bar{u}}$. Figure 11 shows what type this decrease is. For each contour, two of the three parameters e_ℓ, e_h and e_s can be selected arbitrarily. The third parameter can then be determined in such a way as to minimize the deviation of the velocity $u(\eta)$ from the average value $\bar{u}$. The minimum is reached when, as is shown in the top of Fig.11, the velocity at the centerline equals the velocity along the contour. Calculations have resulted in further important results of the present analysis, indicating that the magnitude of this minimum as a good approximation only depends on e_ℓ, e_h, e_s and $\left.\frac{\Delta u}{\bar{u}}\right|_{uk}$. The magnitude of this minimum and the appropriate set of parameters e_ℓ, e_h and e_s therefore hardly vary with different contour curves (i.e., at different w_ℓ, w_h, w_s) at the same $\left.\frac{\Delta u}{\bar{u}}\right|_{uk}$.

From the auxiliary condition (4.2) it follows that the velocity /56 profile in the exit cross section of the contraction is:

$$\frac{\Delta u}{\bar{u}} = \frac{u_{max} - u_{min}}{\bar{u}} \leq 0{,}0014 \qquad (4.13)$$

Together with the requirement of identical velocity at the centerline and at the contour of the exit cross section, described above and in Fig.11, these are two conditions for the determination of the four values e_ℓ, e_h, e_s and $\left.\frac{\Delta u}{\bar{u}}\right|_{uk}$. Thus two of these values can be arbitrarily selected, the other two being calculated. This relationship is represented in Fig.12. Each point of diagram Fig.12 represents a set of parameter values e_ℓ, e_h, e_s and $\left.\frac{\Delta u}{\bar{u}}\right|_{uk}$,

of which the auxiliary condition (4.13) is satisfied, guaranteeing that the velocity along contour and centerline in the exit cross section $\xi = \xi_E$ are equal.

A general relationship followed from the calculations: as $\left.\frac{\Delta u}{\bar{u}}\right|_{uk}$ increases, the length of the contraction decreases. In order to minimize the length of the contraction $\left.\frac{\Delta u}{\bar{u}}\right|_{uk}$ must be chosen as great as possible. However, the magnitude of $\left.\frac{\Delta u}{\bar{u}}\right|_{uk}$ is limited to a certain range.

Inspecting the velocity curves along the contour in Fig.11, it will be clear that by means of correction the contour downstream of the velocity maximum causes a steep velocity decrease, and therefore also a greater pressure gradient. At this point the two pressure gradients, the one resulting from the decrease of the contour curvature and the one resulting from the cross section increase, aggregate. At the boundary layer of the flow the pressure gradient effects a decrease of the wall-friction coefficient c_{f2}. As stated in (4.4) c_{f2} may not be less than 0.0025. Large values of $\left.\frac{\Delta u}{\bar{u}}\right|_{uk}$ require correspondingly significant correction to achieve constant test section velocities. The areas of increased pressure, thus resulting, can make compliance with the auxiliary condition (4.4) impossible for significant corrections. In general, it can be assumed that, for different contraction ratios k, different sets of parameter values for $w_\ell, w_h, w_s, e_\ell, e_h, e_s$ lead to the minimal contraction length L. In establishing the sets of parameters, three of the six parameters can be varied independently from one another. However, as explained above, no more than two of the correction parameters e_ℓ, e_h, e_s may be included in these. The other three must always be determined, in order to satisfy the auxiliary conditions (4.2), (4.3), and (4.4).

/57

To further simplify the optimization problem calculations with differing parameter values were carried out, each time establishing the appropriate contraction length L. The results indicate that a variation of the inversion point parameters w_ℓ, w_h, w_s affect the length significantly more than variation of the correction parameters if e_ℓ, e_h, e_s are changed in the area of significant values for $\left.\frac{\Delta u}{\bar{u}}\right|_{uk}$, corresponding to Fig.12. Values for $\left.\frac{\Delta u}{\bar{u}}\right|_{uk}$ are considered significant in line with the preceding discussion, if they allow the auxiliary condition (4.4) to be satisfied. /58

A variation of the correction parameters e_ℓ, e_h, e_s influences the contraction length L only to a technically insignificant degree. On the other hand, variation computation with variation of three parameters, even on a fast calculator such as the RUB TR 440, which was used for the computations in the present work, resulted in computation times of about 25 hours. The computation time is this high largely because the determination of parameters on the basis of auxiliary condition (4.4) is only possible iteratively.

For the reasons mentioned it was decided to not completely solve the optimization problem mathematically. Instead, the test computations were based on the following constant values:

two dimensional	axi-symmetrical	
$e_h = 0.05$	$e_h = 0.05$	(4.14)
$e_s = 3.0$	$e_s = 3.0$	(4.15)

From Diagram Fig.12:

$e_\ell = 1.5$	$e_\ell = 1.45$	(4.16)
$\left.\frac{\Delta u}{\bar{u}}\right\|_{uk} = 0.0123$	$\left.\frac{\Delta u}{\bar{u}}\right\|_{uk} = 0.0114$	(4.17)

From the examples in Figs.23 through 26, it can be seen that the values selected here result in very short exit zones.

A further advantage of keeping the constant parameter values e_ℓ, e_h, e_s and $\frac{\Delta u}{\bar{u}}\Big|_{uk}$ is indicated in Section 4.7. It makes it very simple to compensate for the displacement effect of the boundary layer. After introduction of the fixed parameters $w_\ell, w_h, w_s, e_\ell, e_h, e_s$ instead of the general contour curve y(x), and the largely arbitrary choice of constant values for e_n and e_s the present method can no longer presume to have solved the optimization problem of wind tunnel contractions mathematically exactly. Rather, we have here a probably fully adequate approximation solution. /59

4.6 Determination of the Contraction Length

With the values (4.14), (4.15), (4.16) and (4.17), as well as the boundary curves of Fig.9, the different inversion point locations w_h, inversion point slopes w_s, and contraction ratios k (or the countour-ordinate values η_E at the exit of the contraction), potential-flow and boundary layer calculations were carried out. These flows satisfy the stated conditions (4.1), (4.2) and (4.3). The value for η_E was varied, keeping all other values constant, until the auxiliary condition (4.4) was satisfied. The process of determining the appropriate value η_E was simplified by the fact that the relationship $\eta_E(c_{f2})$ very closely approximated linearity. This allowed linear interpolation of very accurate intermediate values. The result of these calculations is shown in Fig.13. The relative contraction length over w_s is plotted there. The diagram shows lines of constant η_E values. For each value of η_E (also for each contraction ratio k), another value combination w_h, w_s therefore leads to a minimal contraction length L_{min}.

The minimal values of the $L(w_s)$ curves were expected on the basis of Fig.9. Surprisingly the relative contraction length of optimal wind tunnel contractions had a maximum at a certain value for η_E (see the connection line of the minima for the $L(w_s)$ curves). While with increasing w_h (i.e., decreasing η_{WP} and η_E) the length w_ℓ of the supply zone increases (Fig.9), the length of the exit zone decreases. This decrease is somewhat less for greater η_E values than the increase of w_ℓ. As η_E decreases, the contour velocity close to the inversion point WP increases. Since the velocity increase begins upstream of point WP, the boundary layer at that point is safe from separation and the contour can be curved in relatively pronouncedly. For decreasing η_E the length w_ℓ increases relatively less than for a greater value of η_E. Thus the length decrease for low η_E of the exit flow exceeds the length increase of the entry zone. /60

With the results of the calculations just described, a series of diagrams was compiled, from which for a given contraction ratio k, or η_E the parameters for the contraction contour can be determined. These are the following diagrams: /61

$w_\ell(\eta_E)$	Fig.14
$w_h(\eta_E)$	Fig.15
$w_s(\eta_E)$	Fig.16
$L(\eta_E)$	Fig.17
$\eta_{WP} - \eta_E(\eta_E)$	Fig.18

The discontinuity in the curve of Fig.16 indicates that the suppression of the length increase of the supply zone, just described, at decreasing η_E values quite suddenly occurs at a certain value for η_E.

4.7 Compensation for the Boundary Layer Displacement

In Section 3.3.2 it was demonstrated that it suffices to compensate for the boundary layer displacement in the exit zone of a wind tunnel contraction. The curve for the wall friction coefficient c_f is practically independent of the Reynolds number of the contraction flow. It can, like the curve for the potential flow, be represented as a dimensionless function of the contraction dimension.

The displacement thickness, on the other hand, is more dependent on the Reynolds number. There can, however, be connections between the contour curve, Reynolds number and displacement thickness, /62 making it possible to draw conclusions about the displacement of the core flow in the exit zone, without a complete boundary layer calculation. This is made possible in the first place by the equality of e_ℓ, e_h, e_s and $\left.\frac{\Delta u}{\bar{u}}\right|_{uk}$ for all occurring wind tunnel contractions. The curve for the contour velocity in the exit flow zone of all these contractions is therefore practically equalized, if represented relative to the exit wall distance y_E (compare Figs.23-26). Sample calculations have shown that the increase of the displacement thickness in these areas at differing contraction ratios k is almost equal, when only y_E and $\bar{u}$ correspond. As described in Section 3.3, the boundary layer becomes extremely thin at the point of the greatest contour velocity. Downstream of this point the boundary layer increases in thickness again. In order to compensate for the displacement of the boundary layer in the exit zone, the difference between the displacement thickness δ^+ and the displacement thickness at the point of the greatest velocity $\delta^+_{u_{max}}$ are added for the contour established for the section from the point of highest velocity, for frictionless flow. For the curve of the difference $\delta^+ - \delta^+_{u_{max}}$ as a function of $\frac{x}{y_E}$,

an analytical approach was chosen, accurately simulating the curve except for one factor. This factor depends on the Reynolds number:

$$Re = \frac{\bar{u}\, y_E}{\nu} \tag{4.18}$$

Details about this procedure can be found in Appendix 5. The /63 function was normalized, so that the factor is equal to the difference

$$d = \frac{\Delta\delta^+}{y_E} = \frac{\delta_E^+ - \delta_B^+}{y_E} \tag{4.19}$$

between the displacement thickness at point E and a reference value. Figure 19 shows d as a function of Re. As the displacement thickness shall be compensated for, downstream of the point of maximum contour velocity, also the location of this point must be known. It can be taken from Fig.20 for the respective value η_E.

4.8 Application Example and Accuracy Check

In the preceding sections a number of diagrams were prepared, from which, for an assumed contraction ratio k (or η_E respectively), the absolute value of the contraction (possibly in the form of the greatest ordinate value y_A) and of the velocity $\bar{u}$ in the test section, all parameters can be determined, establishing the curve for the contour of a wind tunnel contraction. In Appendix 6 a relatively simple computer program is provided, with the aid of which the contour of the contraction can be calculated point by point from the parameters. The method and the accuracy of this calculation will be detailed in the following example.

Be it assumed that the contour for a two dimensional wind tunnel contraction is required. In the entry cross section the distance between the contour and the centerline is:

$$y_A = 1.5m \qquad (4.20)$$ /64

The required contraction ratio:

$$k = 3 \qquad (4.21)$$

or:

$$\eta_E = 0.333 \qquad (4.22)$$

The designed velocity for the test section:

$$\bar{u} = 60\frac{m}{s} \qquad (4.23)$$

The required contour is calculated point-by-point with the aid of the computer program discussed in Appendix 6. For this purpose, the following set of parameters can be obtained from the diagrams (the center column contains the designations used in the computer program):

y_A	= RMAX	= 1.5m	(given)
η_E	= EM	= 0.333	(given)
L	= XL	= 1.82	(from Fig.17)
w_h	= WH	= 0.581	(from Figs.15 & 18)
w_ℓ	= WL	= 1.248	(from Fig.14)
w_s	= WS	=-2.325	(from Fig.16)
d	= DD	= 0.0047	(from Fig.19)
$\frac{\xi_E - \xi_{u_{max}}}{\eta_E}$	= XV	= 1.45	(from Fig.20)
Δx	= DX	= 0.1m	(given)

The value Δx gives the required distance of the x values of the point, in which the contour ordinate values shall be calculated.

The table for y(x), reproduced at the end of Appendix 6, was /65 calculated with the aid of this program based on these data. As a result of the boundary layer displacement, the exit cross section y becomes greater than $y_A \cdot \eta_E$. This achieves that the contraction of the flow more accurately represents the contraction ratio k than would be the case without compensation for the boundary layer displacement.

With this example a check shall be made of which errors are caused due to ignoring the boundary layer displacement in the supply zone, and by the analytical approach for the boundary layer displacement in the exit zone. The computer program of Chapter 2 is initially used to calculate the appropriate potential flow. This is based on a contour curve without compensation for boundary layer displacement in the exit zone. The result of this computation is represented in Fig.21 as a plotting diagram.

A boundary layer computation in accordance with Section 3.4 is carried out with regard to this potential flow, starting at the entry of the flow at the section with constant flow, up to the entry of the flow in the test section. The example has been chosen in such a way as not to include the re-formation of laminar flow. Thus the curve for the entire boundary layer can be calculated. From the contour curve, which led to Fig.21, the displacement density is now subtracted. Only in the area of the exit zone, in which the displacement effect can be compensated for, in accordance with Section 4.7, not the displacement thickness, but the value $\delta^+_{u_{max}}$ (compare Section 4.7) is subtracted.

For the contour curve, so obtained, the potential flow is /66 computed with the program from Chapter 2. This potential flow

results in the sample contraction with compensation for the boundary layer displacement along the entire contraction wall and the constant flow section wall. The result is represented in Fig.22. A comparison of Fig.21 and Fig.22 demonstrates that the velocity profiles in the exit flow cross sections virtually coincide. This demonstrates that the compensation for the boundary layer displacement, in accordance with Section 4.7, is fully adequate to satisfy the requirements of the auxiliary condition (4.2). Furthermore the velocity curve $u(\xi)$ coincides so accurately, that non-compliance with the auxiliary condition (4.3), caused by ignoring the boundary layer displacement in the supply zone can also be ignored.

4.9 Discussion of the Results /67

Analyzing the curve for the optimal contraction contours in Figs.23-26, the contradiction to the traditional wind tunnel contractions is immediately noticed, in that the contours show significant curvature relatively close to the exit cross section, in other words, that the contour inversion points are relatively close to the exit cross section. Conventional contours generally have drawn-out, weakly curved exit zones. The reason for this is shown in Fig.11. For an uncorrected contour curve, the contour velocity in the exit zone approaches the average value $\bar{u}$ of the velocity in the exit cross section asymptotically. With increasing exit zone length, the velocity profile in the exit cross section becomes more constant. As the effect of the contour corrections cannot be accurately predetermined up to now, the contours were opened up slightly only immediately upstream of the exit cross section, in order to improve the profile. Disadvantages of such contours, compared to those developed in the present work, are a greater length, increased by about 20-30%, and relatively thick boundary layers in the exit cross section.

In order to demonstrate this comparison, the computational checking method, developed in the present work, was used to calculate the steady flow section and contraction of the 0.5m wind tunnel of the Institute for Thermodynamics and Fluid Dynamics at the Ruhr University at Bochum. The plotter-drawing of Fig.28 /68 shows the results. A boundary layer calculation showed that immediately upstream of the contraction the boundary layer separates. From the $u(\xi)$-curve in Fig.28 it can be seen that the pressure increases significantly at that point. Tests at the contraction showed that the pressure increase in reality is less pronounced than the calculated value. Also this indicates boundary layer separation. A filament probe, entered into the contraction from the test length, however, did not show any separation with return flow along the wall. Rather, eddies were found with axes in the flow direction. This phenomenon suggests a wall-curvature-effect similar to the Taylor-Görtler vortex formation. What probably occurred there is that the wall friction, decelerating the flow, is forced away from the wall due to centrifugal action. The boundary layer equations are set up under the assumption that the boundary layer thickness is of a lesser order of magnitude than the longitudinal curvature radius of the wall. Nearly separated boundary layers are so thick, that this condition is no longer satisfied. Thus the boundary layer calculation would not predict such a phenomenon.

Figure 29 shows the contour and the velocity curve for a contraction suitable for the same wind tunnel, calculated according to the method described in the present work. The essentially lesser velocity decrease in the area of the steady flow section, relative /69 to Fig.28, can be recognized. Furthermore, this contraction is essentially shorter, thus increasing the test length by 0.23m.

5. Summary /70

The present work has attempted to develop a theoretical method for the calculation of optimal contours for two dimensional and axi-symmetrical wind tunnel contractions in the subsonic range.

It has been shown in Chapter 1 that the earlier methods in this area are unsatisfactory, because of the absence of an adequate computational procedure for the flow characteristics. With the aid of electronic computers it has become possible to develop such a computational procedure in which the flow in the interior of the contraction is calculated as a potential flow, while the wall friction has been taken into consideration by means of boundary layer calculations.

In order to calculate the potential flow, vortex sheets are used in Chapter 2 to represent the walls in the singularity model. The local circulation of a layer has been determined satisfying the kinematic flow conditions at a number of points on the layer. The upstream and downstream boundaries of the vortex sheets are represented by source and sink layers. A Fredholm integral equation of the second degree has been derived from this arrangement to represent the circulation distribution of the vortex layer. The integral equation is solved by means of translation into a system of linear equations. As has been shown in Chapter 3, certain /71
demands should be made of a method to calculate boundary layers at the walls of wind tunnel contractions. This is due to the fact that the pressure gradient changes sign several times between the entry of the flow into the steady flow section and the exit at the test length. For this reason, the boundary layer calculations have been carried out with the use of a method developed by Bradshaw et al. [30]. This method solves a hyperbolic system of three partial differential equations for the mass transport, the

impulse transport, and the turbulent energy transport, from which the boundary layer properties are determined. This method was particularly suitable to the present problem as, including the turbulent energy transport, the history of the boundary layer is relatively well compensated, even at changing external conditions.

The computational method is used in Chapter 4 for the optimization of wind tunnel contractions. An attempt was made to find the shortest contractions possible, satisfying the conditions of a given contraction ratio, a given homogeneity of the flow velocity at the contraction exit, and the requirement that the contour should eliminate the possibility of boundary layer separation. It was shown that the contour of satisfactory contractions can be determined by means of fixed parameters. For some of these parameters the above mentioned auxiliary conditions are the determinants. By means of varying some of the other /72
parameters, it has been shown that they do not essentially affect the contraction length. By means of varying the other parameters, with the aid of the computational method, diagrams were developed from which it was possible to determine an optimal contraction contour for each required contraction ratio. For this purpose a computer program has been prepared, which calculates the contour curve point-by-point from the parameters.

REFERENCES

[1] Whitehead, L.G., Wu, L.Y., and Waters, M.H.L., "Contracting Ducts of Finite Length," The Aeronautical Quarterly. London 1951, Vol.2, p.254-271.

[2] Szczeniowski, B. "Contraction Cone for a Wind Tunnel," Journal of Aeronautical Science, New York 1943, Vol.10, pp.311-312.

[3] Jordinson, R. "Design of Wind Tunnel Contractions," Aircraft Engineering, London 1961, Vol.33, pp.294-297.

[4] Cohen, M.J., Ritchie, N.J.B. "Low-speed Three-dimensional Contraction Design," Journal of the Royal Aeronautical Society, London 1962, Vol.66, pp.231-236.

[5] Witoszynski, E. "On Flow Expansion and Flow Baffling," Vorträge aus dem Gebiete der Hydro- und Aerodynamik (Innsbruck 1922). Hrsg. Kármán, Th.v.; Levi-Civita, T.; Berlin 1924, pp.248-251.

[6] Tsien, H.-S. "On the Design of Contractions for Wind Tunnels," J. Aeron. Sci., New York, 1943, Vol.10, pp.68-70.

[7] Thwaites, B. "On the Design of Contractions for Wind Tunnels," A.R.C., R.&.M. No.2278, London 1946.

[8] Mills, R.D., "Some Finite Two-dimensional Contractions," The Aeron. Quart., London 1968, Vol.19, pp.91-104.

[9] Prandtl, L. "The Production of Perfect Air Flows (Wind Tunnels)," Handbuch der Experimentalphysik, Leipzig 1932, Vol.4, No.2, pp.65-106.

[10] Hughes, N.J.S., "Stream Expansion with a Discontinuity in Velocity on the Boundary," A.R.C., R.&.M. No.1978, London 1944.

[11] Cheers, F., "Note on Wind Tunnel Contractions," A.R.C.,R.&.M., No.2137, London 1945.

[12] Libby, P.A. and Weiss, H.R., "The Design of Two-dimensional Contracting Sections," Quarterly of Applied Mathematics, London 1951, Vo.2, pp. 95-98.

[13] Gibbings, J.C. "The Choice of a Hodograph Boundary for Contracting Ducts," J.Roy.Aeron.Soc., London 1964, Vol.68, pp.420-422.

[14] Gibbings, J.C. "On the Effective 'Length' of Two-dimensional Contracting Ducts," J. Roy. Aeron. Soc., London 1966, Vol.70,p.676.

[15] Lau, W.T.F. "An Analytical Method for the Design of Two-dimensional Contractions," J.Roy.Aeron.Soc., London 1964, [illegible].

[16] Lau, W.H.F."On the Length of Two-dimensional Contractions," J.Roy.Aeron.Soc., London 1966, Vol.70, pp.673-675.

[17] Batchelor, G.K. and Shaw, F.S., "A Consideration of the Design of Wind Tunnel Contractions," Australian Council for Aeronautics, Report ACA-4, Melbourne 1944.

[18] Küchemann, D. and Weber, J., "Aerodynamics of Propulsion," McGraw-Hill Publications in Aeronautical Science, Hrag. Hunsaker, J.C.; New York, 1953.

[19] Vandrey, F., "A Direct Iteration Method for the Calculation of the Velocity Distribution of Bodies of Revolution and Symmetrical Profiles," A.R.C., R.&.M., No.3374, London 1951 and 1964.

[20] Hucho, W.-H., Untersuchungen über den Einfluß einer Heckschraube auf die Druckverteilung und die Grenzschicht schiffsähnlicher Körper. [Research about the Affect of a Tail Rotor on the Pressure Distribution and the Boundary Layer of Ship-like Bodies]. Thesis. Technical University, Braunschweig 1967.

[21] Abramowitz, M. and Stegun, J.A., Handbook of Mathematical Functions. Dover Publicatios, New York, 1965.

[22] Bradshaw, P., "The Effect of Wind Tunnel Screens on Nominally Two-dimensional Boundary Layers," Journal of Fluid Mechanics, Cambridge, U.K. 1965, Vol.22, pp.679-687.

[23] Bradshaw, P., "Turbulent Boundary Layers," J.Roy.Aeron.Soc, London 1968, Vo.72, pp.451-458.

[24] Kline, S.J., Morkovin, M.V., Sovran, G., and Cockrell, D.J., Computation of Turbulent Boundary Layers -- 1968 AFOSR-IFP -- Stanford Conference. Stanford, 1968, Vol.1.

[25] Coles, D.E. and Hirst, E.A., Computation of Turbulent Boundary Layers, -- 1968 AFOSR-IFP -- Stanford Conference. Stanford, 1968, Vol.1.

[26] Bradshaw, P., "A Note on Reverse Transition," J. Fluid Mech., Cambridge, U.K. 1969, Vol.35, pp.387-390.

[27] Brinich, P.F., and Neumann,H.E., Some Characteristics of Turbulent Boundary Layers in Rapidly Accelerated Flows. NASA TN D-6587, Washington, D.C., 1971.

[28] Narasimha, R. and Sreenivasan, K.R., "Reverse Transition in Highly Accelerated Boundary Layers," Rep.71 FM 9 of the Dept. Aeron. Engng., Indian Inst. of Science, Bangalore, India 1971.

[29] Walz, A., Boundary Layers of Flow and Temperature, University Press, Cambridge Mass. and London, U.K. 1969.

[30] Bradshaw, P. Ferris, D.H. and Atwell, N.P., "Calculation of Boundary Layer Development Using the Turbulent Energy Equation," J.Fluid Mech., Cambridge, U.K. 1967, Vol.28, Part 3, pp.593-616.

[31] Bradshaw,P., Calculation of Boundary Layer Development Using the Turbulent Energy Equation. IX:Summary. NPL Aero Report 1287 -- A.R.C., 30 909, Teddington 1969.

[32] Ferris,D.H., and Bradshaw, P., A Computer Program for the Calculation of Boundary Layer Development Using the Turbulent Energy Equation. NPL Aero Report 1269, Teddington 1968.

[33] Gersten, K., "The Wind Tunnel for Moderate Velocities," Archiv für Technisches Messen, No.250, Munich 1956, pp.241-244.

[34] Pope, A. and Harper, J.J., Low Speed Wind Tunnel Testing. Wiley & Sons, Inc., New York, London, Sydney, 1966.

[35] Schlichting, H., Grenzschicht-Theorie, [Boundary Layer Theory]. 5th Ed., Verlag G. Braun, Karlsruhe 1965.

[36] Rechenberg, I., Optimierung technischer Systeme nach Prinzipien der biologischen Evolution. [Optimization of Technical System According to the Principles of Biological Evolution]. Friedrich Frommann, Stuttgart-Bad Cannstatt 1972.

Appendix 1

/78

Analysis of the Kernel Function $G(\xi,\xi')$ for the Range $\xi \approx \xi'$ Axi-Symmetrical Flow

The kernel function $G(\xi,\xi')$ is given in Eqs.(2.27), (2.5) and (2.7). For the range $\xi \approx \xi'$ it is treated similarly to Hucho's treatment [20].

$$G(\xi,\xi') = \left\{u^+(\xi,\xi') + v^+(\xi,\xi')\,\frac{d\eta}{d\xi}\right\} y_A \qquad \text{(A1.1)}$$

$$\begin{aligned} G_r(\xi,\xi') = {} & \frac{1}{\sqrt{(\xi-\xi')^2+(\eta+\eta')^2}}\left\{K(k)-\left\{1+\frac{2\,(\eta-\eta')\,\eta'}{(\xi-\xi')^2+(\eta-\eta')^2}\right\}E(k)\right\} - \\ & - \frac{d\eta}{d\xi}\,\frac{(\xi-\xi')}{\eta\sqrt{(\xi-\xi')^2+(\eta+\eta')^2}}\left\{K(k)-\left\{1+\frac{2\,\eta\,\eta'}{(\xi-\xi')^2+(\eta-\eta')^2}\right\}E(k)\right\} \\ = {} & \frac{1}{\sqrt{(\xi-\xi')^2+(\eta+\eta')^2}}\left\{\{K(k)-E(k)\}\left\{1-\frac{d\eta}{d\xi}\,\frac{(\xi-\xi')}{\eta}\right\} - \right. \\ & \left. - E(k)\left\{\frac{2\,\eta'}{(\xi-\xi')^2+(\eta-\eta')^2}\right\}\left\{(\eta-\eta') - \frac{d\eta}{d\xi}\,(\xi-\xi')\right\}\right\} \end{aligned} \qquad \text{(A1.2)}$$

with

$$k = 2\sqrt{\frac{\eta\,\eta'}{(\xi-\xi')^2+(\eta+\eta')^2}} \qquad \text{(A1.3)}$$

The value η' is developed as a Taylor series for $(\xi-\xi')$:

$$\eta' = \eta - \frac{d\eta}{d\xi}(\xi-\xi') + \frac{d^2\eta}{d\xi^2}\,\frac{(\xi-\xi')^2}{2} - \ldots. \qquad \text{(A1.4)}$$

The series is not extended beyond the third term. Substituting Eq.(A1.4) in Eq.(A1.2) results in:

$$G_r(\xi,\xi') = \frac{1}{\sqrt{(\xi-\xi')^2+\left\{\eta+\eta-(\xi-\xi')\frac{d\eta}{d\xi}+\frac{1}{2}(\xi-\xi')^2\frac{d^2\eta}{d\xi^2}\right\}^2}} \cdot$$

$$\cdot \left\{\left\{K(k)-E(k)\right\}\left\{1-\frac{d\eta}{d\xi}\frac{(\xi-\xi')}{\eta}\right\} - \right.$$

$$-E(k)\left\{\frac{2\eta-2(\xi-\xi')\frac{d\eta}{d\xi}+(\xi-\xi')^2\frac{d^2\eta}{d\xi^2}}{(\xi-\xi')^2+\left\{(\xi-\xi')\frac{d\eta}{d\xi}-\frac{1}{2}(\xi-\xi')^2\frac{d^2\eta}{d\xi^2}\right\}^2}\right\} \cdot$$

$$\left. \cdot \left\{(\xi-\xi')\frac{d\eta}{d\xi}-\frac{1}{2}(\xi-\xi')^2\frac{d^2\eta}{d\xi^2}-\frac{d\eta}{d\xi}(\xi-\xi')\right\}\right\} \qquad \text{(A1.5)}$$

Substituting Eq.(A1.4) in Eq.(A1.3) results in:

$$k = 2\sqrt{\frac{\eta^2-\eta(\xi-\xi')\frac{d\eta}{d\xi}+\frac{\eta}{2}(\xi-\xi')^2\frac{d^2\eta}{d\xi^2}}{(\xi-\xi')^2+\left\{2\eta-(\xi-\xi')\frac{d\eta}{d\xi}+\frac{1}{2}(\xi-\xi')^2\frac{d^2\eta}{d\xi^2}\right\}^2}} \qquad \text{(A1.6)}$$

for the argument k of the elliptical integral E(k) and K(k).

From Eq.(A1.6):

$$\lim_{\xi\to\xi'} k = 1 \qquad \text{(A1.7)}$$

Abramowitz and Stegun [21] (p.591 and 592, Eqs.17.3.26 and 17.3.35) gives the following approximations for the argument k in this limiting case:

$$\lim_{k\to 1} K(k) = \frac{1}{2} \ln \frac{16}{1-k^2} = \ln \frac{4}{\sqrt{1-k^2}} \qquad \text{(A1.8)}$$

$$\lim_{k\to 1} E(k) = 1 \qquad \text{(A1.9)}$$

Substituting Eq.(A1.6) in Eq.(A1.8) results in:

/80

$$K(\zeta=\xi') = \ln \frac{4}{\sqrt{1-4\dfrac{\eta^2 - \eta(\xi-\xi')\frac{d\eta}{d\xi} + \frac{\eta}{2}(\xi-\xi')^2\frac{d^2\eta}{d\xi^2}}{(\xi-\xi')^2+\left\{2\eta-(\xi-\xi')\frac{d\eta}{d\xi}+\frac{1}{2}(\xi-\xi')^2\frac{d^2\eta}{d\xi^2}\right\}^2}}} \qquad \text{(A1.10)}$$

Eq.(A1.10) can be restated:

$$K(\xi=\xi') = \ln \frac{8\eta}{|\xi-\xi'| \sqrt{\dfrac{4\eta^2\left\{1+\left(\frac{d\eta}{d\xi}-\frac{1}{2}(\xi-\xi')\frac{d^2\eta}{d\xi^2}\right)^2\right\}}{(\xi-\xi')^2+\left(2\eta-(\xi-\xi')\frac{d\eta}{d\xi}+\frac{1}{2}(\xi-\xi')^2\frac{d^2\eta}{d\xi^2}\right)^2}}} \qquad \text{(A1.11)}$$

This results in:

$$G_r(\xi=\xi') = \frac{1}{\sqrt{(\xi-\xi')^2+\left(2\eta-(\xi-\xi')\frac{d\eta}{d\xi}+\frac{1}{2}(\xi-\xi')^2\frac{d^2\eta}{d\xi^2}\right)^2}} \cdot$$

$$\cdot \left\{ \left\{ \ln \frac{8\eta}{|\xi-\xi'|\sqrt{\frac{4\eta^2\left\{1+\left(\frac{d\eta}{d\xi}-\frac{1}{2}(\xi-\xi')\frac{d^2\eta}{d\xi^2}\right)^2\right\}}{(\xi-\xi')^2+\left(2\eta-(\xi-\xi')\frac{d\eta}{d\xi}+\frac{1}{2}(\xi-\xi')^2\frac{d^2\eta}{d\xi^2}\right)^2}}} - \right.\right.$$

$$\left.\left. \cdot \left\{1-\frac{d\eta}{d\xi}\frac{(\xi-\xi')}{\eta}\right\} - \left\{\frac{2\eta-2(\xi-\xi')\frac{d\eta}{d\xi}+(\xi-\xi')^2\frac{d^2\eta}{d\xi^2}}{1+\left(\frac{d\eta}{d\xi}-\frac{1}{2}(\xi-\xi')\frac{d^2\eta}{d\xi^2}\right)^2}\right\}\left\{-\frac{1}{2}\frac{d^2\eta}{d\xi^2}\right\}\right\}$$

(A1.12)

For axi-symmetrical flow this results in:

$$G_r(\xi=\xi') = \frac{1}{2\eta}\left\{\ln\frac{8\eta}{|\xi-\xi'|\sqrt{1+\left(\frac{d\eta}{d\xi}\right)^2}} - 1 + \frac{\eta}{1+\left(\frac{d\eta}{d\xi}\right)^2}\frac{d^2\eta}{d\xi^2}\right\} \qquad \text{(A1.13)}$$

Two Dimensional Flow

/81

The kernel function $G(\xi,\xi')$ is given in Eqs.(2.27), (2.9) and (2.11). It is developed in the range $\xi=\xi'$ in such a way as to eliminate the unknowns. When Eq.(2.9) and (2.11) are also substituted in Eq.(2.27), the following results:

$$G_e(\xi,\xi') = -\frac{\eta-\eta'}{(\xi-\xi')^2+(\eta-\eta')^2} + \frac{\eta+\eta'}{(\xi-\xi')^2+(\eta+\eta')^2} +$$

$$+\frac{d\eta}{d\xi}\frac{\xi-\xi'}{(\xi-\xi')^2+(\eta-\eta')^2} - \frac{d\eta}{d\xi}\frac{\xi-\xi'}{(\xi-\xi')^2+(\eta+\eta')^2} \qquad \text{(A1.14)}$$

Eq.(A1.4) is substituted in Eq.(A1.14) and expressions with identical denominator are combined:

$$G_e(\xi=\xi') = \frac{-(\xi-\xi')\frac{d\eta}{d\xi} + \frac{1}{2}(\xi-\xi')^2\frac{d^2\eta}{d\xi^2} + (\xi-\xi')\frac{d\eta}{d\xi}}{(\xi-\xi')^2 + \left((\xi-\xi')\frac{d\eta}{d\xi} - \frac{1}{2}(\xi-\xi')^2\frac{d^2\eta}{d\xi^2}\right)^2} +$$

$$+ \frac{2\eta - (\xi-\xi')\frac{d\eta}{d\xi} + \frac{1}{2}(\xi-\xi')^2\frac{d^2\eta}{d\xi^2} - (\xi-\xi')\frac{d\eta}{d\xi}}{(\xi-\xi')^2 + \left(2\eta - (\xi-\xi')\frac{d\eta}{d\xi} + \frac{1}{2}(\xi-\xi')^2\frac{d^2\eta}{d\xi^2}\right)^2} \qquad \text{(A1.15)}$$

After simplifying and ignoring all terms in which $(\xi-\xi')$ occurs as a factor, this results in:

$$G_e(\xi=\xi') = \frac{1}{2}\left\{\frac{\frac{d^2\eta}{d\xi^2}}{1+\left(\frac{d\eta}{d\xi}\right)^2} + \frac{1}{\eta}\right\} \qquad \text{(A1.16)}$$

Appendix 2

Analytical Computation of the Residual Integral from Eq.(2.35) at Constant $\dot{\omega}$, for $\xi \approx \xi'$ in Axi-symmetrical Flow

The integral of Eq.(2.35) restated:

$$I = \int_{\alpha_\mu - \frac{\Delta\alpha}{2}}^{\alpha_\mu + \frac{\Delta\alpha}{2}} \hat{G}(\alpha_\mu, \alpha')\, d\alpha' \qquad \text{(A2.1)}$$

The following equations were derived under the assumption $\Delta\alpha \ll 1$. Eq.(A1.13) is copied from Appendix 1. Substituting Eqs.(2.31), (2.32) and (2.33) changes this equations into:

$$\hat{G}_r(\xi \approx \xi') = \frac{\dot{\xi}}{2\eta} \left\{ \ln \frac{8\,\eta}{|\xi - \xi'| \sqrt{1 + \left(\frac{\eta}{\xi}\right)^2}} - 1 + \frac{\eta}{1 + \left(\frac{\eta}{\xi}\right)^2} \frac{\ddot{\eta}\dot{\xi} - \dot{\eta}\ddot{\xi}}{\dot{\xi}^3} \right\} \qquad \text{(A2.2)}$$

Eq.(A2.2) is substituted into Eq.(A2.1). From this, two partial integrals are formed:

$$I_r = I_1 + I_2 \qquad \text{(A2.3)}$$

In integral I_1 the integrand is fully independent of α':

$$I_1 = \frac{\dot{\xi}}{2\eta}\left\{\ln\frac{8\,\eta}{\sqrt{1+\left(\frac{\dot{\eta}}{\dot{\xi}}\right)^2}} - 1 + \frac{\eta}{\xi}\,\frac{\ddot{\eta}\dot{\xi}-\dot{\eta}\ddot{\xi}}{\dot{\xi}^2+\dot{\eta}^2}\right\}\int_{\alpha_\mu-\frac{\Delta\alpha}{2}}^{\alpha_\mu+\frac{\Delta\alpha}{2}} d\alpha'$$

$$= \Delta\alpha\left(\frac{\dot{\xi}}{2\eta}\left\{\ln\frac{8\,\eta}{\sqrt{1+\left(\frac{\dot{\eta}}{\dot{\xi}}\right)^2}} - 1\right\} + \frac{\ddot{\eta}\dot{\xi}-\dot{\eta}\ddot{\xi}}{2\left(\dot{\xi}^2+\dot{\eta}^2\right)}\right) \qquad \text{(A2.4)}$$

Integral I_2 is: /83

$$I_2 = -\int_{\alpha_\mu-\frac{\Delta\alpha}{2}}^{\alpha_\mu+\frac{\Delta\alpha}{2}} \frac{\dot{\xi}}{2\eta}\,\ln|\xi-\xi'|\,d\alpha' \qquad \text{(A2.5)}$$

In Eq.(A2.5) α and α' shall be substituted by ξ and ξ':

$$d\alpha' = \frac{d\xi'}{\dot{\xi}} \qquad \text{(A2.6)}$$

The integration limits of I_2 can be developed in Taylor series:

$$\xi_o = \xi\left(\alpha_\mu+\frac{\Delta\alpha}{2}\right) = \xi(\alpha_\mu) + \dot{\xi}(\alpha_\mu)\,\frac{\Delta\alpha}{2} + \ddot{\xi}(\alpha_\mu)\,\frac{\Delta\alpha^2}{8} \qquad \text{(A2.7)}$$

$$\xi_u = \xi\left(\alpha_\mu-\frac{\Delta\alpha}{2}\right) = \xi(\alpha_\mu) - \dot{\xi}(\alpha_\mu)\,\frac{\Delta\alpha}{2} + \ddot{\xi}(\alpha_\mu)\,\frac{\Delta\alpha^2}{8} \qquad \text{(A2.8)}$$

If the assumption $\Delta\alpha \ll 1$ applies:

$$\dot{\xi} = \dot{\xi}' \tag{A2.9}$$

Thus I_2 becomes:

$$I_2 = -\frac{1}{2\eta} \int_{\xi_u}^{\xi_o} \ln|\xi-\xi'| \, d\xi'$$

$$= \frac{1}{2\eta} \left[(\xi-\xi')(\ln|\xi-\xi'| - 1) \right]_{\xi'=\xi_u}^{\xi'=\xi_o} \tag{A2.10}$$

$$= \frac{1}{2\eta} \left\{ (\xi-\xi_o)(\ln|\xi-\xi_o| - 1) - (\xi-\xi_u)(\ln|\xi-\xi_u| - 1) \right\}$$

/84

$$I_2 = -\frac{\Delta\alpha}{4\eta} \left\{ (\dot{\xi}+\ddot{\xi}\frac{\Delta\alpha}{4}) \left(\ln(\dot{\xi}\frac{\Delta\alpha}{2}+\ddot{\xi}\frac{\Delta\alpha^2}{8})-1\right) + (\dot{\xi}-\ddot{\xi}\frac{\Delta\alpha}{4}) \left(\ln(\dot{\xi}\frac{\Delta\alpha}{2}-\ddot{\xi}\frac{\Delta\alpha^2}{8})-1\right) \right\} \tag{A2.11}$$

$$I_r = I_1+I_2 = \frac{\Delta\alpha}{2} \left\{ \frac{\dot{\xi}}{\eta} \left(\ln \frac{8\,\eta}{\sqrt{1+\left(\frac{\eta}{\xi}\right)^2}} - 1\right) + \frac{\ddot{\eta}\dot{\xi}-\dot{\eta}\ddot{\xi}}{\dot{\xi}^2+\dot{\eta}^2} - \right.$$

$$- \frac{1}{2\eta} \left\{ (\dot{\xi}+\ddot{\xi}\frac{\Delta\alpha}{4}) \left(\ln(\dot{\xi}\frac{\Delta\alpha}{2}+\ddot{\xi}\frac{\Delta\alpha^2}{8})-1\right) + \right.$$

$$\left. \left. + (\dot{\xi}-\ddot{\xi}\frac{\Delta\alpha}{4}) \left(\ln(\dot{\xi}\frac{\Delta\alpha}{2}-\ddot{\xi}\frac{\Delta\alpha^2}{8})-1\right) \right\} \right\} \tag{A2.12}$$

The values for ξ and η occurring in Eq.(A2.12) and their derivatives refer to the point μ.

Appendix 3 /85

Transformation of Eq.(2.35) into a System of Linear Equations for $\hat{\omega}_\mu$, $\mu = 1,2,3,\ldots,n$ for a $\hat{\omega}$ Curve, Quadratically Interpolated from the $\hat{\omega}_\mu$ Values

The development of these linear equations is based on Eq.(2.35):

$$\hat{\omega}_\mu = \frac{1}{\pi} \sum_{\nu=1}^{n} \int_{\alpha_\nu - \frac{\Delta\alpha}{2}}^{\alpha_\nu + \frac{\Delta\alpha}{2}} \hat{\omega}(\hat{\omega}_{\nu-1}, \hat{\omega}_\nu, \hat{\omega}_{\nu+1}, \alpha') \, \hat{G}(\alpha_\mu, \alpha') \, d\alpha' + \hat{\omega}_q(\alpha_\mu)$$

$$\mu = 1,2,3,\cdots,n \qquad (A3.1)$$

This system of equations serves to calculate the n values $\hat{\omega}_\mu$, $\mu = 1,2,3,\ldots,n$. The function $\hat{\omega}(\hat{\omega}_{\nu-1}, \hat{\omega}_\nu, \hat{\omega}_{\nu+1}, \alpha')$, occurring in Eq.(A3.1), is computed with the aid of the Lagrange interpolation method, such as used by Abramovitz and Stegun [21] (p.878, Eqs. 25.2.1 and 25.2.2). For a quadratic interpolation of the $\hat{\omega}$ values it is:

$$\hat{\omega} = \ell_{\nu-1}\hat{\omega}_{\nu-1} + \ell_\nu \hat{\omega}_\nu + \ell_{\nu+1}\hat{\omega}_{\nu+1} \qquad (A3.2)$$

In Eq.(A3.2) the factors ℓ_i are developed from the following equation by means of cyclical substitution of the indices:

$$\ell_\nu = \frac{(\alpha' - \alpha_{\nu-1})(\alpha' - \alpha_{\nu+1})}{(\alpha_\nu - \alpha_{\nu-1})(\alpha_\nu - \alpha_{\nu+1})} \qquad (A3.3)$$

Thus Eq.(A3.1) is developed into the following system of linear equations:

$$\hat{\omega}_{\mu} = \frac{1}{\pi} \sum_{\nu=1}^{n} \left\{ \hat{\omega}_{\nu-1} \int_{\alpha_\nu - \frac{\Delta\alpha}{2}}^{\alpha_\nu + \frac{\Delta\alpha}{2}} \ell_{\nu-1} \hat{G}(\alpha_\mu, \alpha')\, d\alpha' + \right.$$

$$+ \hat{\omega}_{\nu} \int_{\alpha_\nu - \frac{\Delta\alpha}{2}}^{\alpha_\nu + \frac{\Delta\alpha}{2}} \ell_{\nu}\, \hat{G}(\alpha_\mu, \alpha')\, d\alpha' +$$

$$\left. + \hat{\omega}_{\nu+1} \int_{\alpha_\nu - \frac{\Delta\alpha}{2}}^{\alpha_\nu + \frac{\Delta\alpha}{2}} \ell_{\nu+1} \hat{G}(\alpha_\mu, \alpha')\, d\alpha' \right\} + \hat{\omega}_q(\alpha_\mu) \qquad \text{(A3.4}$$

$$\mu = 1, 2, 3, \cdots, n$$

In Eq.(A3.4) the integrals occurring are perfect local functions, which can be calculated without knowing the $\hat{\omega}$ curve. For the present work a computer program was developed, in which the integral values were calculated andassembled in a coefficient matrix. With the aid of this matrix the system of equations was solved for $\hat{\omega}_\mu$. At three points, however, the coefficient calculation had to be modified relative to Eq.(A3.4):

a) at point $\nu=1$
b) at point $\nu=\mu$
c) at point $\nu=n$.

In cases (a) and (c) the value for $\hat{\omega}$ is determined by interpolation or extrapolation respectively, over the first three or the last three values for $\hat{\omega}_\mu$. In case (b) a smaller range to the right and to the left of the singular points of /87
the kernel $\hat{G}_1(\alpha_\mu = \alpha_\nu)$ is selected from the integration for the

axi-symmetrical flow per Eq.(3.4). In this range the analytical solution of the integral from Appendix 2 is substituted, multiplied with the constant value $\hat{\omega}_{\mu}$.

```
      FUNCTION VERD(DLR,X,DL,EMIN,RMAX,DD,XV,ROT)                    /101
C-----------------------------------------------------------------------
C     Compensation Function for Boundary Layer Displacement in a Wind Tunnel Contraction
C     from Subroutine KONTUR
C-----------------------------------------------------------------------
      LOGICAL ERST,ROT
      Y(X)=ST*(X-RK)-SQRT(1.+FS*(X-RK)*(X-RK))*2.+14.2*TANH((X-RK)/12.
      IF(DLR.LT.X) GO TO 10
      ERST=.TRUE.
      VERD=0.
      RETURN
   10 IF(.NOT.ERST) GO TO 20
      ERST=.FALSE.
      IF(ROT) GO TO          15
      ST=.195
      FS=.0041
      AG=58.9
      RK=2.
      GO TO                  16
   15 ST=.3
      FS=.01
      AG=77.2
      RK=10.
   16 XAN=75.-XV*100.
      YAN=Y(XAN)
   20 XL=-(DL-X)/EMIN*100.+75.
      VERD=(Y(XL)-YAN)/AG*DD
      RETURN
      END
```

Contour Curve for a Wind Tunnel Contraction
(Compensation for Boundary Layer Displacement) /102

RMAX = 1,5000000
EM = 0,333000
XL = 1,820000
WH = 0,581000
WL = 1,248000
WS = -2,325000
DC = 0,004700
XV = 1,450000
DX = 0,100000M
ZWEIDIMENSIONALE STROEMUNG (2-dimensional flow)

X	Y
0.0	1.5000
0.1000	1.4998
0.2000	1.4986
0.3000	1.4955
0.4000	1.4894
0.5000	1.4797
0.6000	1.4655
0.7000	1.4458
0.8000	1.4200
0.9000	1.3872
1.0000	1.3466
1.1000	1.2975
1.2000	1.2394
1.3000	1.1718
1.4000	1.0946
1.5000	1.0083
1.6000	0.9137
1.7000	0.8123
1.8000	0.7063
1.9000	0.5994
2.0000	0.5355
2.1000	0.5076
2.2000	0.4943
2.3000	0.4913
2.4000	0.4967
2.5000	0.5004
2.6000	0.5015
2.7000	0.5017
2.7300	0.5018

STOP

ENDE STOP (1.00) 0.32 SEKUNDEN RECHENDAUER

Pages 88 through 100 (comprising Appendices 4-6) are missing in text

Appendix 7 /103

Computation of a General Function for the Contour Curve

The following shows a method which can be used to compute the coordinates of a function, satisfying the conditions set for the contour function y(x). The derivation of the necessary equations is carried out in a general form here, since the same functions are also used in Section 4.4 for the contour correction at the end of the contraction.

Problem

A function shall be computed so as to satisfy the following conditions:

$$x = x_w \rightarrow y = y_w \quad \text{(A7.1)}$$

$$x = x_w \rightarrow \frac{dy}{dx} = 0 \quad \text{(A7.2)}$$

$$x = x_w \rightarrow \frac{d^2y}{dx^2} = 0 \quad \text{(A7.3)}$$

$$x = 0 \rightarrow \frac{dy}{dx} = y'_o \quad \text{(A7.4)}$$

no maximum, minimum or inversion point in the range $0<x<x_w$ (A7.5)

Given

x_w, y_w, y'_o

Solution

Initially a polynomial of the fifth degree is calculated:

$$y = a\,\bar{x}^5 + b\,\bar{x}^3 + c\,\bar{x} \quad \text{(A7.6)}$$

satisfying the conditions (A7.1), (A7.2) and (A7.3), substituting /104
a value $\bar{x}_w$ for the value of the abscissa x_w. The value $\bar{x}_w$ is determined in such a way, that point $(\bar{x}_w, y_w)$ is transformed into the point (x_w, y_w). This transformation is required in order to satisfy condition (A7.4). The transformation must therefore have the following properties:

$$\bar{x}_w \quad \rightarrow \quad x_w \tag{A7.7}$$

$$\left.\frac{dy}{dx}\right|_{\bar{x}_w} = 0 \quad \rightarrow \quad \left.\frac{dy}{dx}\right|_{x_w} = 0 \tag{A7.8}$$

$$\left.\frac{d^2y}{dx^2}\right|_{\bar{x}_w} = 0 \quad \rightarrow \quad \left.\frac{d^2y}{dx^2}\right|_{x_w} = 0 \tag{A7.9}$$

$$\left.\frac{dy}{dx}\right|_{\bar{x}=0} \neq y'_o \quad \rightarrow \quad \left.\frac{dy}{dx}\right|_{x=0} = y'_o \tag{A7.10}$$

No new maxima, minima or inversion points are created (A7.11)

Solution

Part 1: Determination of a Polynomial, Satisfying (A7.1), (A7.2) and (A7.3) for Point $\bar{x} = \bar{x}_w$

Condition (A7.5) is satisfied by the use of (A7.6).

To determine the coefficients a,b and c, it is assumed that Eq.(A7.6) shall satisfy the conditions (A7.1), (A7.2) and (A7.3) for point $\bar{x} = \bar{x}_w$.

(A7.1)→

$$y_w = a\,\bar{x}_w^5 + b\,\bar{x}_w^3 + c\,\bar{x}_w \tag{A7.12}$$

(A7.2)→

$$0 = 5\,a\,\bar{x}_w^4 + 3\,b\,\bar{x}_w^2 + c \tag{A7.13}$$

(A7.3)→

$$0 = 20\, a\, \bar{x}_w^3 + 3\, b\, \bar{x}_w \qquad (A7.14)$$

(A7.14)→

$$a = -\frac{3}{10}\frac{b}{\bar{x}_w^2} \qquad (A7.15)$$

(A7.15) in (A7.13)→

$$0 = -\frac{3}{2}\, b\, \bar{x}_w^2 + 3\, b\, \bar{x}_w^2 + c$$

$$b = -\frac{2}{3}\frac{c}{\bar{x}_w^2} \qquad (A7.16)$$

(A7.16) in (A7.15)→

$$a = \frac{1}{5}\frac{c}{\bar{x}_w^2} \qquad (A7.17)$$

(A7.16) and (A7.17) in (A7.12)→

$$y_w = \frac{1}{5}\, c\, \bar{x}_w - \frac{2}{3}\, c\, \bar{x}_w + c\, \bar{x}_w$$

$$c = \frac{15}{8}\frac{y_w}{\bar{x}_w} \qquad (A7.18)$$

(A7.18) in (A7.16)→

$$b = -\frac{5}{4}\frac{y_w}{\bar{x}_w^3} \qquad (A7.19)$$

(A7.18) in (A7.17)→

$$a = \frac{3}{8}\frac{y_w}{\bar{x}_w^5} \qquad (A7.20)$$

The slope at the coordinate origin therefore is:

$$\left.\frac{dy}{d\bar{x}}\right|_{\bar{x}=0} = \frac{15}{8}\frac{y_w}{\bar{x}_w} \qquad (A7.21)$$

From (A7.21) it follows that condition (A7.4) can generally not be satisfied with (A7.6).

Part 2: Transformation of Equation (A7.6)

Eq.(A7.6) must be transformed in such a way, that Eq.(A7.4) applies, without losing the applicability of the conditions (A7.1), (A7.2) and (A7.3). As will be shown below, the transformation /106 equation

$$\bar{x} = x + py \tag{A7.22}$$

satisfied this requirement. With this transformation the y values remain, and only the x values are changed. For $y = y_w$, in accordance with (A7.1) and (A7.2):

$$\left.\frac{dy}{dx}\right|_{x_w} = \underbrace{\left.\frac{dy}{d\bar{x}}\right|_{\bar{x}_w}}_{=0,\ \text{Eq. (A7.13)}} \cdot \left.\frac{d\bar{x}}{dx}\right|_{x_w} = 0 \tag{A7.23}$$

Similarly for $y = y_w$, in accordance with (A7.1) and (A7.3):

$$\left.\frac{d^2y}{dx^2}\right|_{x_w} = \left\{\underbrace{\left.\frac{d^2y}{d\bar{x}^2}\right|_{\bar{x}_w}}_{=0,\ \text{Eq. (A7.14)}} \cdot \left.\frac{d\bar{x}}{dx}\right|_{x_w} + \underbrace{\left.\frac{dy}{d\bar{x}}\right|_{\bar{x}_w}}_{=0,\ \text{Eq. (A7.13)}} \cdot \left.\frac{d\left[\left.\frac{d\bar{x}}{dx}\right|_{x_w}\right]}{d\bar{x}}\right|_{\bar{x}_w}\right\} \left.\frac{d\bar{x}}{dx}\right|_{x_w} = 0 \tag{A7.24}$$

In accordance with Eq.(A7.21):

$$\left.\frac{dy}{dx}\right|_{x=0} = y'_0 = \left.\frac{dy}{d\bar{x}}\right|_{\bar{x}=0} \cdot \left.\frac{d\bar{x}}{dx}\right|_{x=0}$$

$$= \frac{15}{8}\frac{y_w}{\bar{x}_w}\left(1 + p\underbrace{\left.\frac{dy}{dx}\right|_{x=0}}_{y'_0}\right)$$

$$p = -\frac{1}{y'_0} + \frac{8}{15}\frac{\bar{x}_w}{y_w} \tag{A7.25}$$

Eq.(A8.22) thus becomes:

$$\bar{x} = x + y \left(\frac{8}{15} \frac{\bar{x}_w}{y_w} - \frac{1}{y'_o}\right) \qquad \text{(A7.26)}$$

For point $x = x_w$:

$$\bar{x}_w = x_w + y_w \left(\frac{8}{15} \frac{\bar{x}_w}{y_w} - \frac{1}{y'_o}\right)$$

$$\bar{x}_w = \frac{15}{7} \left(x_w - \frac{y_w}{y'_o}\right) \qquad \text{(A7.27)}$$

Result

/107

The function required is:

$$y = \frac{3}{8} \frac{y_w}{\bar{x}_w^5} \bar{x}^5 - \frac{5}{4} \frac{y_w}{\bar{x}_w^3} \bar{x}^3 + \frac{15}{8} \frac{y_w}{\bar{x}_w} \qquad \text{(A7.28)}$$

with:

$$\bar{x}_w = \frac{15}{7} \left(x_w - \frac{y_w}{y'_o}\right)$$

and:

$$x = \bar{x} - y \left(\frac{8}{15} \frac{\bar{x}_w}{y_w} - \frac{1}{y'_o}\right) \qquad \text{(A7.30)}$$

Numerical Representation

In the present work the value for the function (A7.28) is required at discrete points. For this reason the value $\bar{x}_w$ is calculated first from Eq.(A7.29) from the given values x_w, y_w and y'_o. Subsequently a series of points $(\bar{x},y)$ are computed with Eq.(A7.28) and transformed into x values with the aid of Eq.(A7.30).

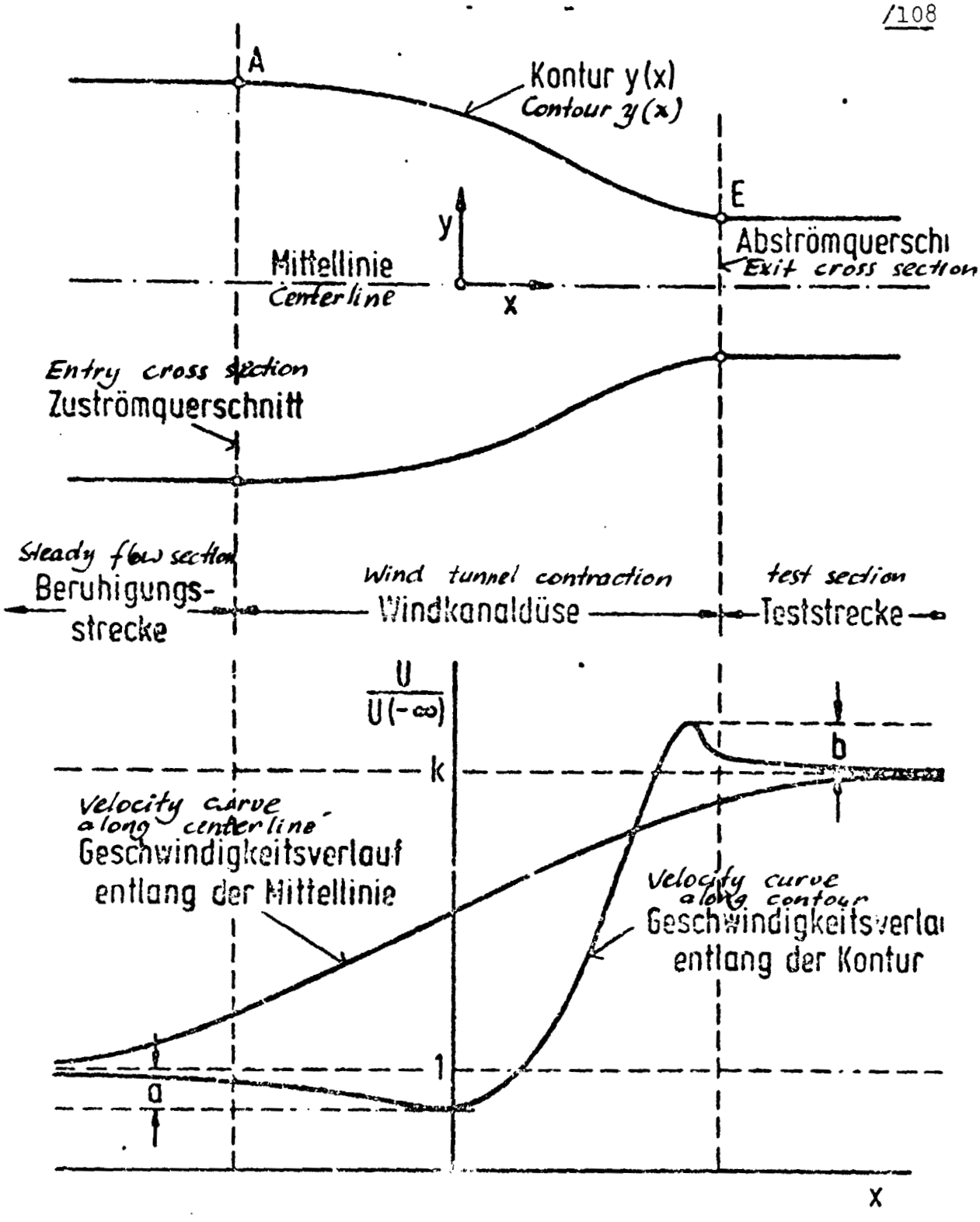

Fig.1 Top: Schematic sketch of a wind tunnel contraction (longitudinal cross section)
Bottom: Schematic velocity curve at the contour and at the center line

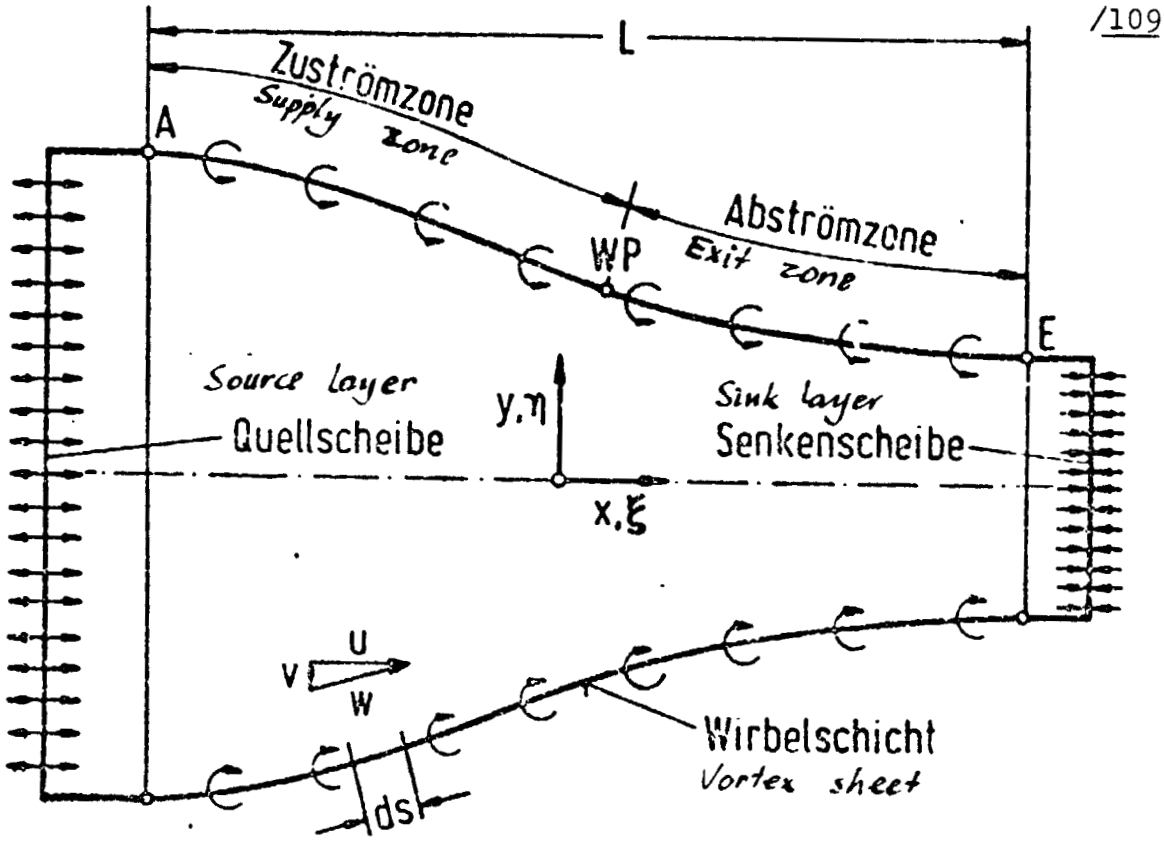

Fig.2 Singularity model for the potential flow through a wind tunnel contraction

/110

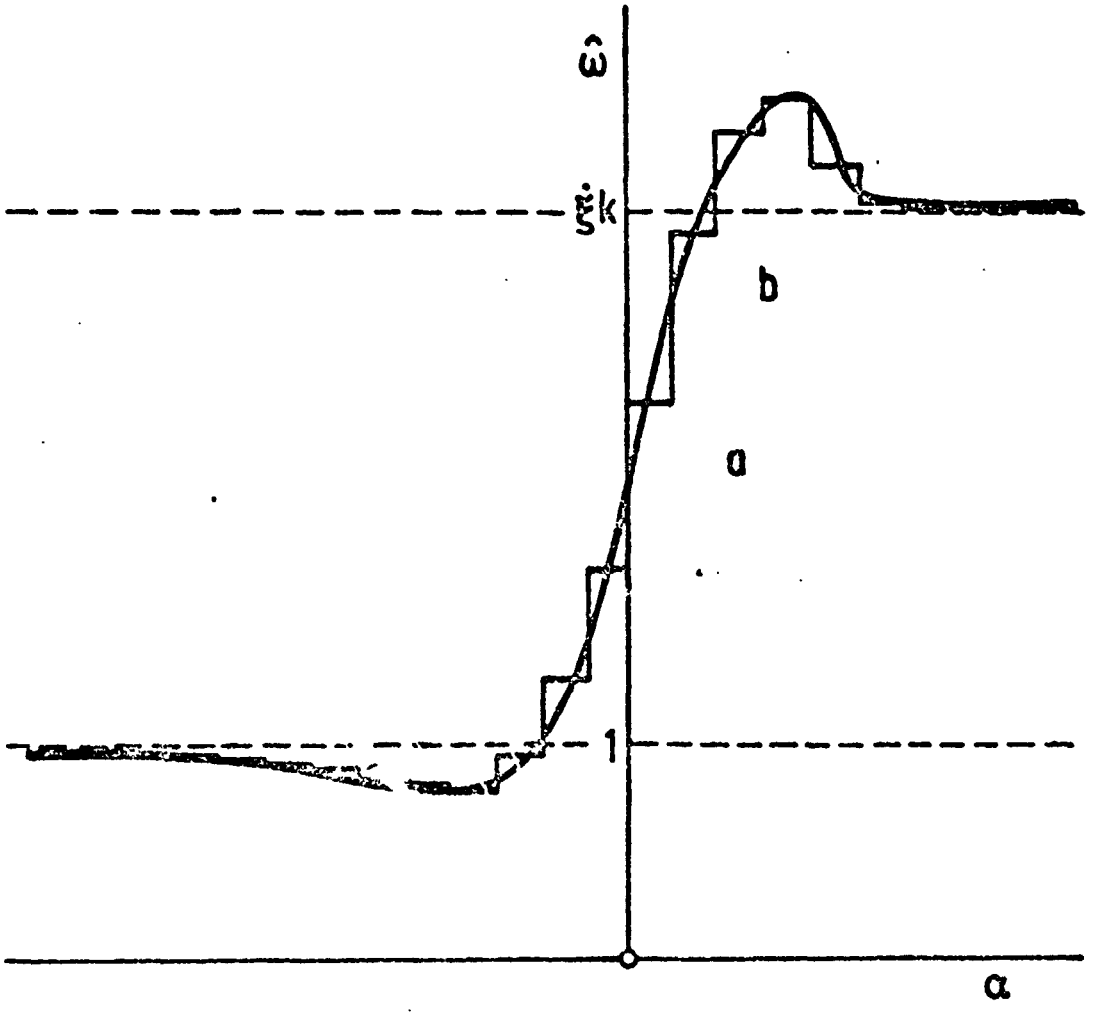

Fig.3 Schematic curve for $\hat{\omega}(\alpha)$ along the contour of a wind tunnel contraction

(a) simulated with a stepped function curve
(b) simulated by means of quadratic interpolation between the interval midpoints

/111

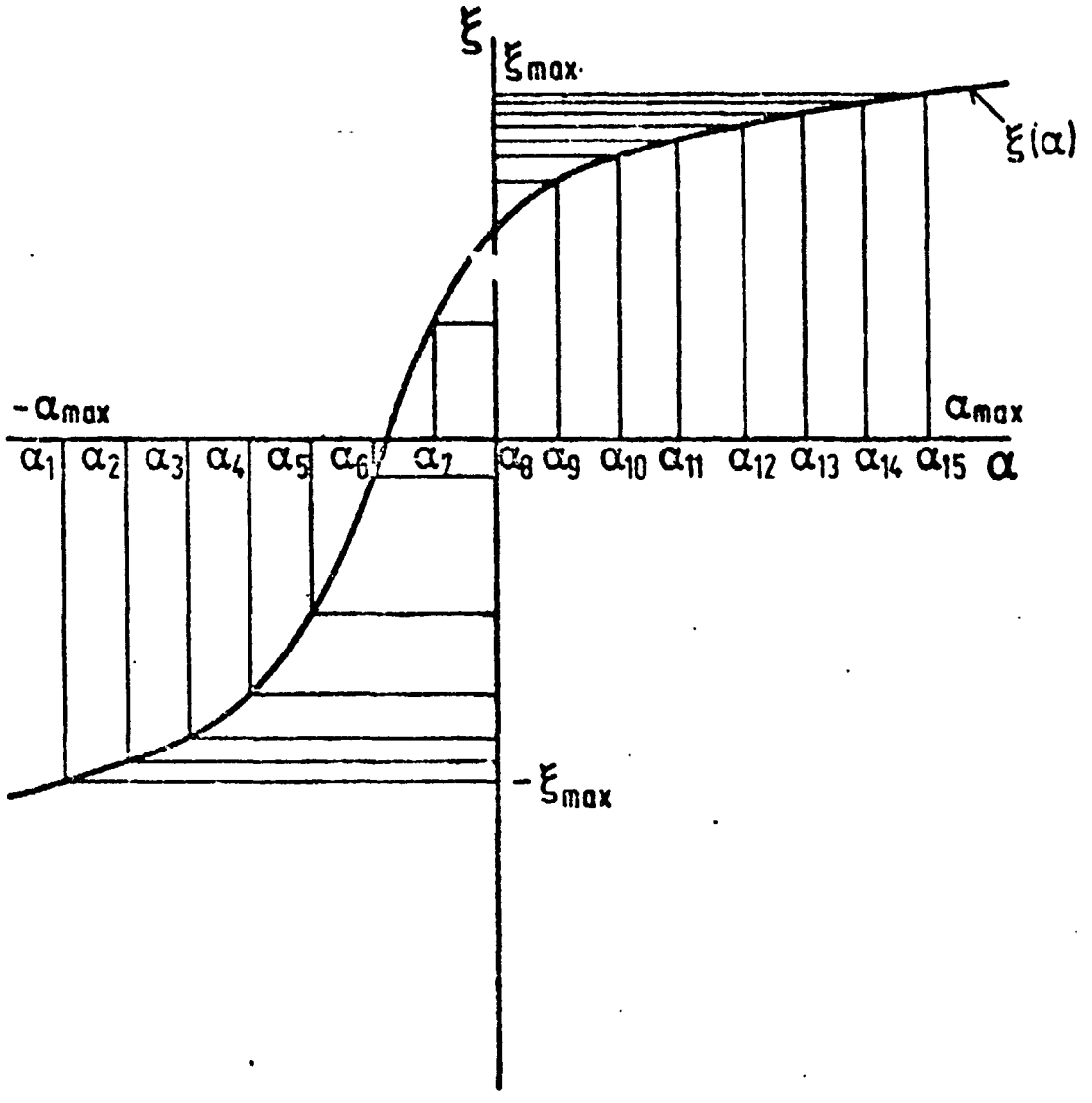

Fig.4 Parameter representation of coordinates $\xi(\alpha)$

/112

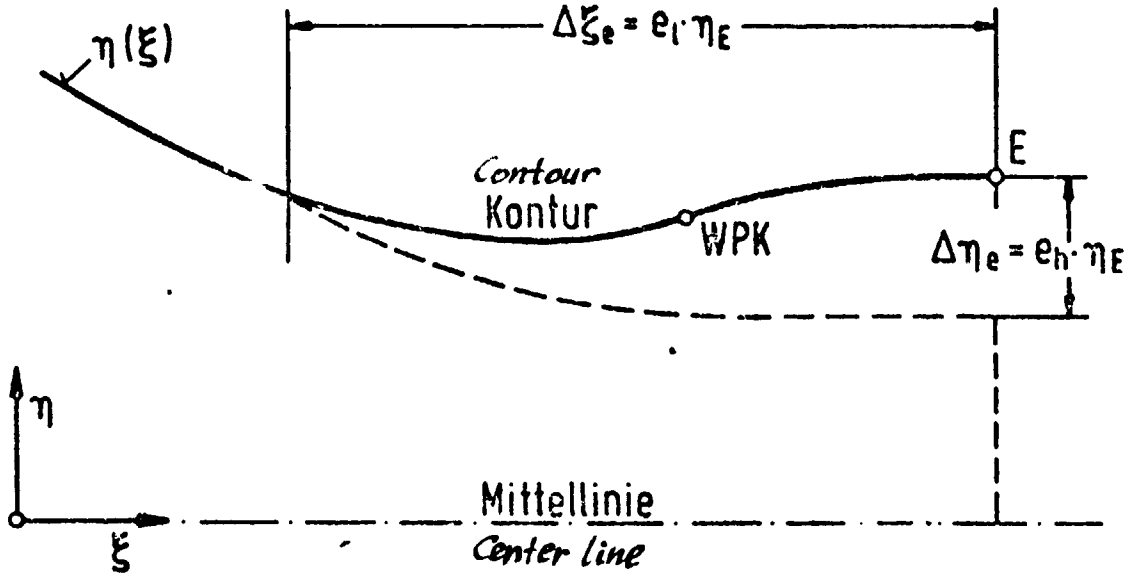

Fig.5 Correction for contraction contour in the exit zone

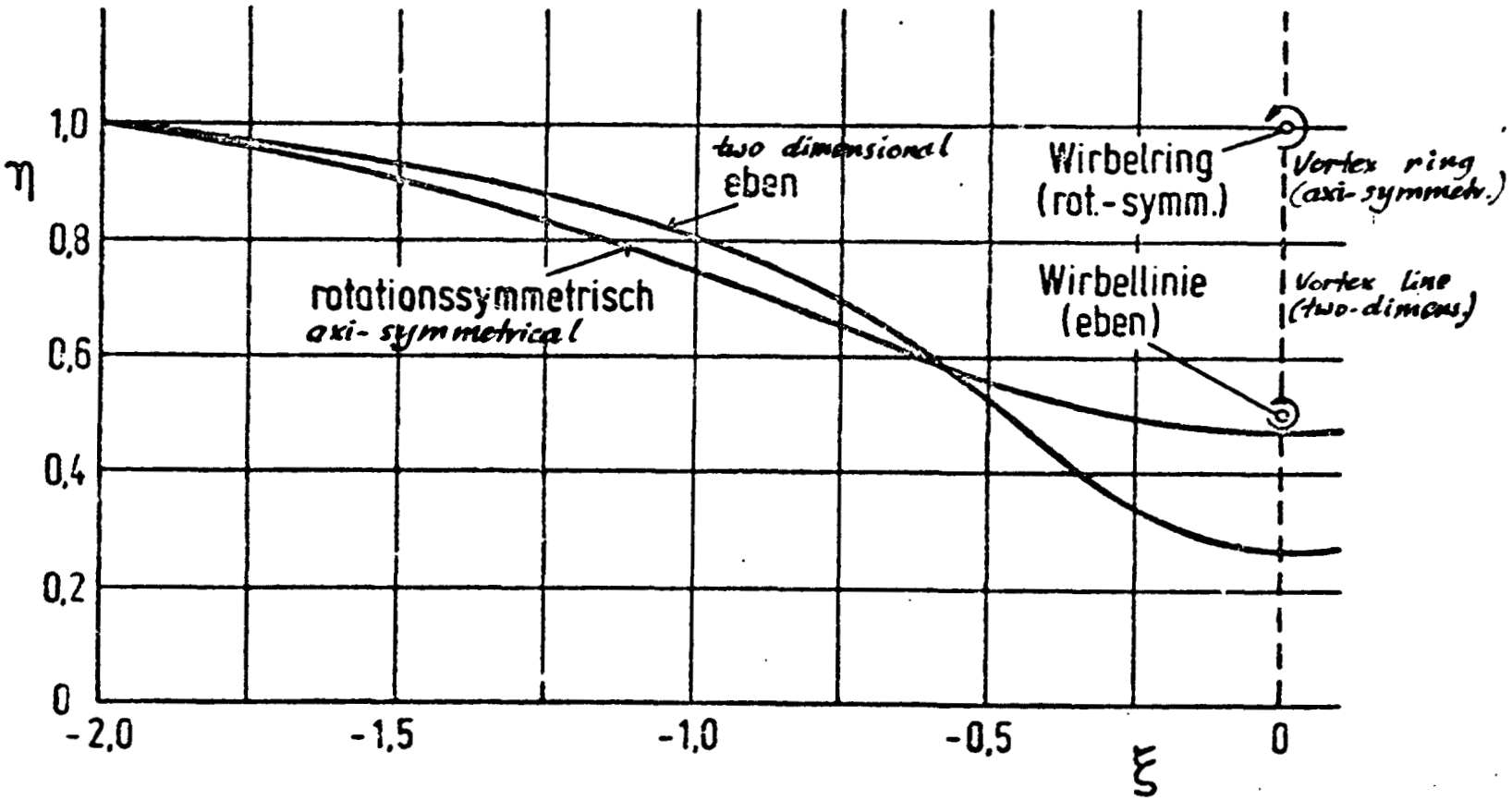

Fig.6 Contour curve for comparative flows

/113

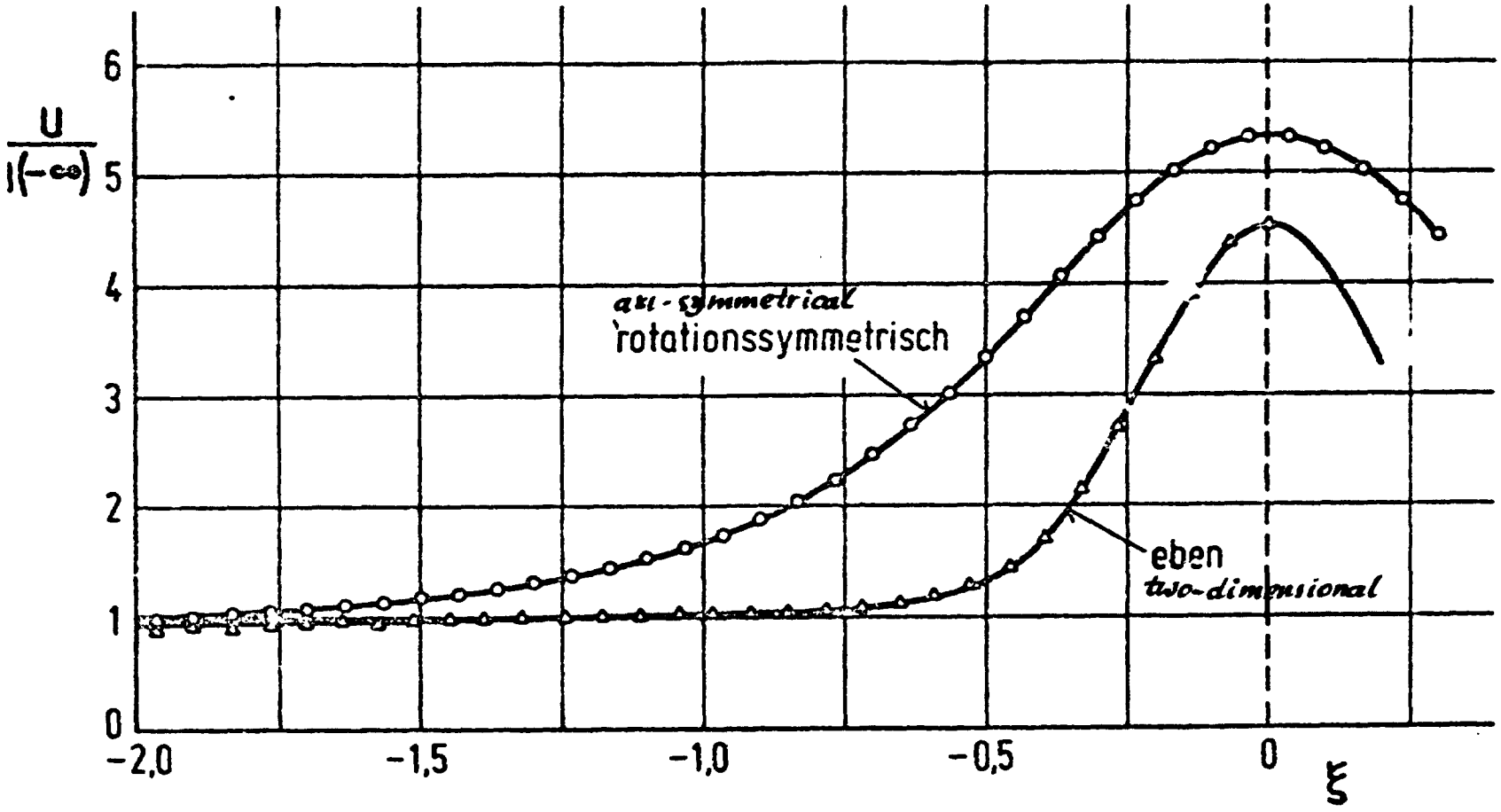

Fig.7 Curve for contour velocities of comparison flows
continuous lines: parallel flows with torque lines or torque ring
point symbols: vortex sheets with source and sink discs

/114

/115

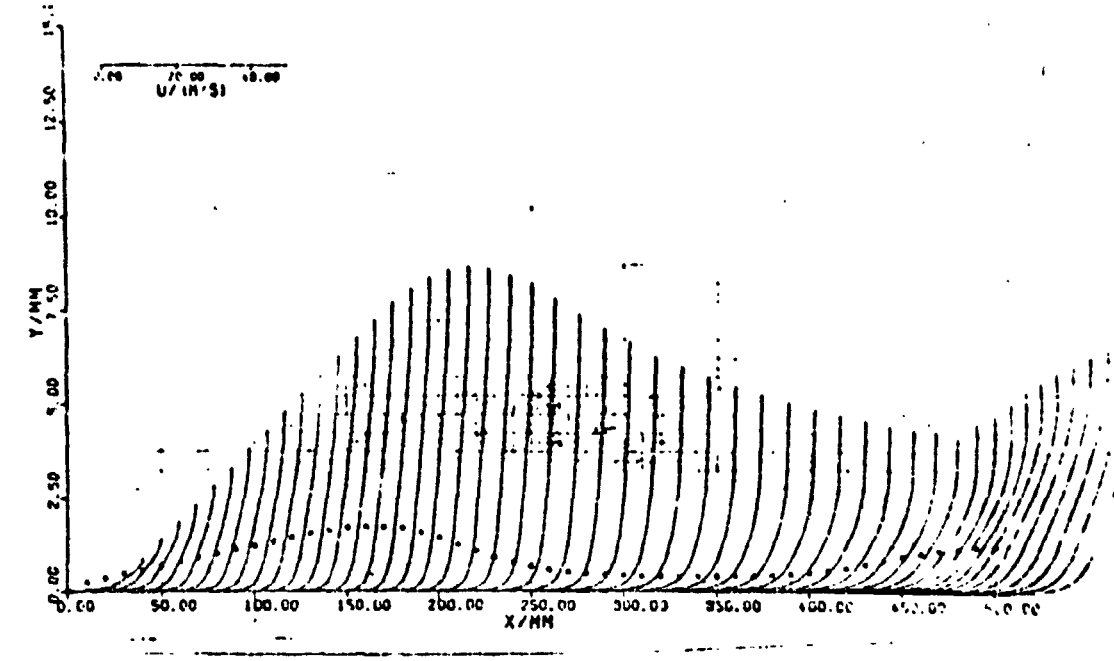

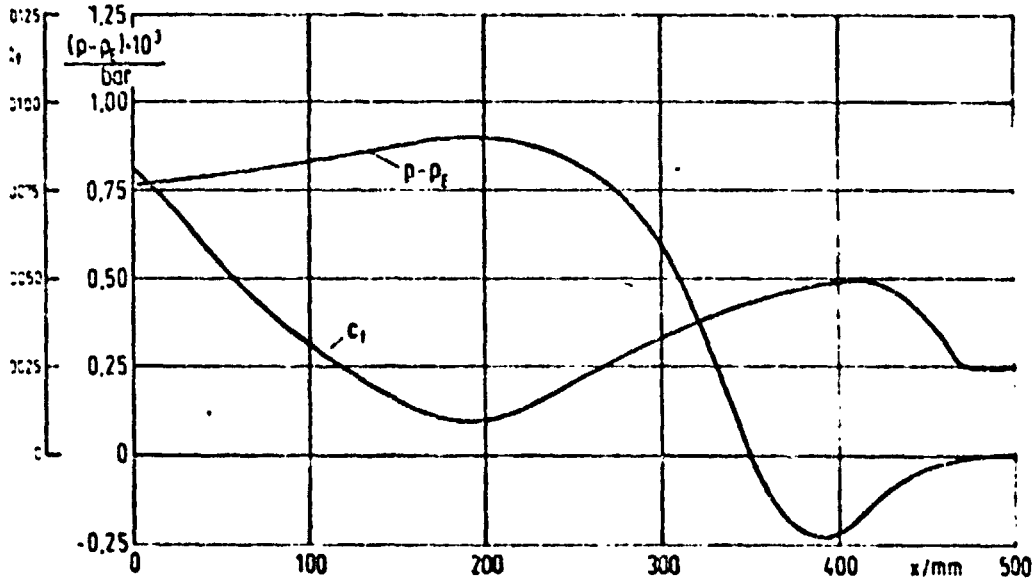

Fig.8 Boundary layer curve along the contour of a wind tunnel contraction

Top: velocity profile in the boundary layer at the base points of the profile represented; point symbols show the curve for the displacement thickness

Bottom: curve for the pressure relative to the pressure in the exit cross section and curve for the wall friction factor c_f

/116

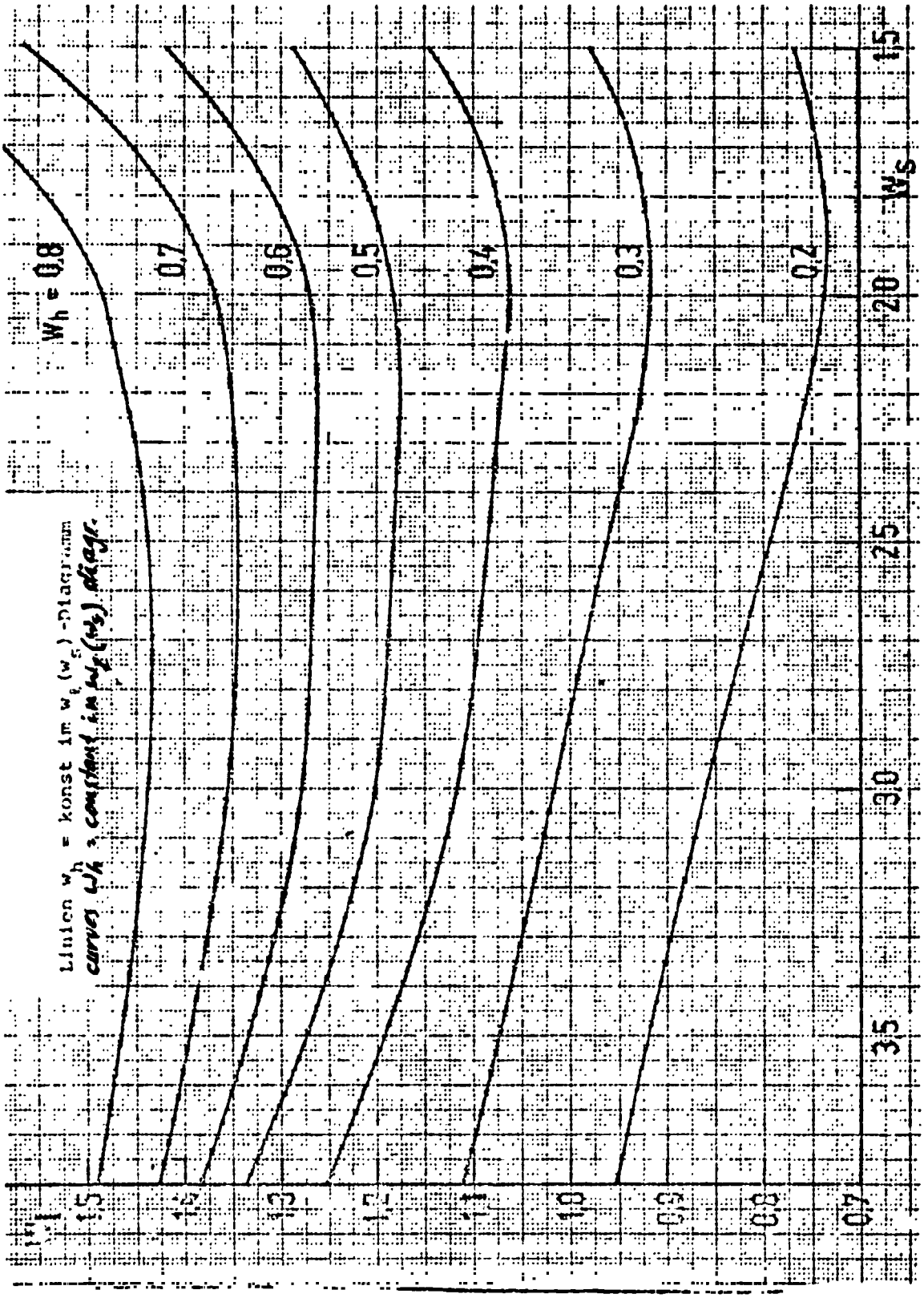

Fig. 9e (Two-dimensional)

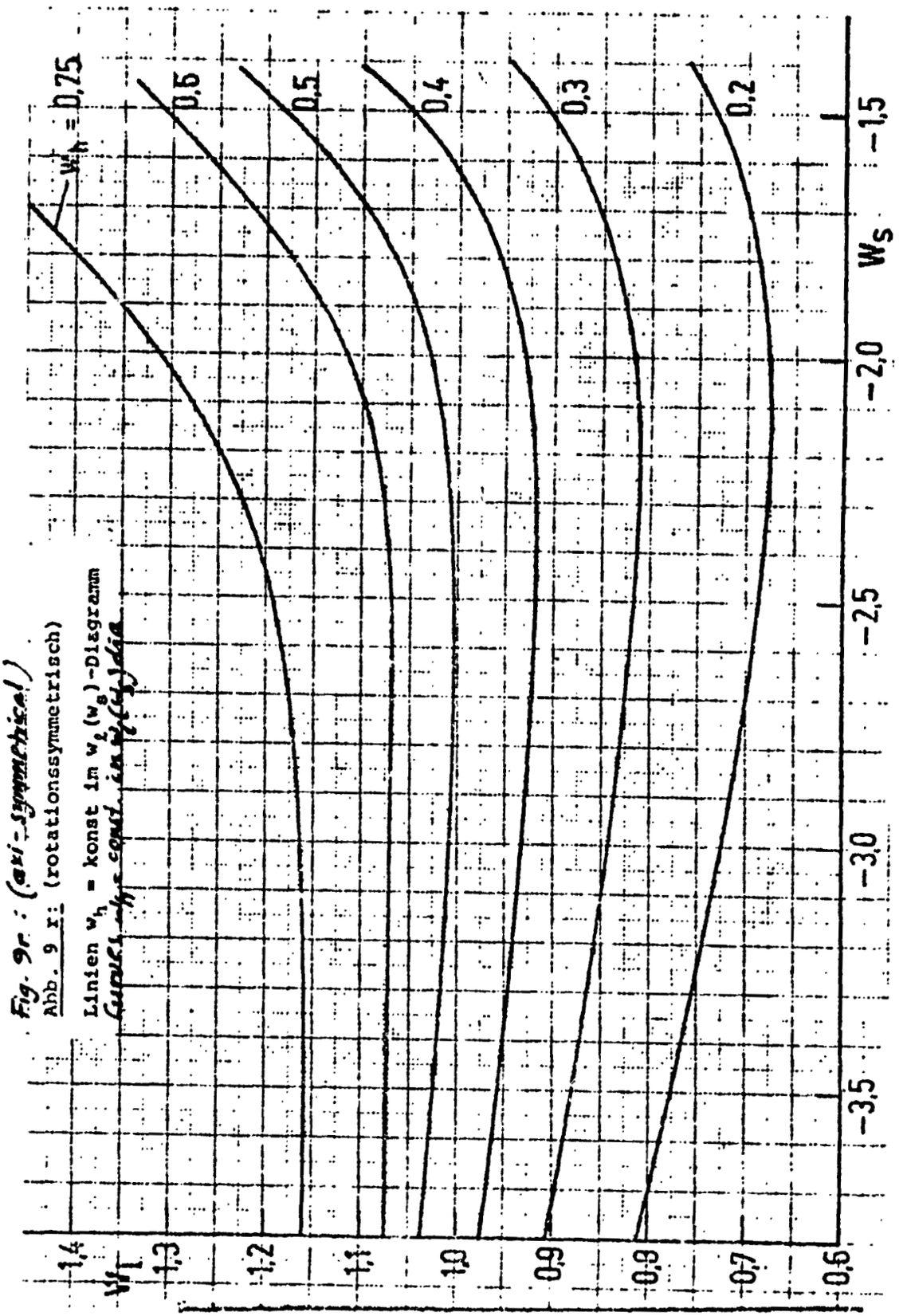

Fig. 9r : (axi-symmetrical)
Abb. 9 r: (rotationssymmetrisch)
Linien w_h = konst im $w_1(w_s)$-Diagramm
Curves w_h = const in $w_1(w_s)$ diagram

/118

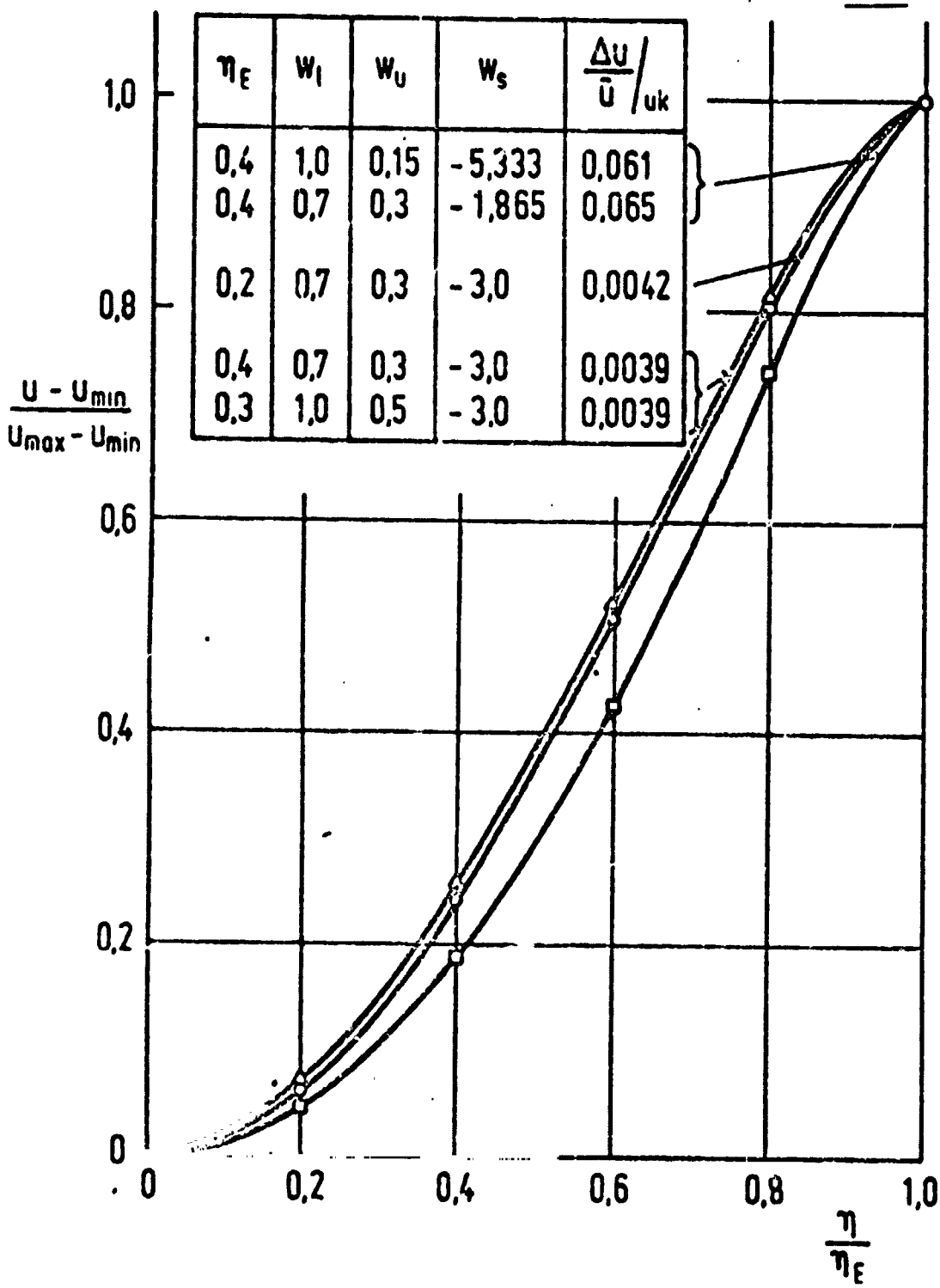

Fig.10 Normalized velocity profile in exit cross section $\xi=\xi_E$ uncorrected contractions

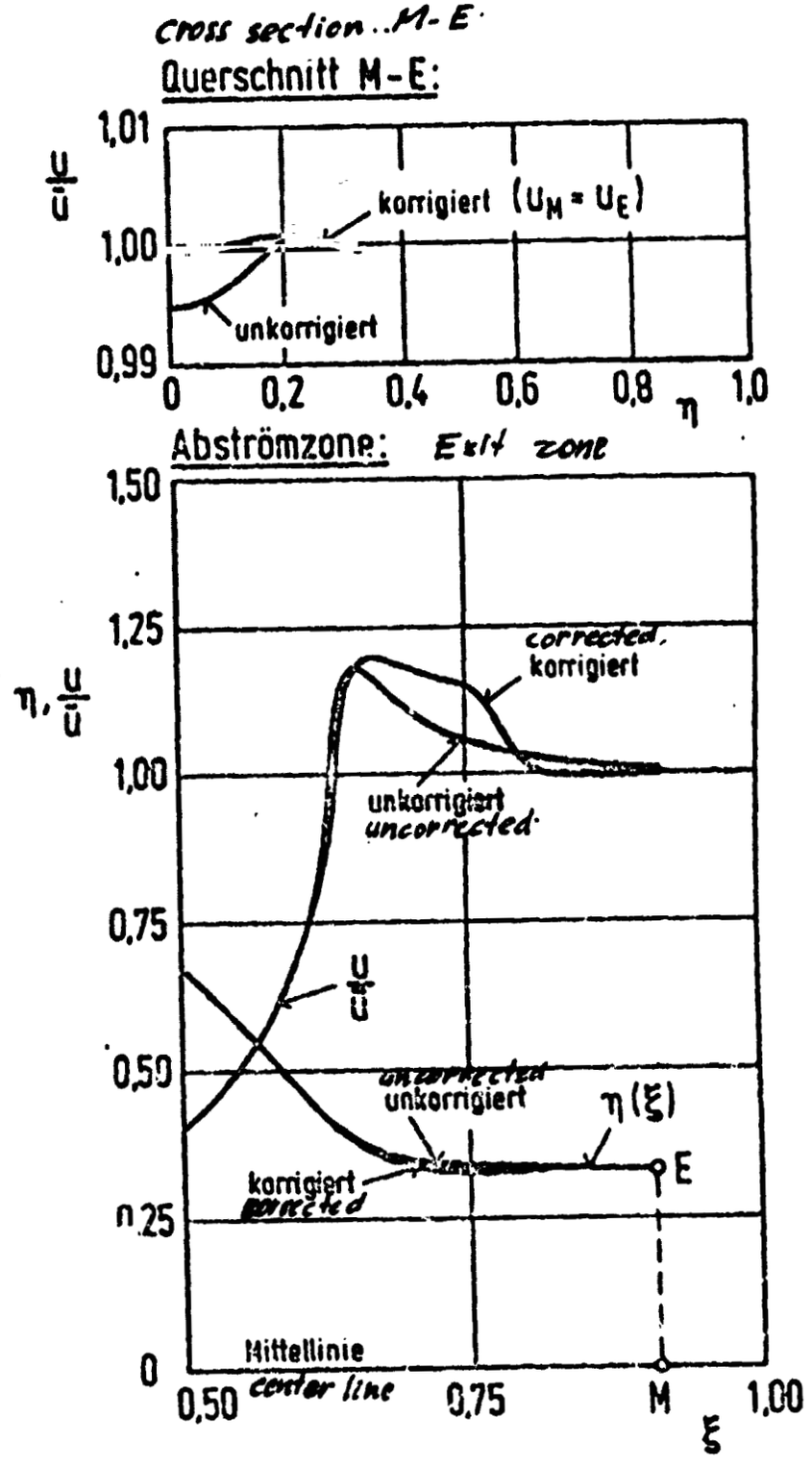

Fig.11 Exit zone for a corrected and an uncorrected two dimensional contraction

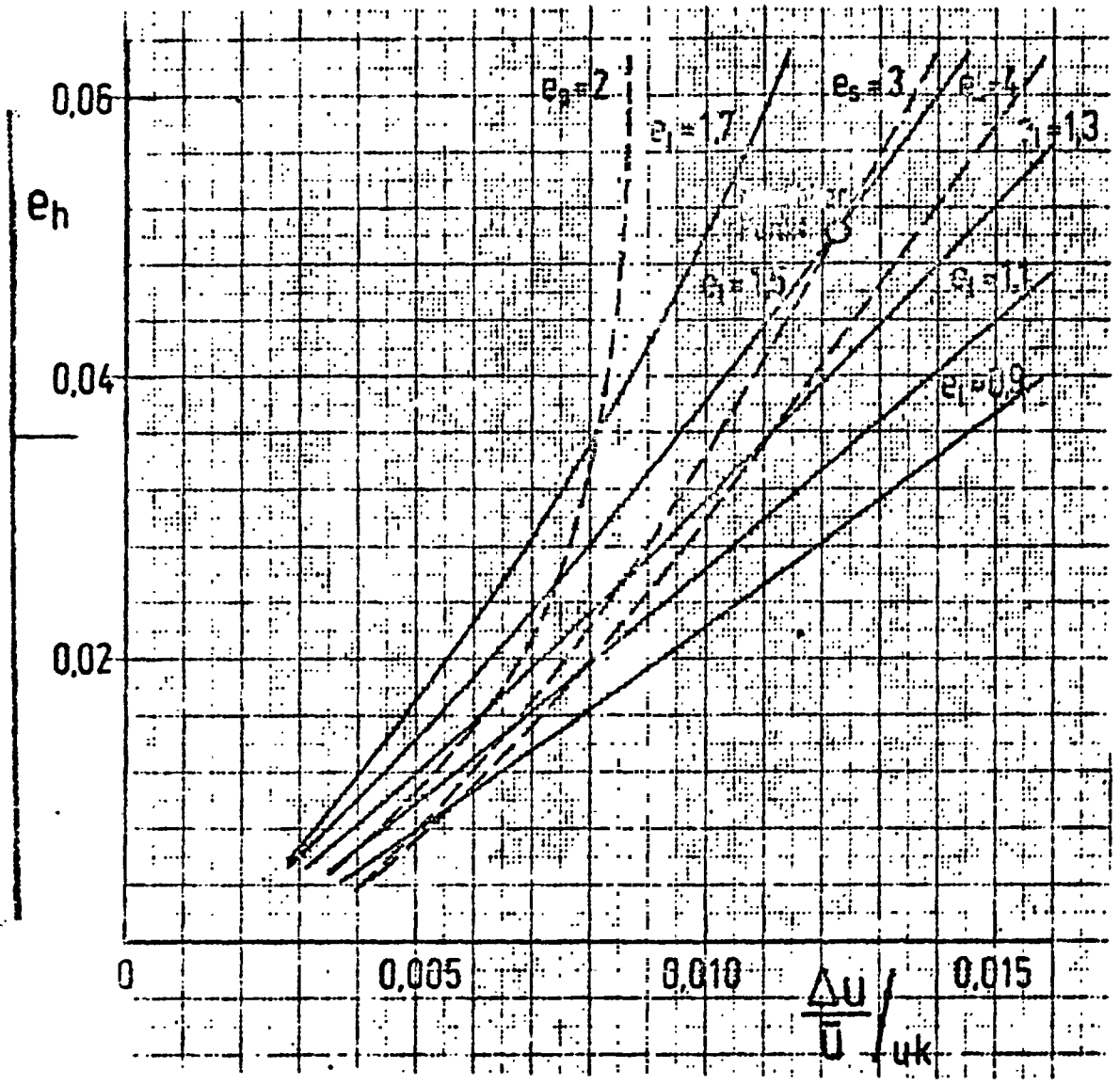

Fig. 12 e: (2-dim)

Linie e_s = Const. and

e_l = Const. in

e_h, $\frac{\Delta u}{u}\Big|_{uk}$-Diagram

/120

Fig.12e

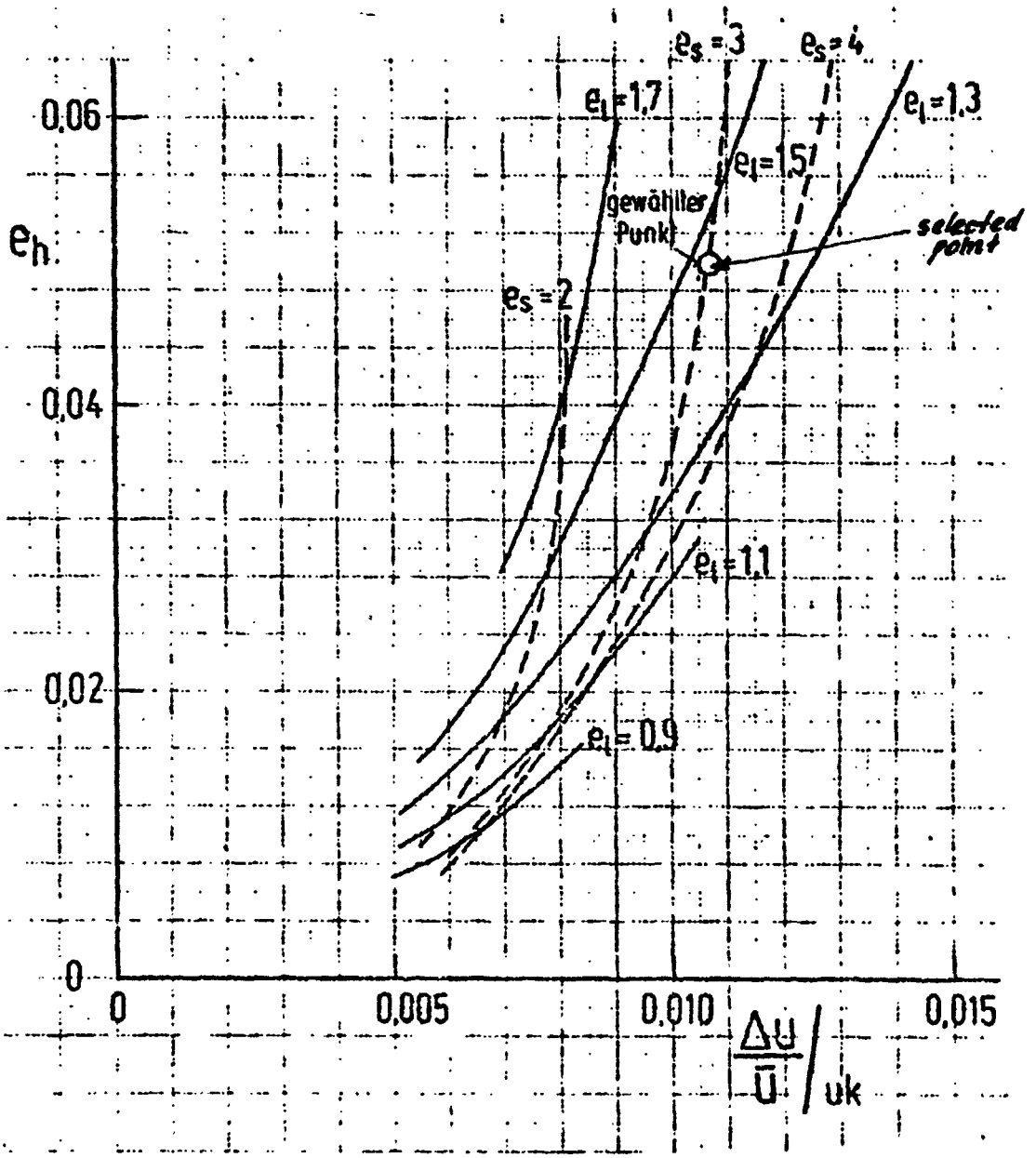

Fig. 12 r: (axi- symmetrical)

Linie e_s = Const. and e_l = Const. in e_h,

$\frac{\Delta u}{\bar{u}}\Big|_{uk}$-Diagram

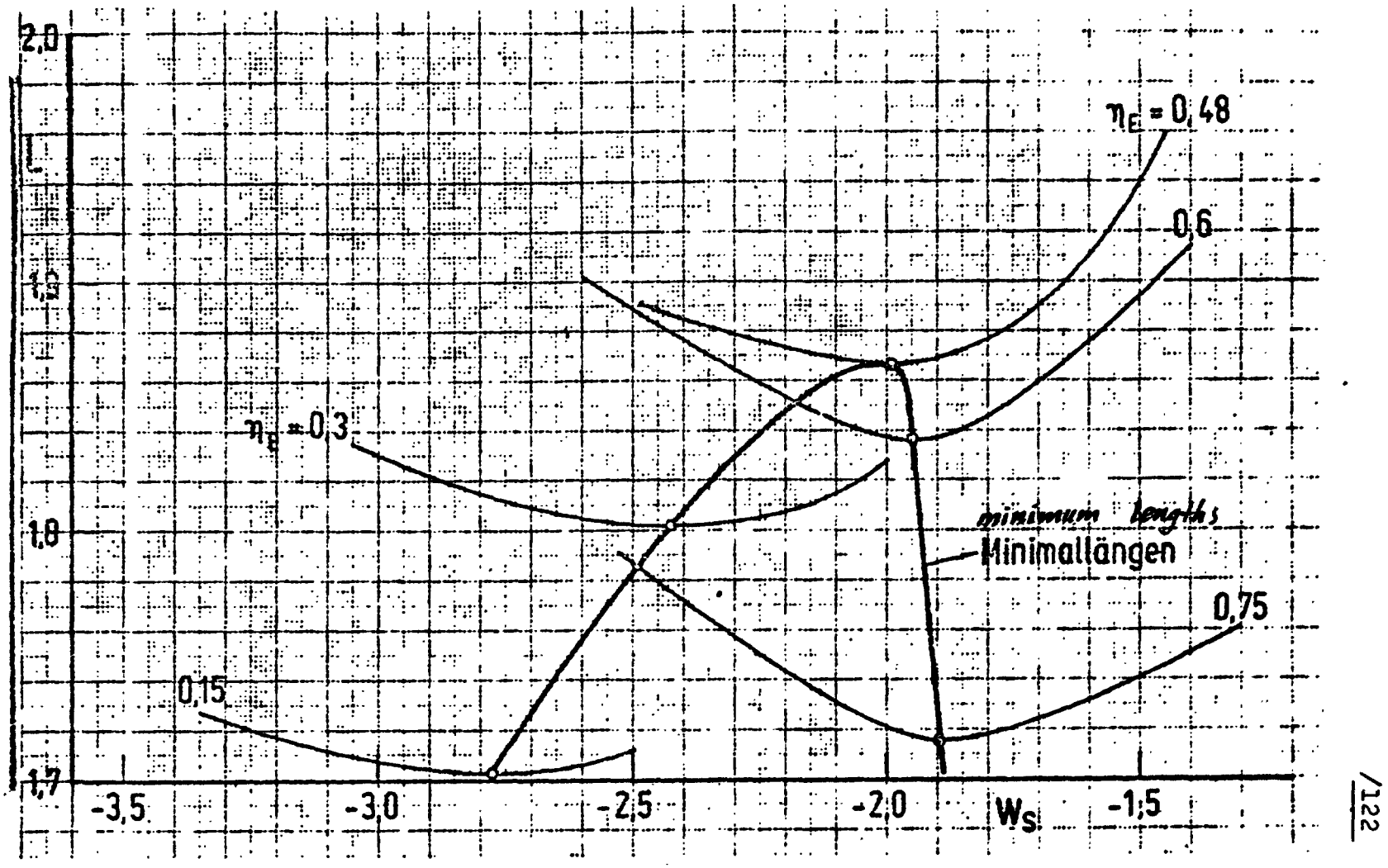

/122

Fig.13e (Two dimensional) Lines η_E = constant in $L(w_s)$ diagram

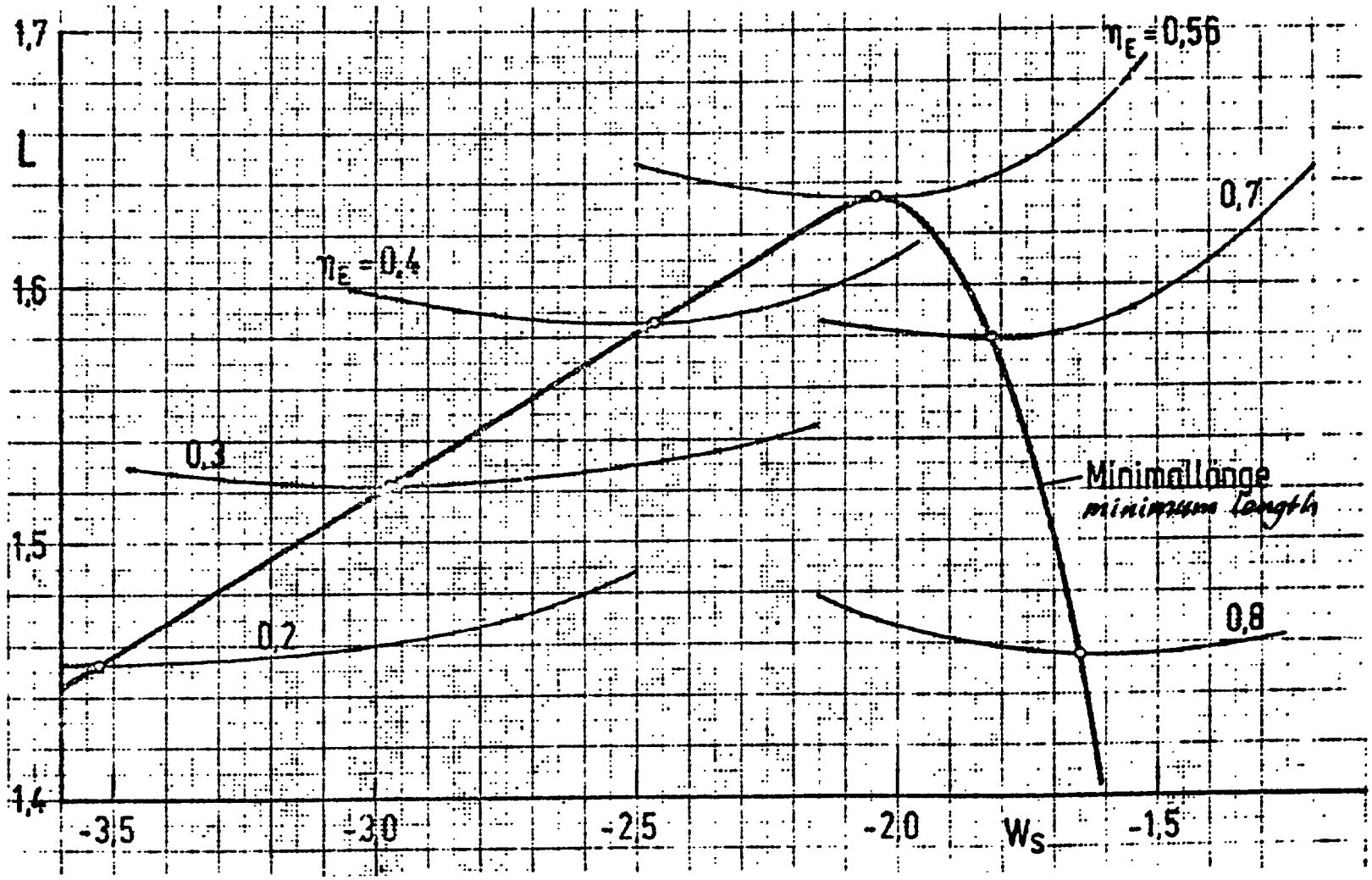

Fig.13r (Axi-symmetrical) Lines η_E = constant in $L(w_s)$ diagram

/123

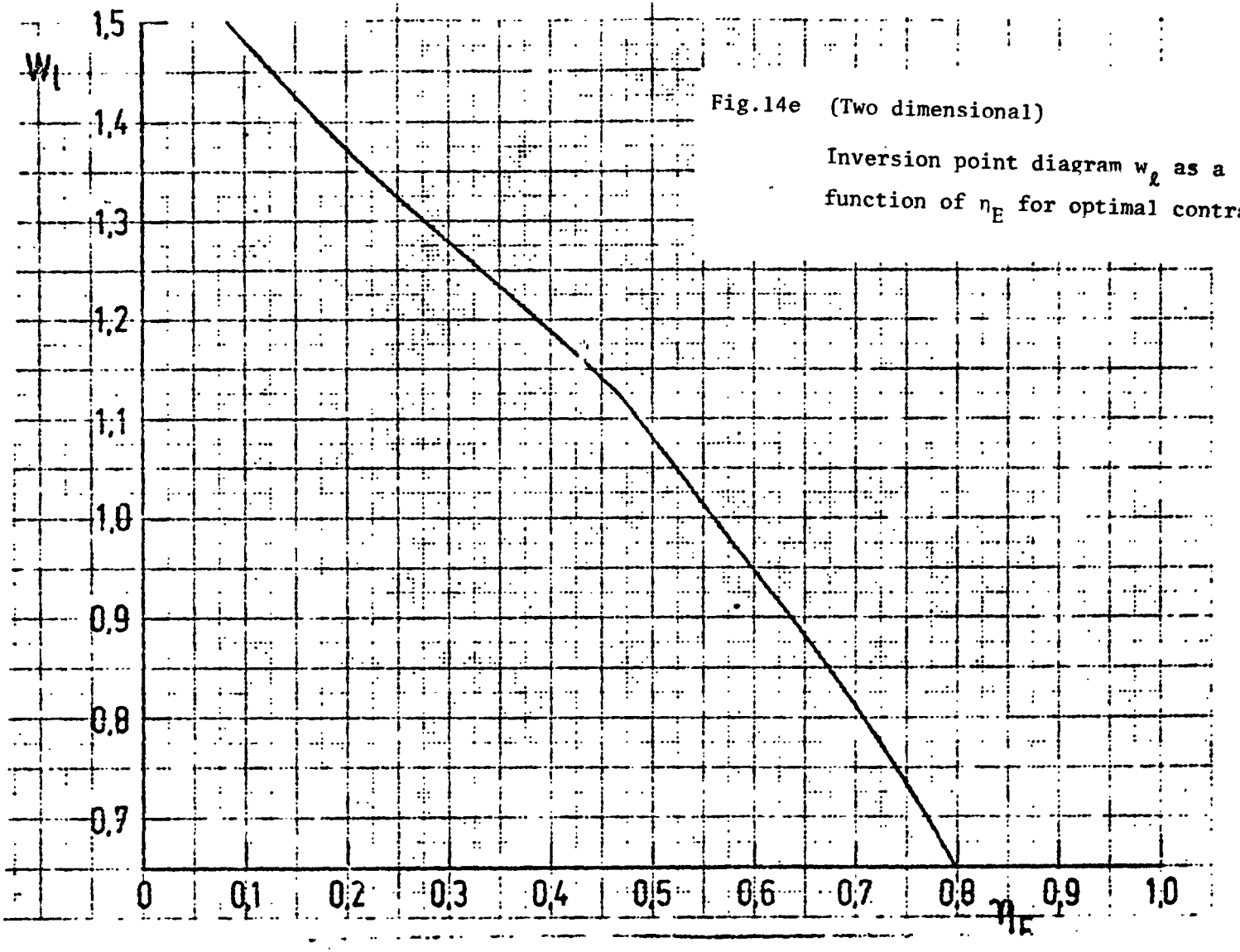

Fig.14e (Two dimensional)

Inversion point diagram w_ℓ as a function of η_E for optimal contractions

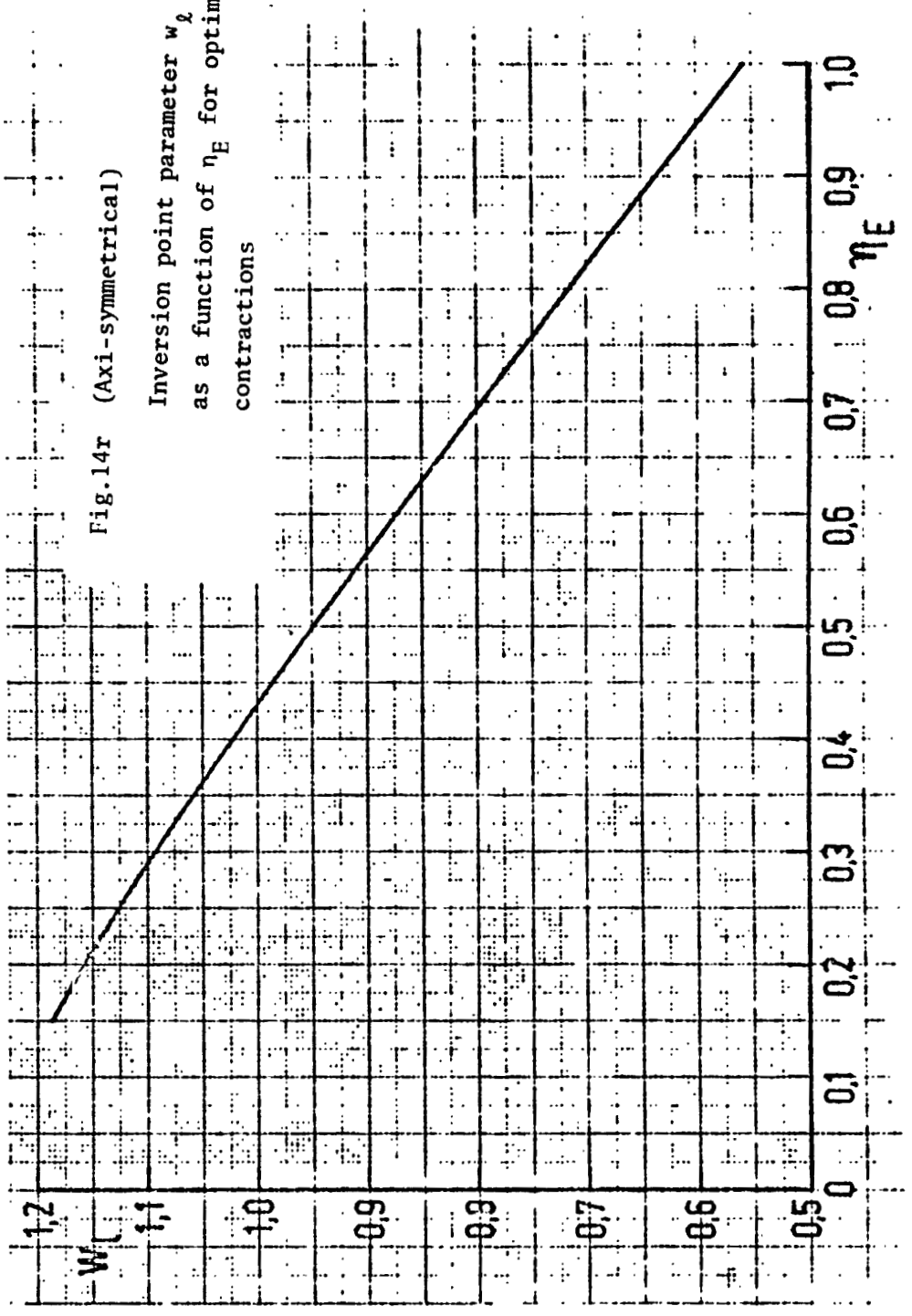

Fig.14r (Axi-symmetrical)

Inversion point parameter w_ℓ as a function of η_E for optimal contractions

/126

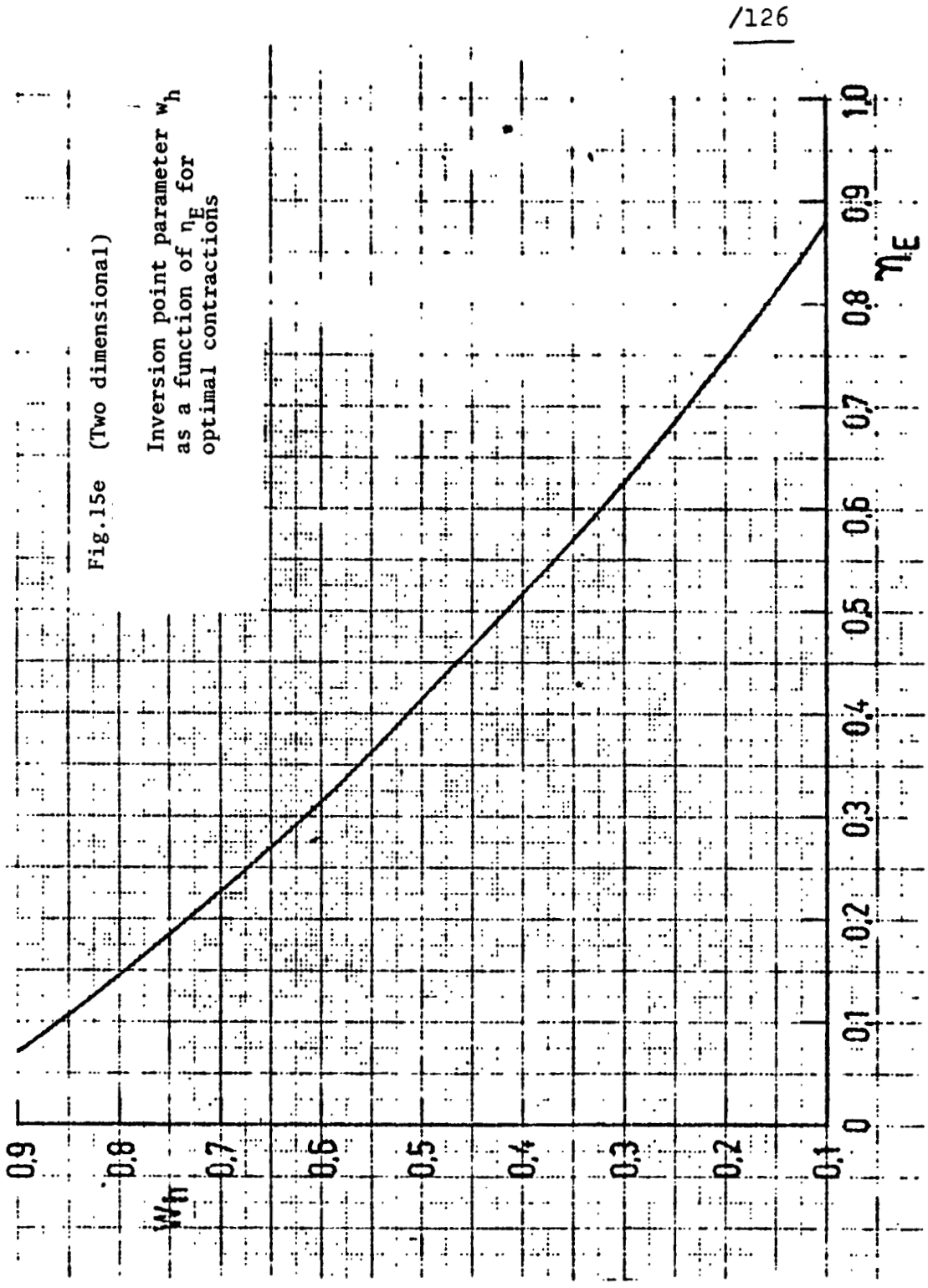

Fig.15e (Two dimensional)

Inversion point parameter w_h as a function of η_E for optimal contractions

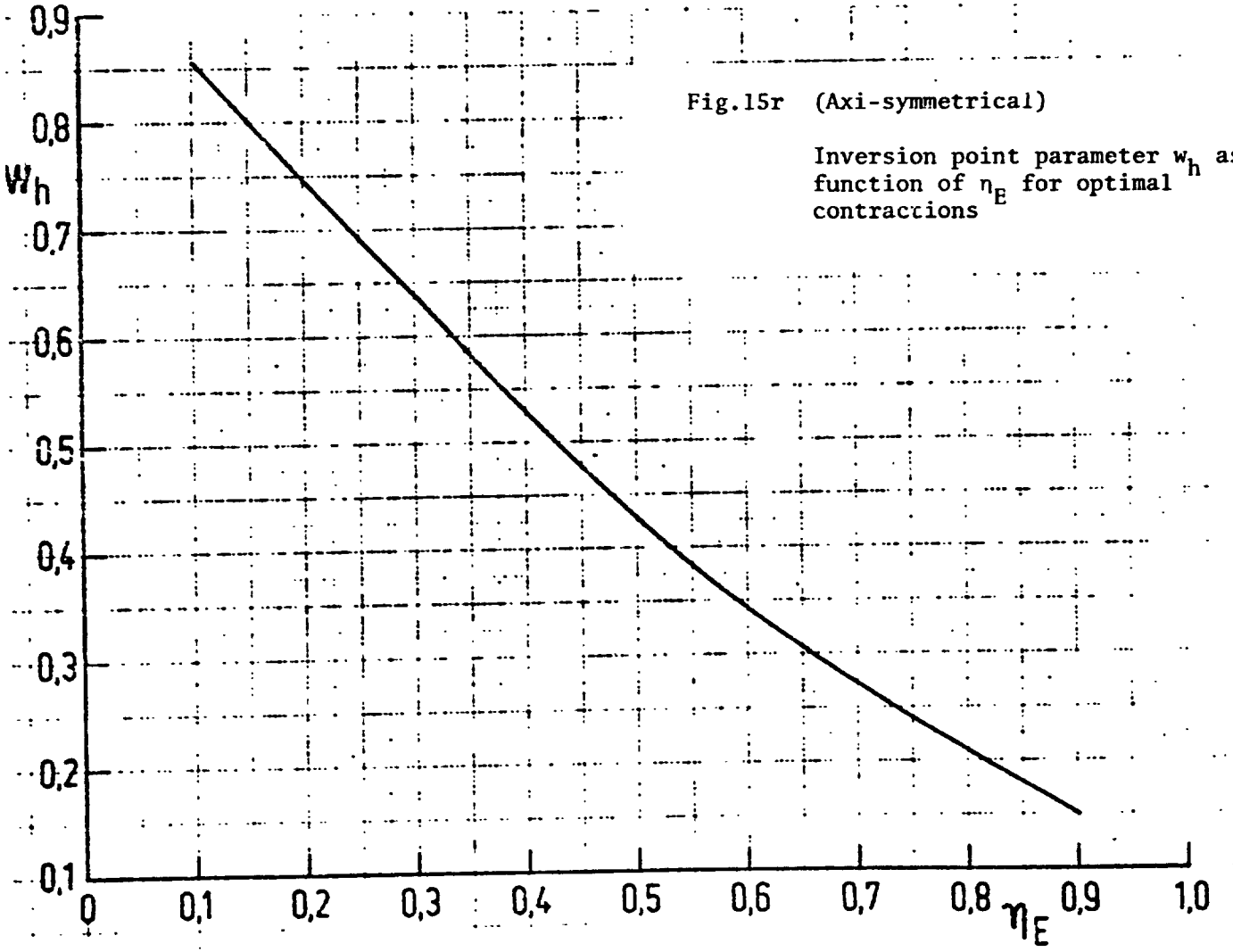

Fig.15r (Axi-symmetrical)

Inversion point parameter w_h as a function of η_E for optimal contractions

/127

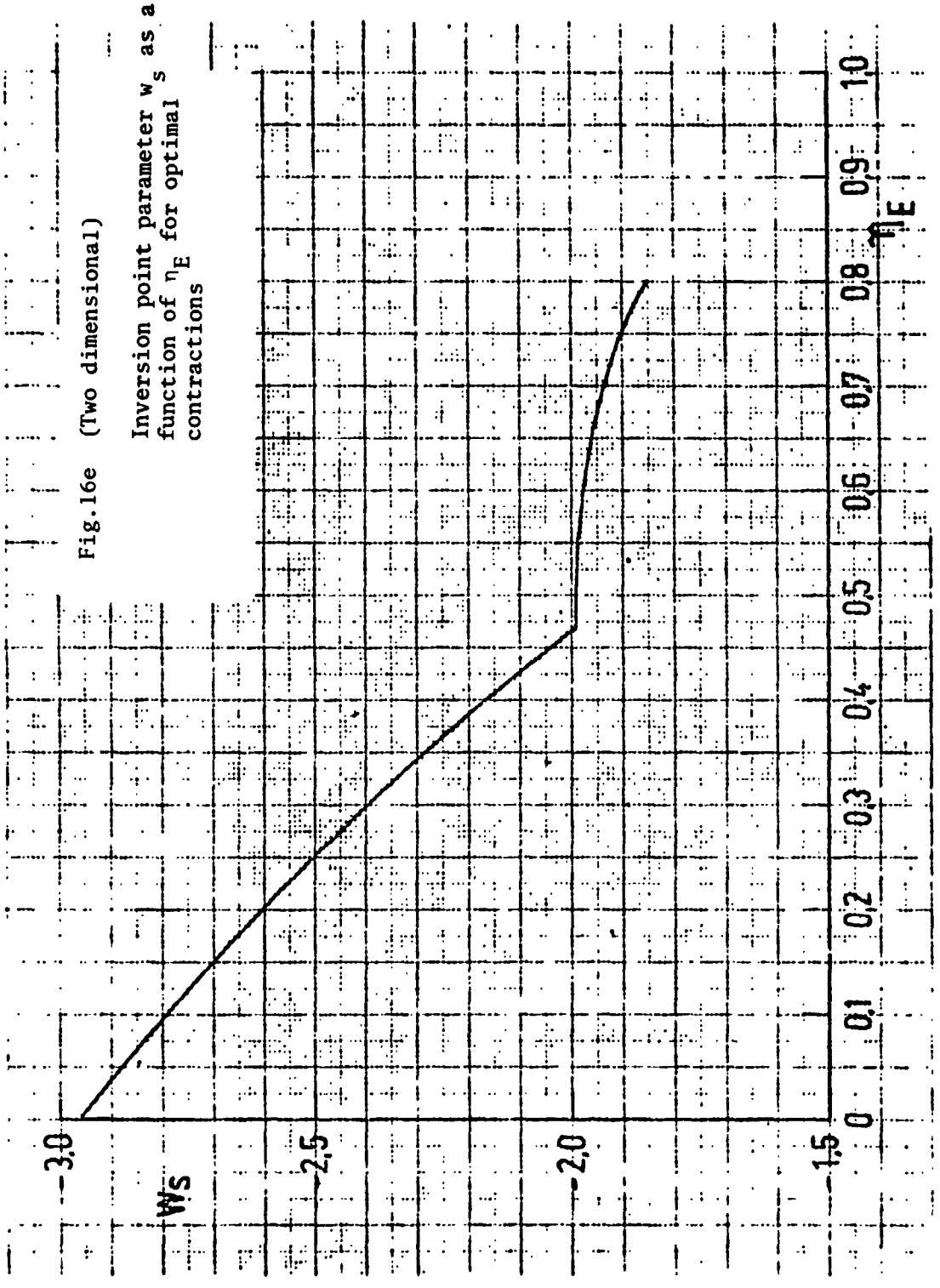

Fig.16e (Two dimensional)

Inversion point parameter w_s as a function of η_E for optimal contractions

/129

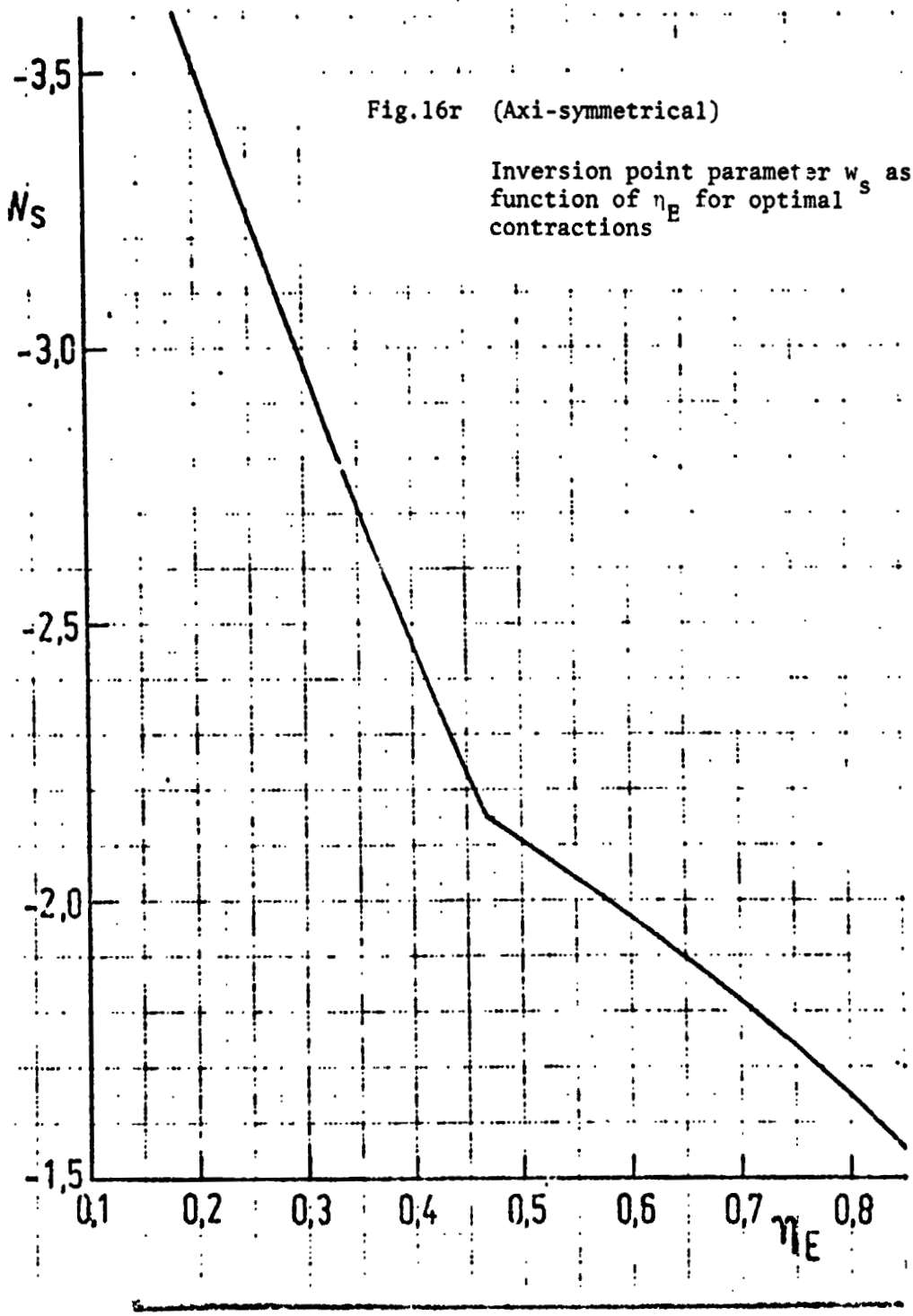

Fig.16r (Axi-symmetrical)

Inversion point parameter w_s as a function of η_E for optimal contractions

/130

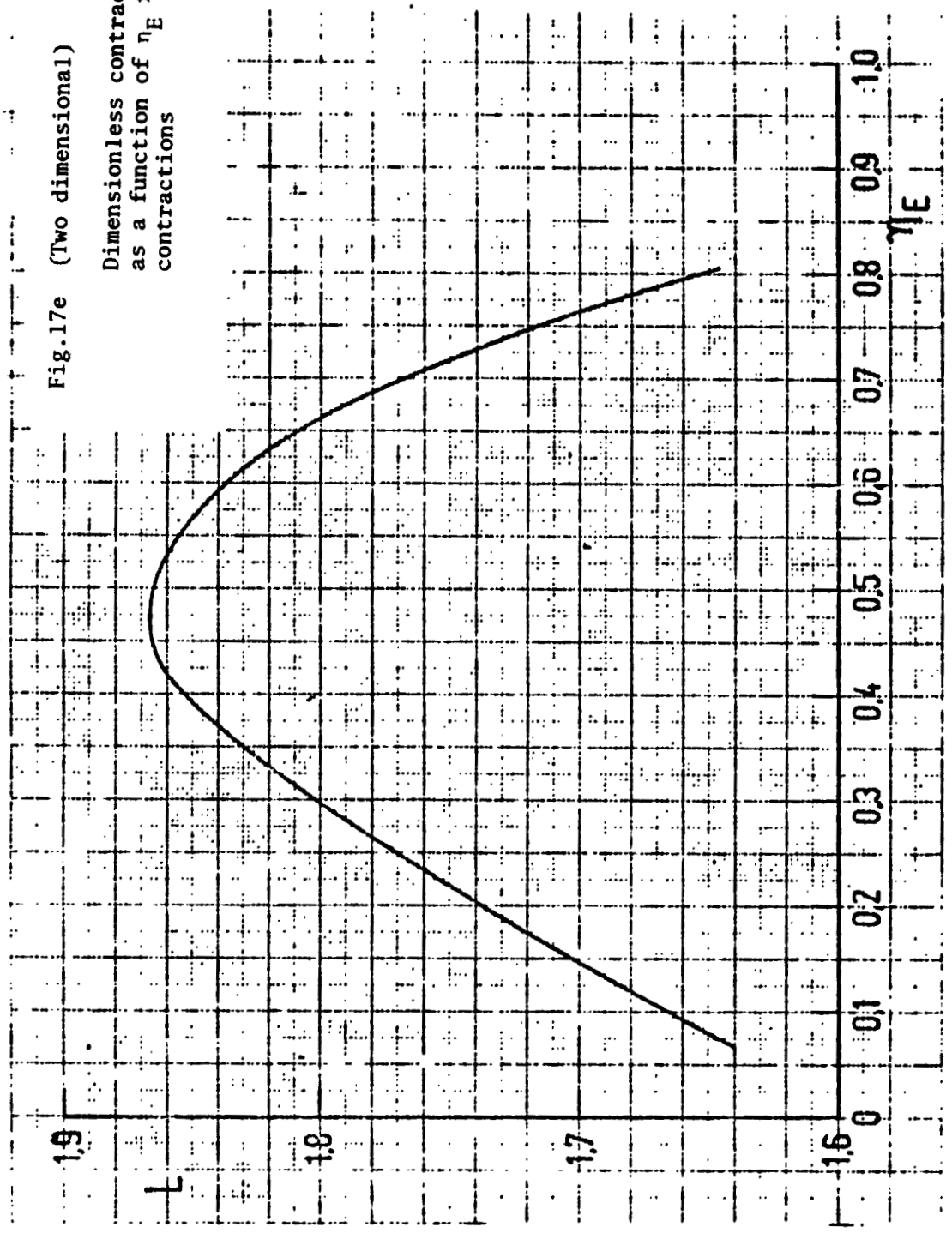

Fig.17e (Two dimensional)

Dimensionless contraction length L as a function of η_E for optimal contractions

/131

Fig.17r (Axi-symmetrical)

Dimensionless expansion lenght L as a function of η_E for optimal contractions.

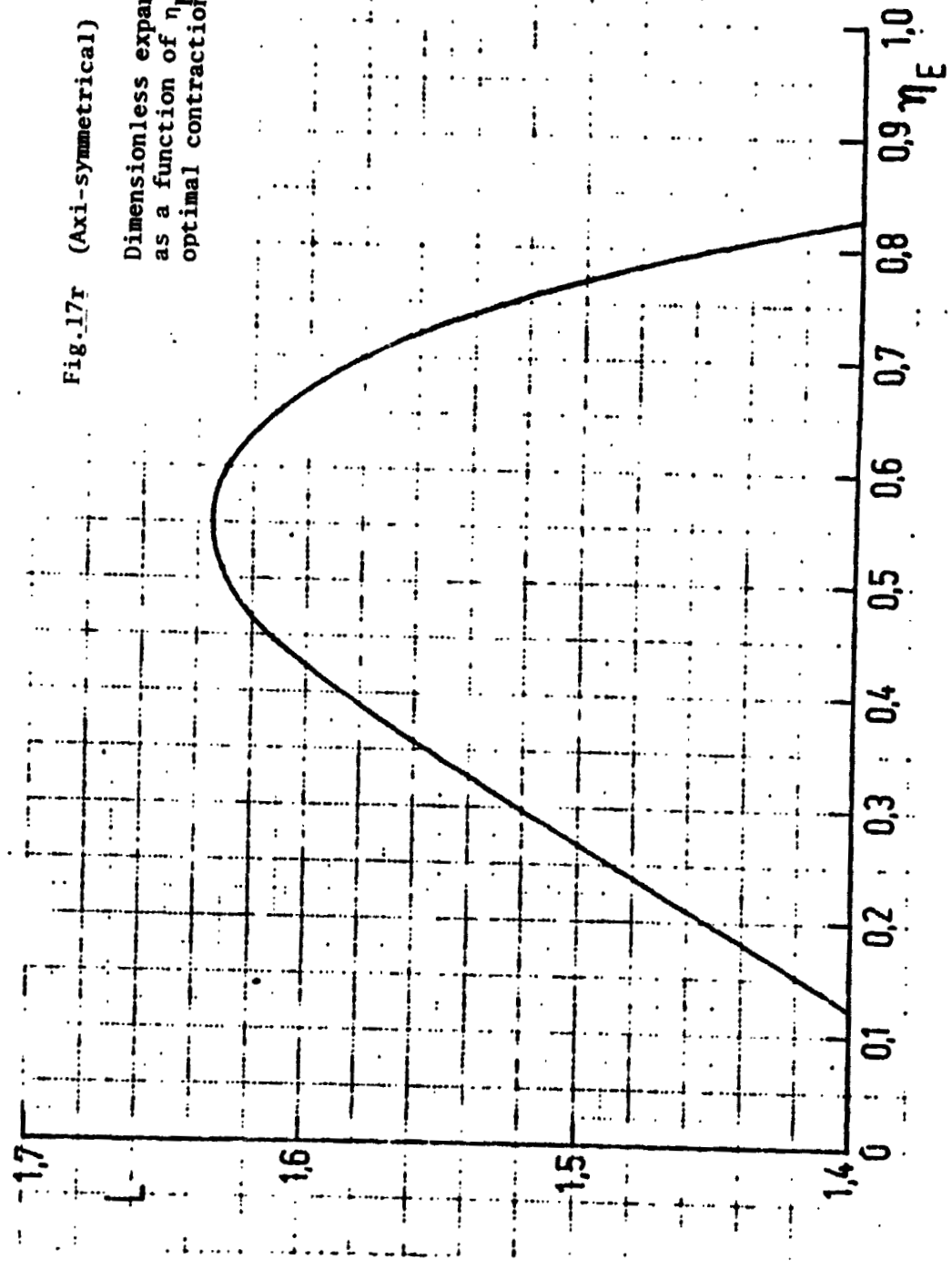

/132

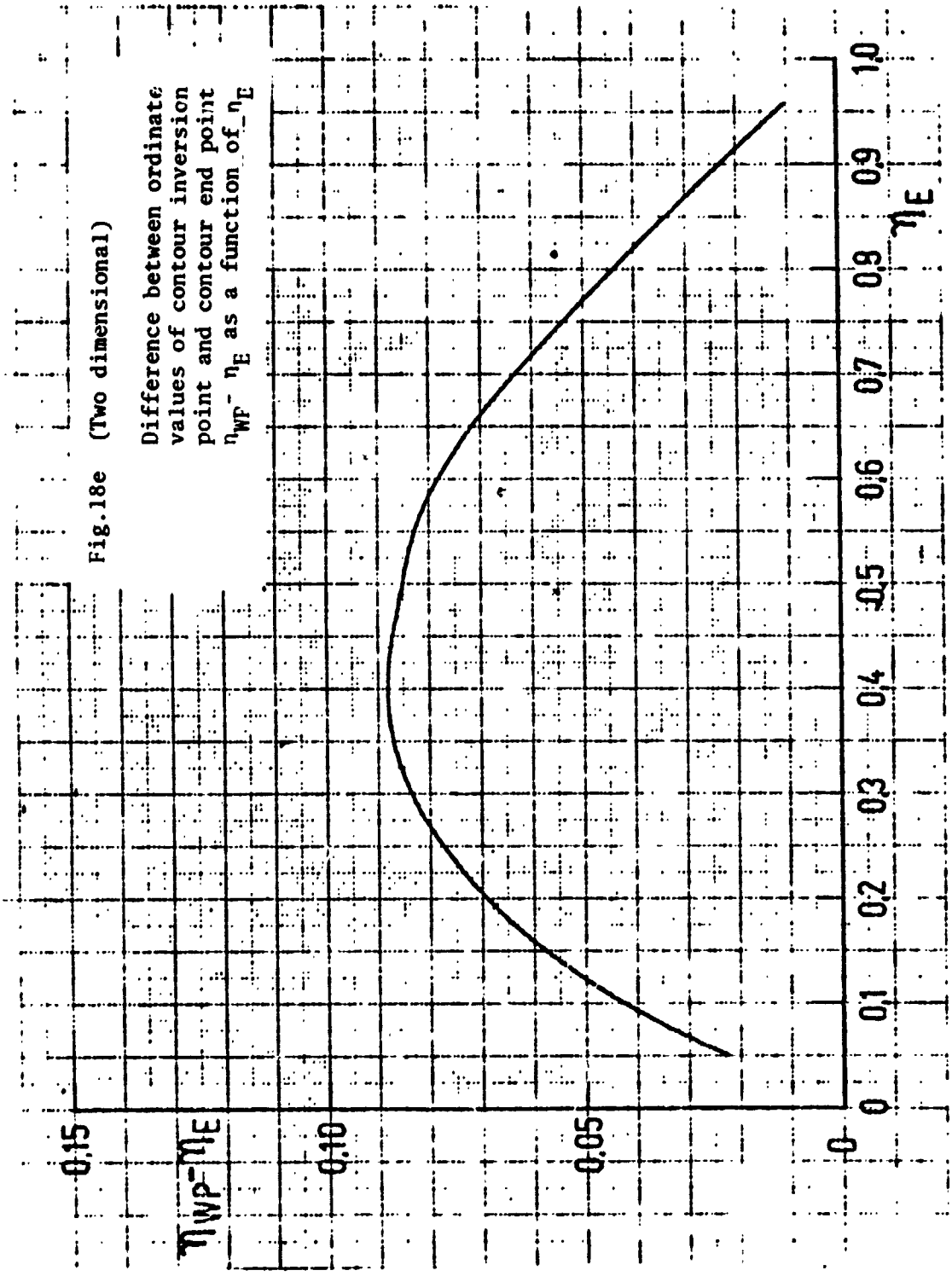

Fig.18e (Two dimensional)

Difference between ordinate values of contour inversion point and contour end point $\eta_{WF} - \eta_E$ as a function of η_E

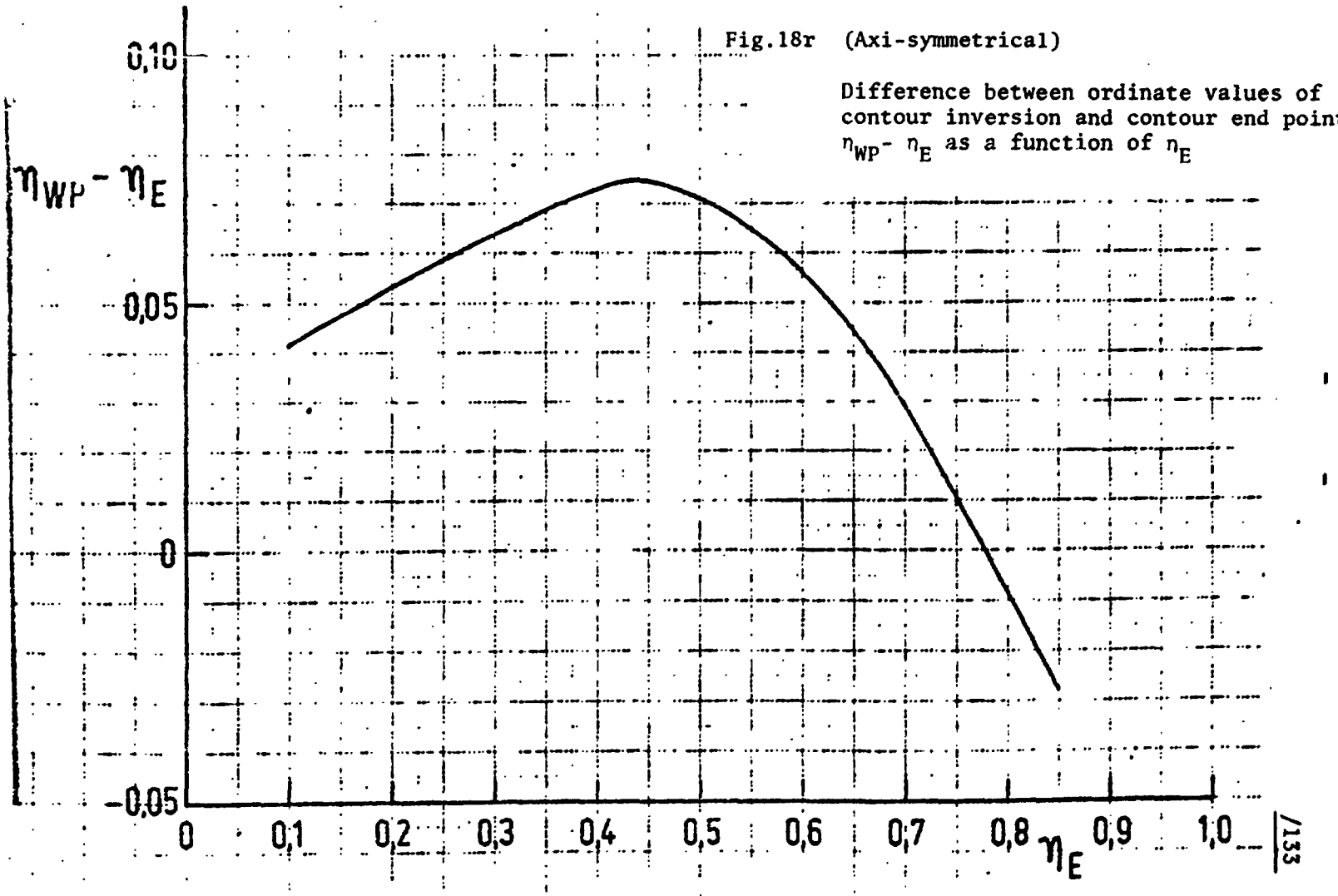

Fig.18r (Axi-symmetrical)

Difference between ordinate values of contour inversion and contour end point $\eta_{WP} - \eta_E$ as a function of η_E

/133

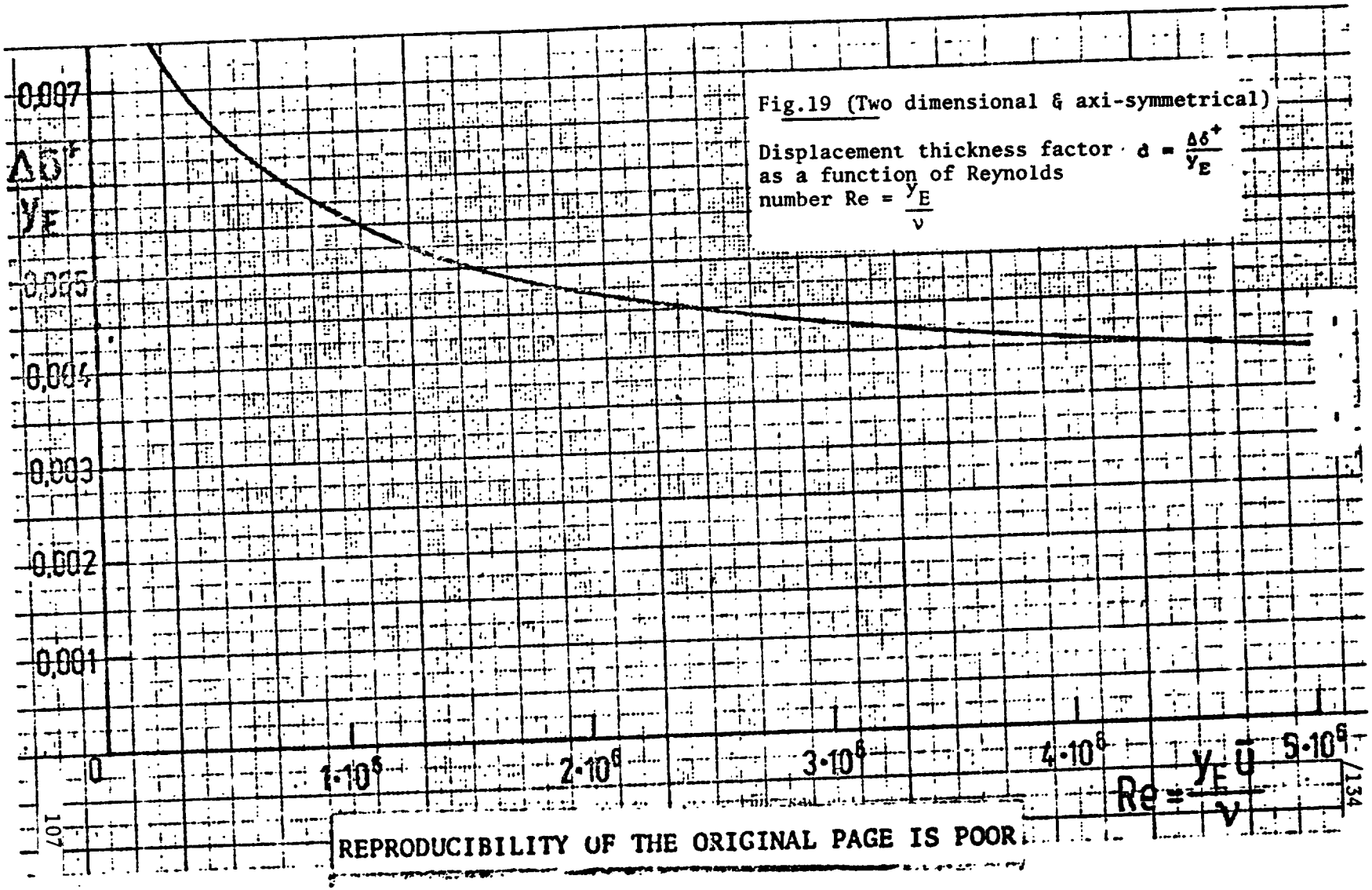

Fig.19 (Two dimensional & axi-symmetrical)

Displacement thickness factor $d = \frac{\Delta\delta^+}{y_E}$ as a function of Reynolds number $Re = \frac{y_E}{\nu}$

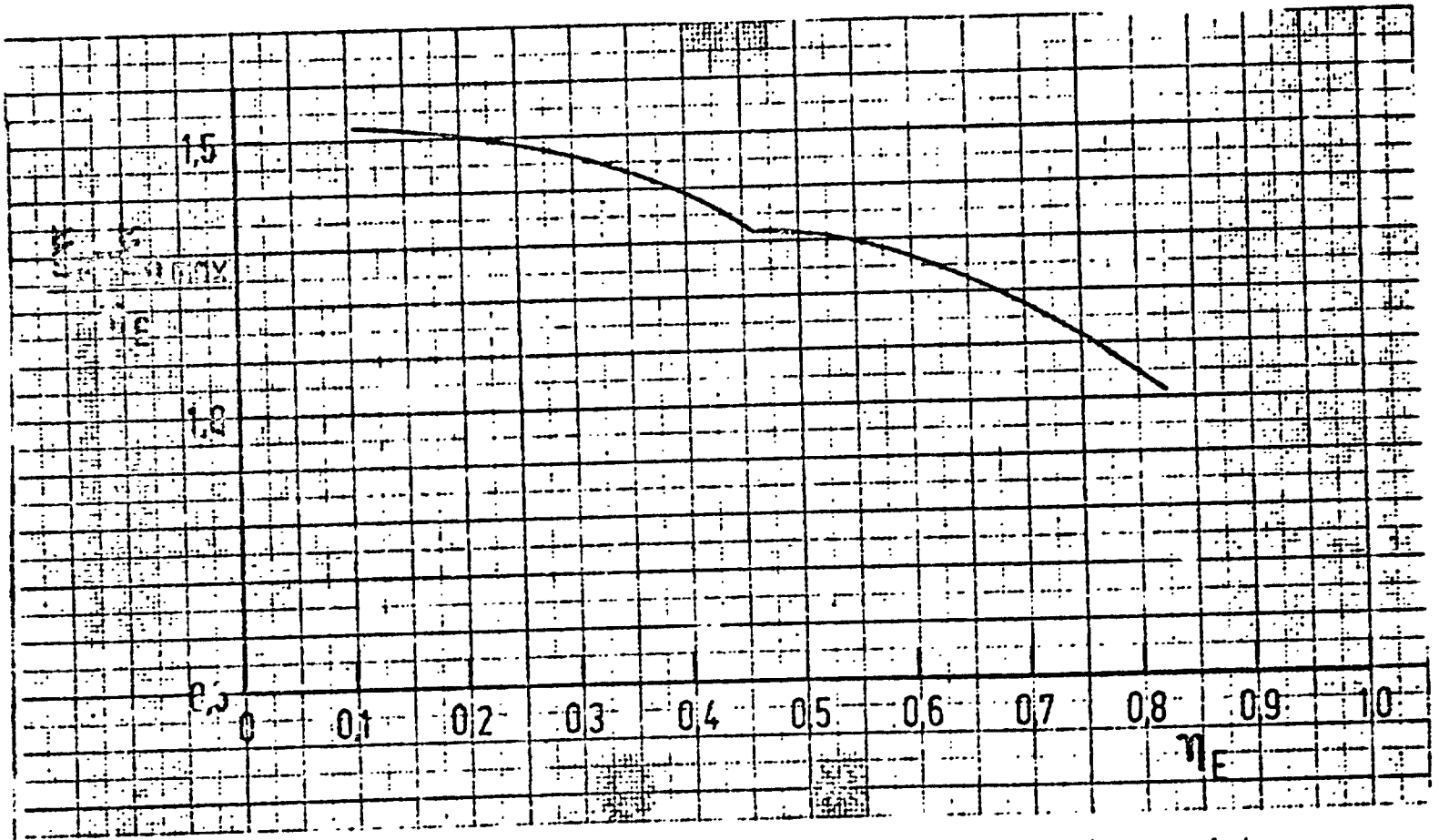

Fig.20e (Two dimensional) Distance between the contour point of maximum velocity and the countour end point $\frac{\xi_E - \xi_{u_{max}}}{\eta}$ as a function of η_E

/135

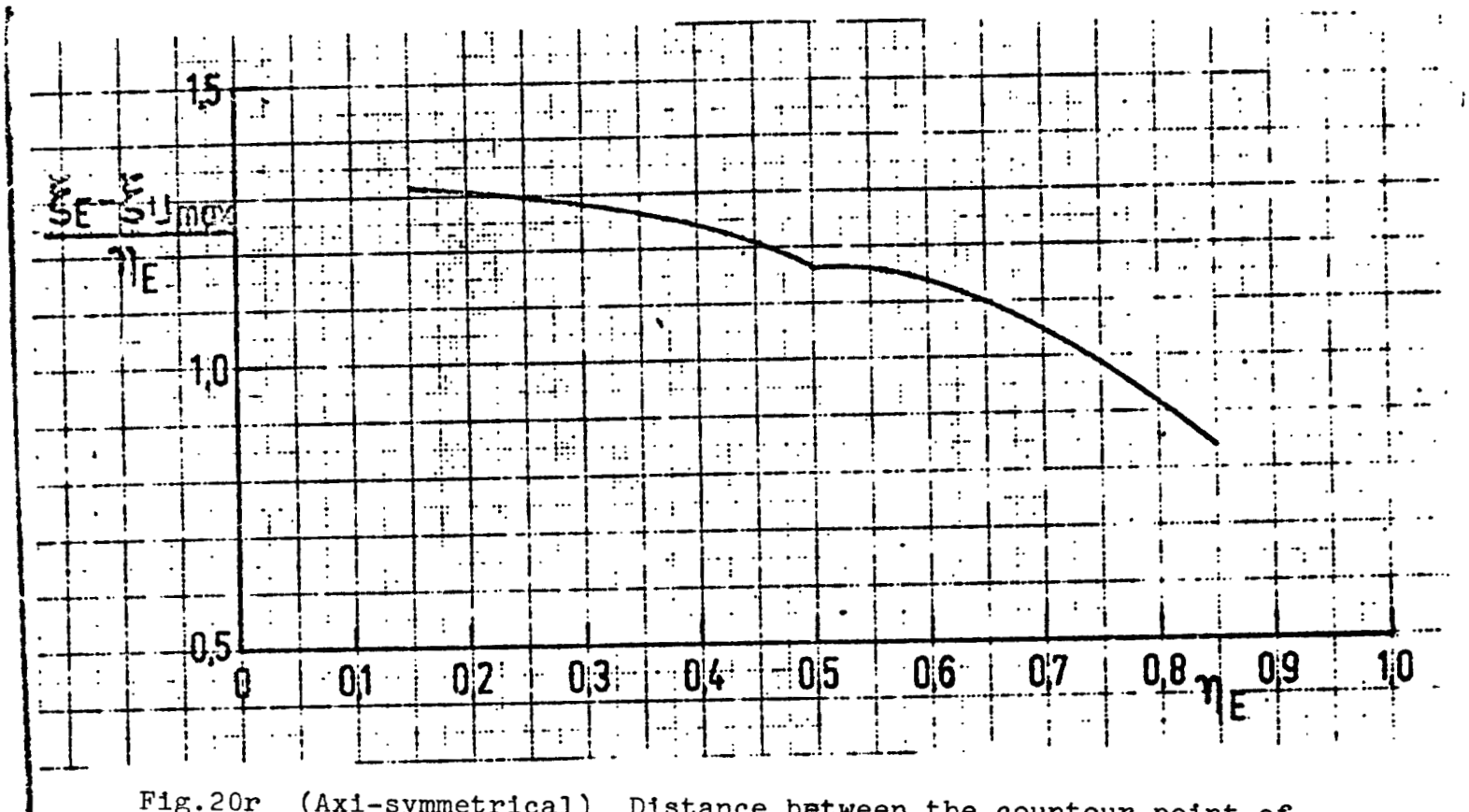

Fig.20r (Axi-symmetrical) Distance between the countour point of maximum velocity and the contour end point $\frac{\xi_E - \xi_{u_{max}}}{\eta_E}$ as a function of η_E

/136

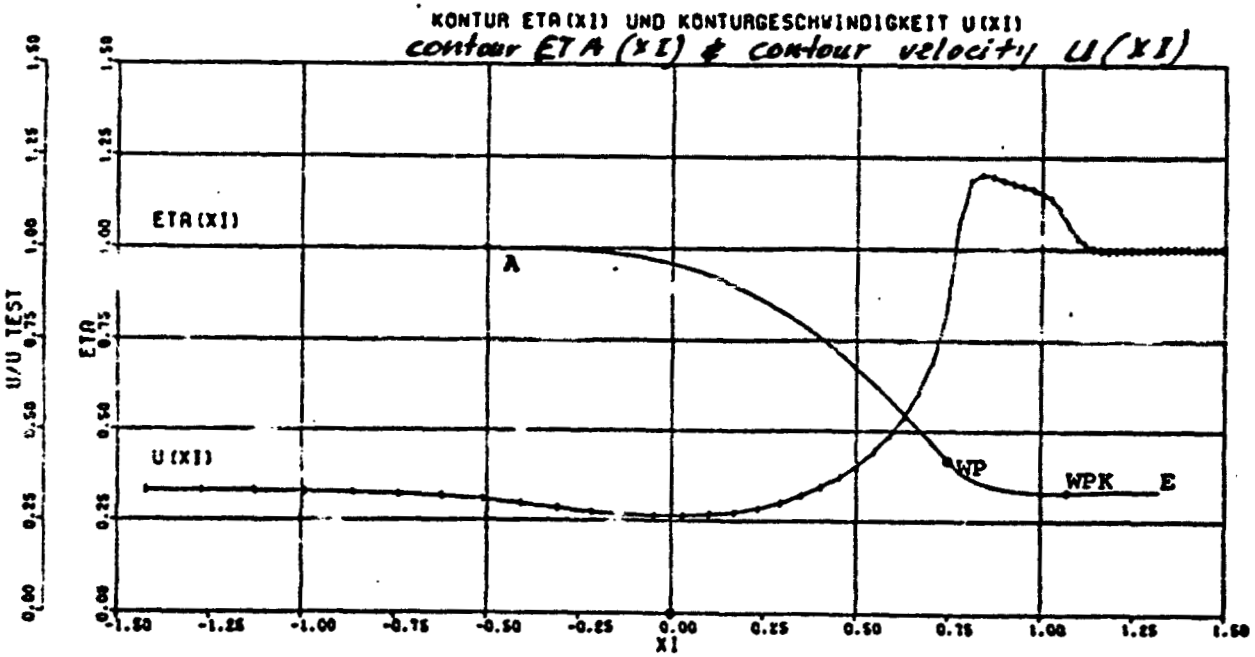

Fig.21 Plotter drawing for calculation of a two dimensional contraction flow without boundary layer compensation

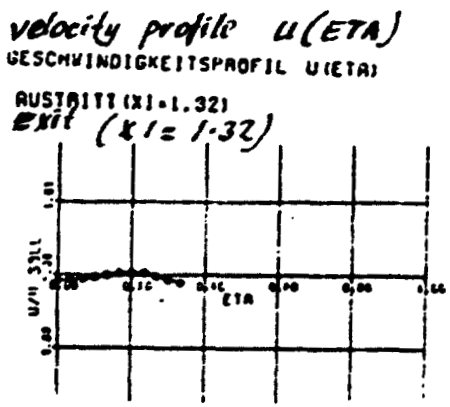

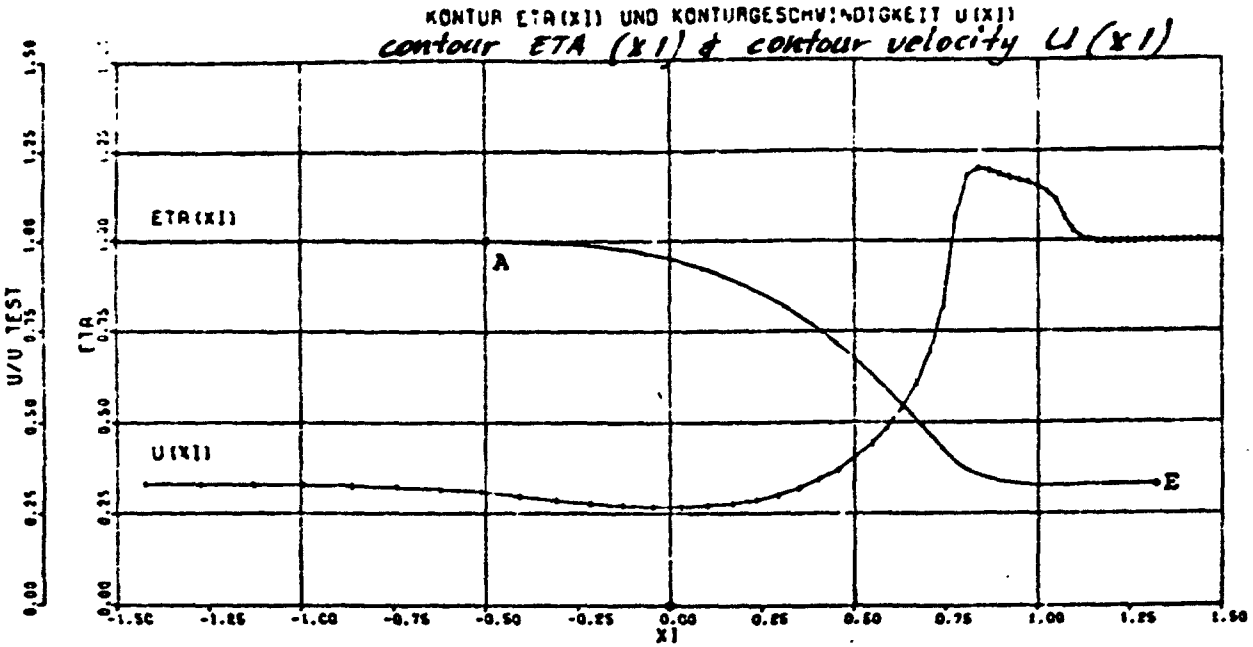

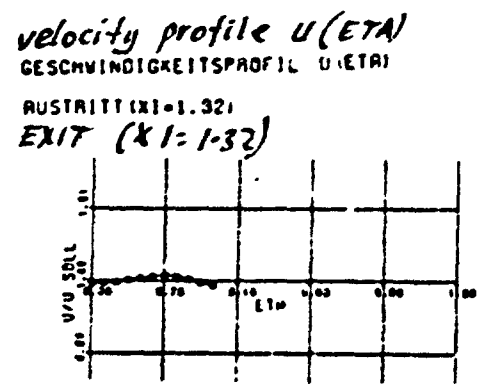

Fig.22 Plotter drawing to calculate the contraction flow of Fig.21 with compensation for displacement effects of the boundary layer

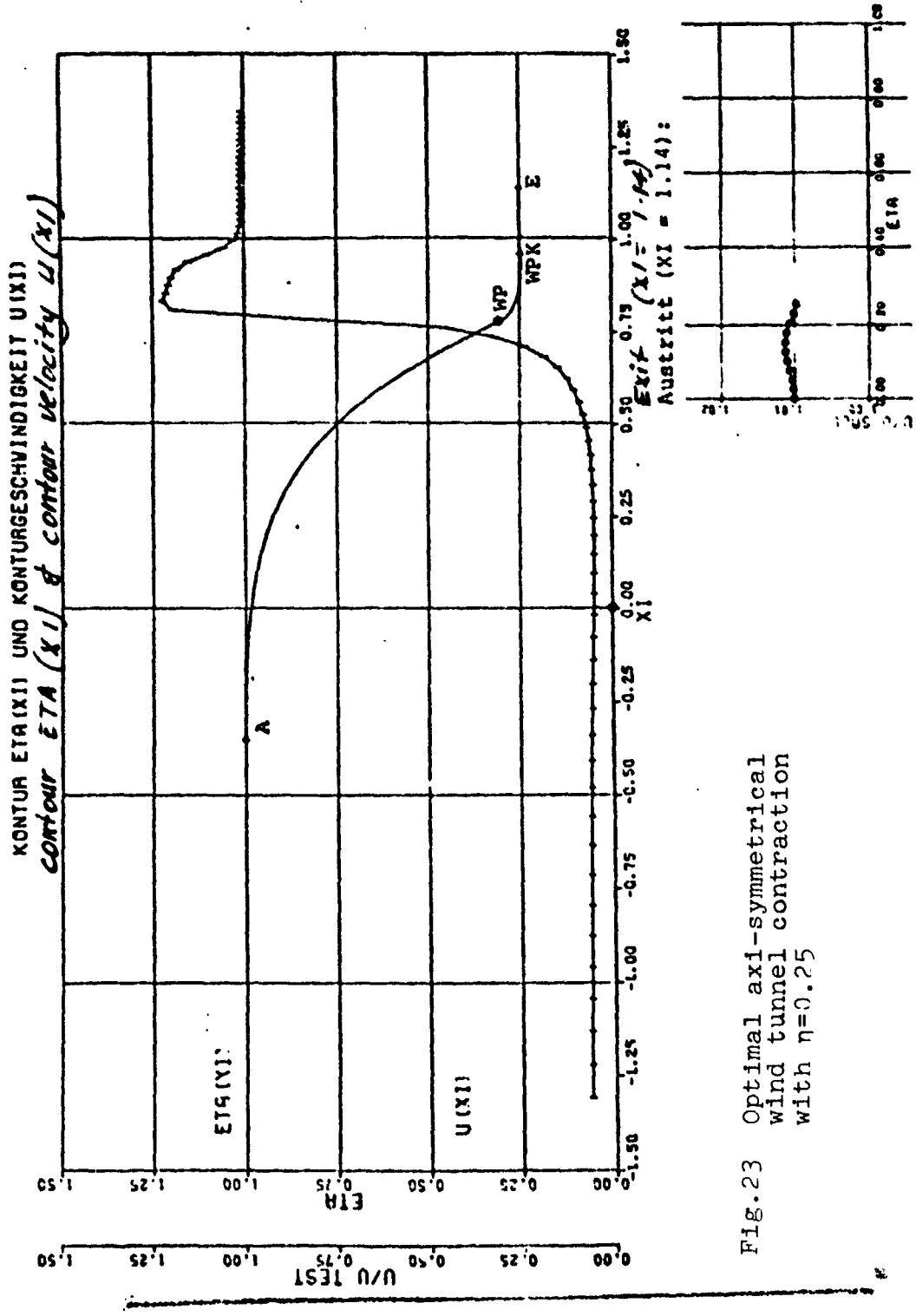

Fig.23 Optimal axi-symmetrical wind tunnel contraction with η=0.25

/140

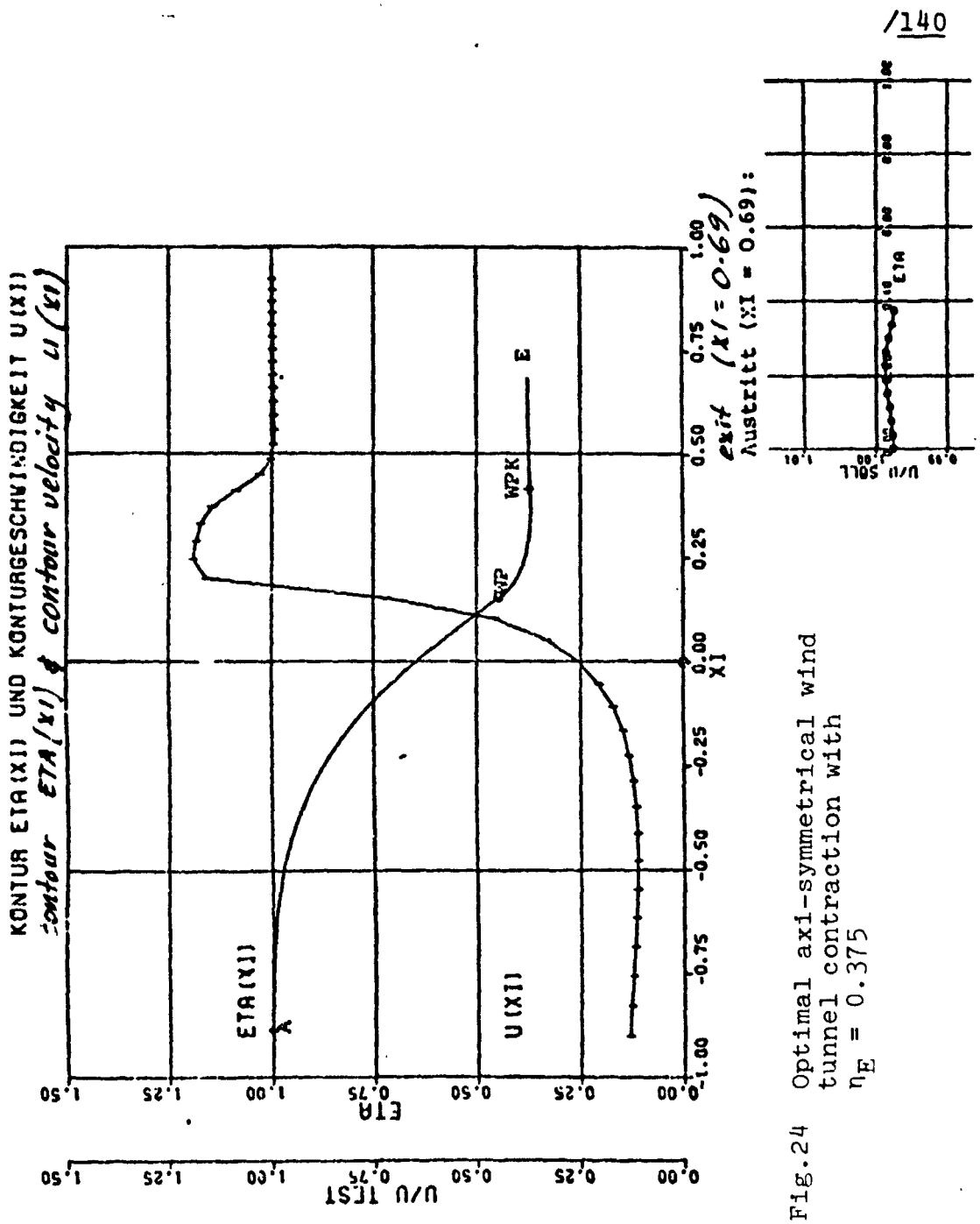

Fig.24 Optimal axi-symmetrical wind tunnel contraction with $\eta_E = 0.375$

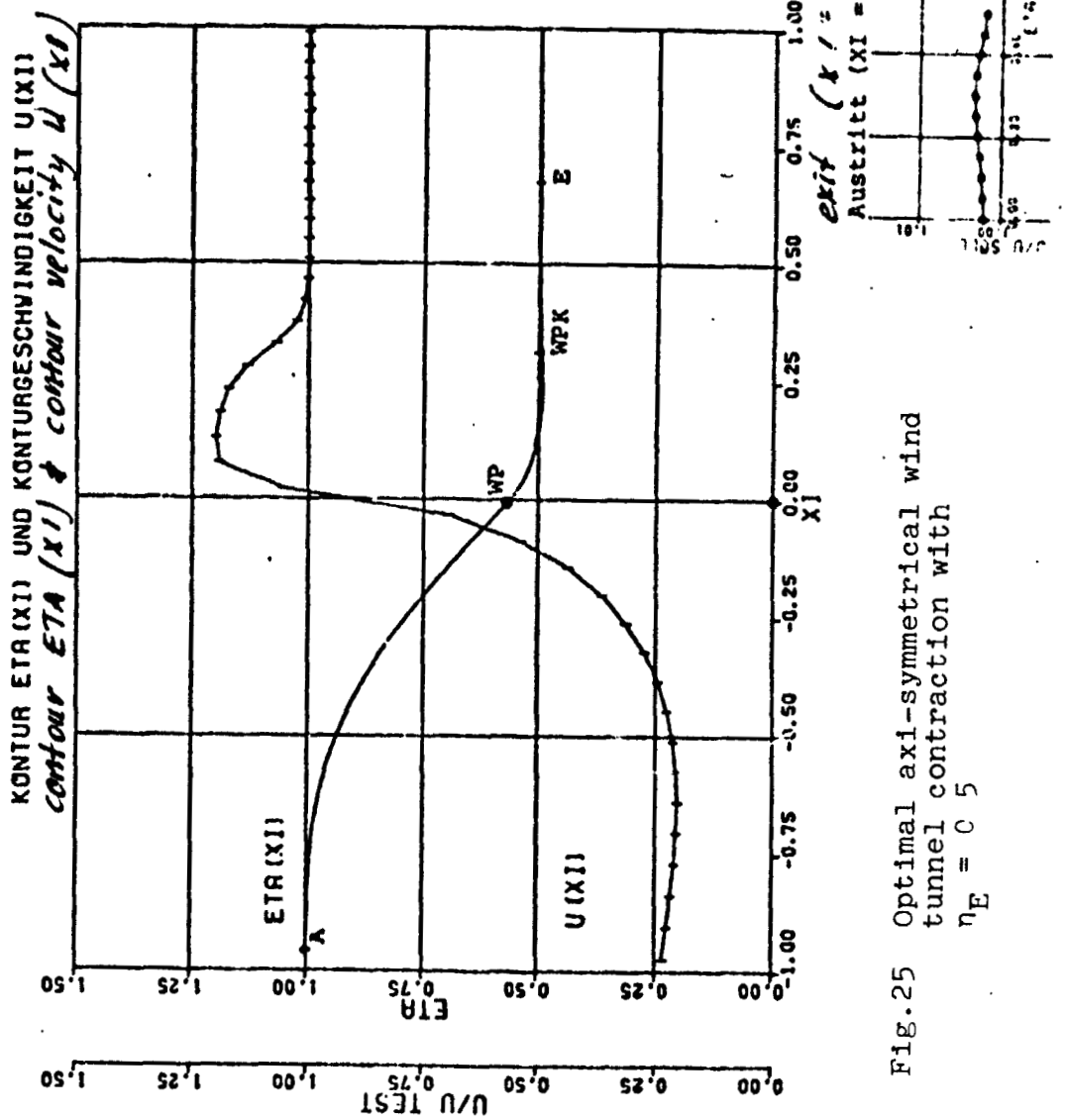

Fig.25 Optimal axi-symmetrical wind tunnel contraction with $\eta_E = 0.5$

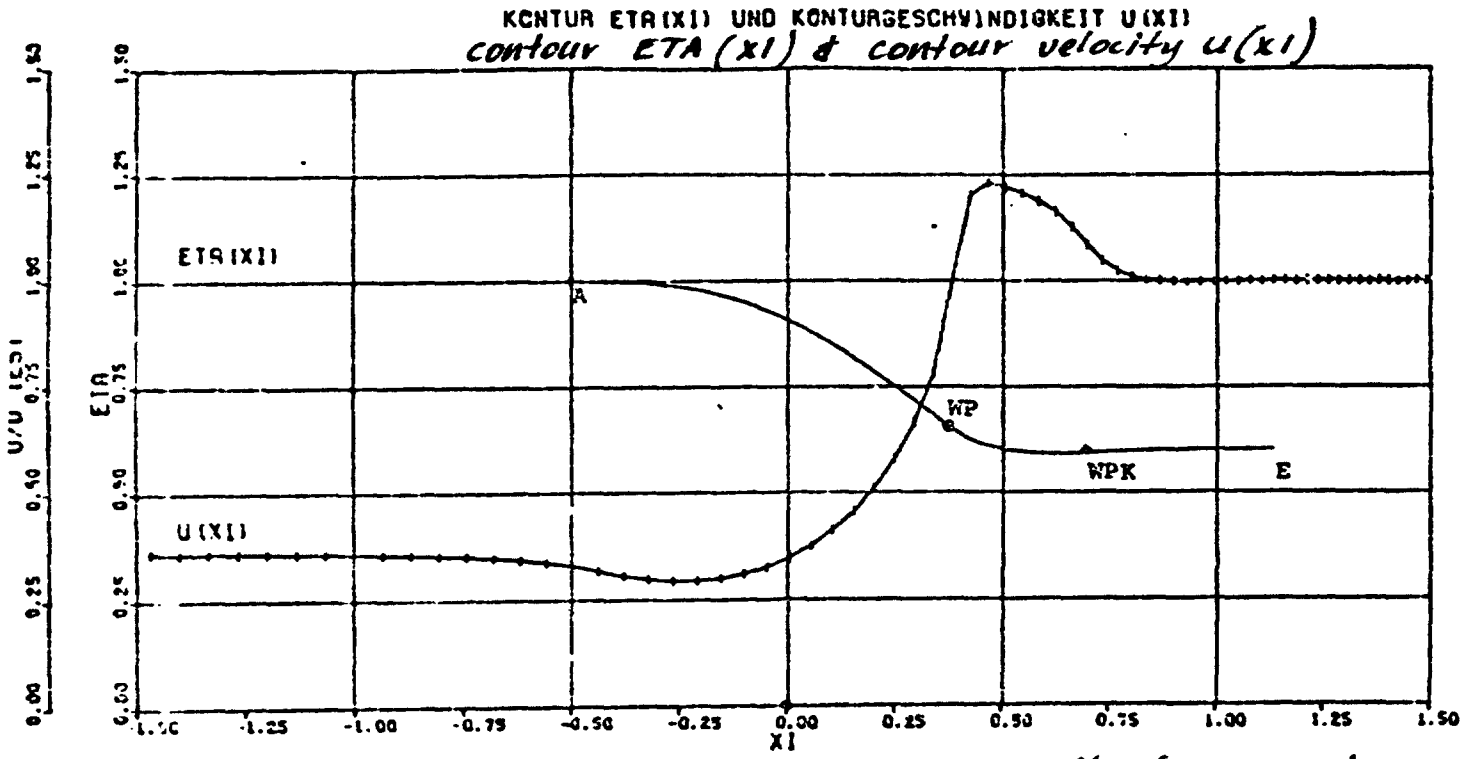

exit (X1 = 1.13)

Austritt (XI = 1.13):

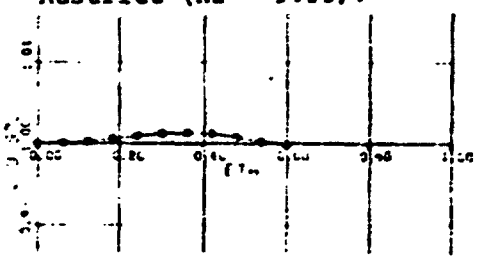

Fig.26 Optimal axi-symmetrical wind tunnel contraction with $\eta_E = 0.6$

/142

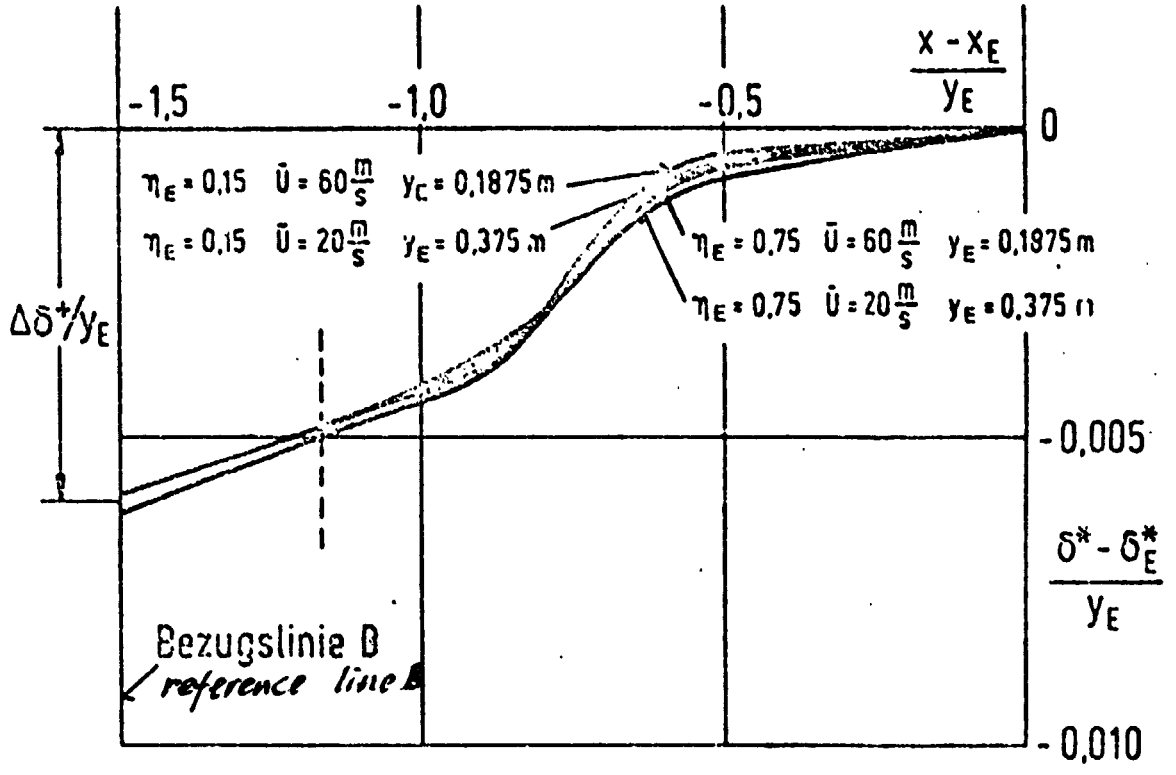

Fig.27 Curve for the displacement thicknesses of different (two dimensional) contractions in the exit zone

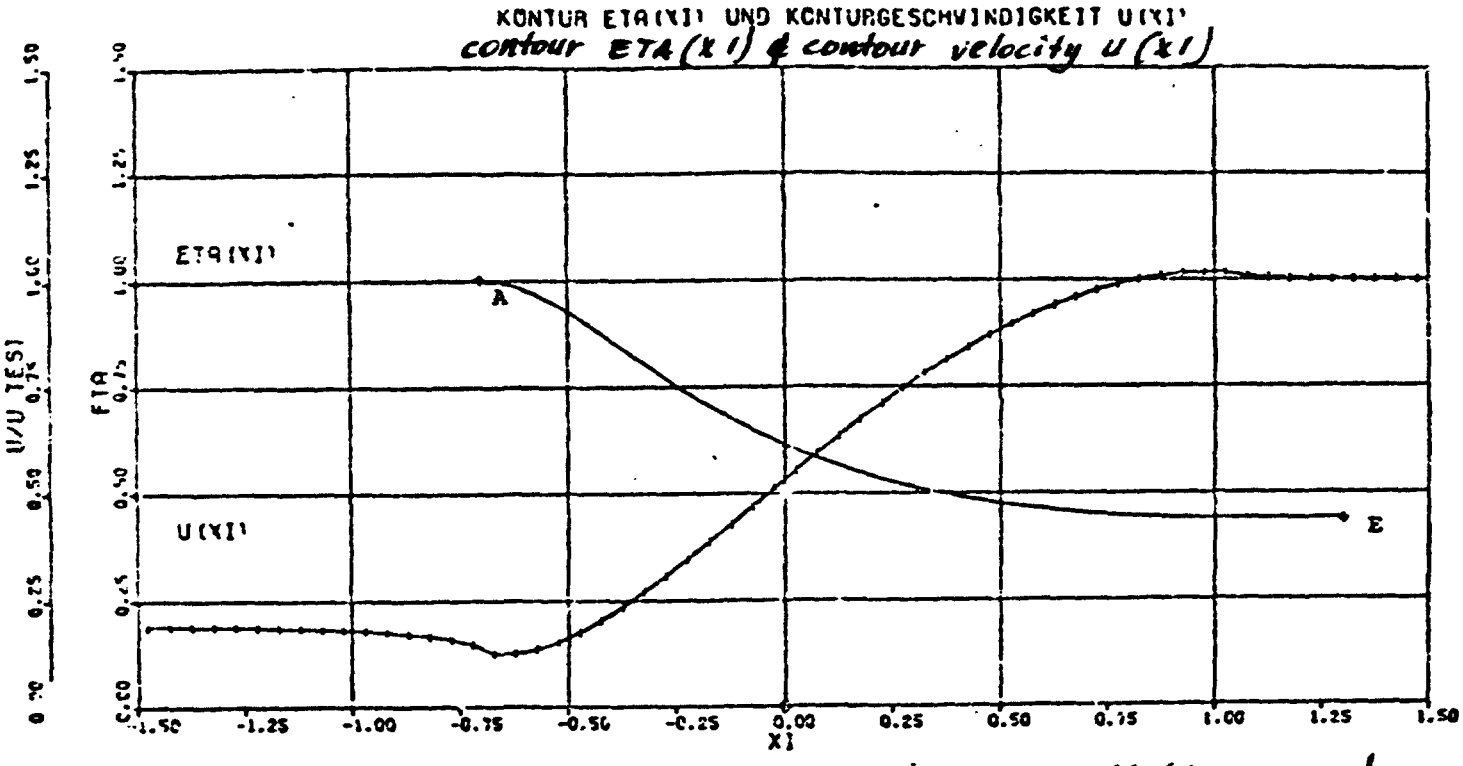

Fig.28 Axi-symmetrical wind tunnel contraction according to Witoszynski [5] with $\eta_E = 0.439$

exit (X I = 1.30)

Austritt (XI = 1.30):

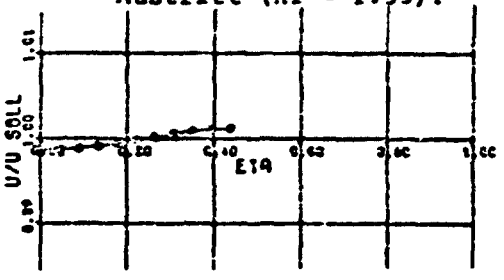

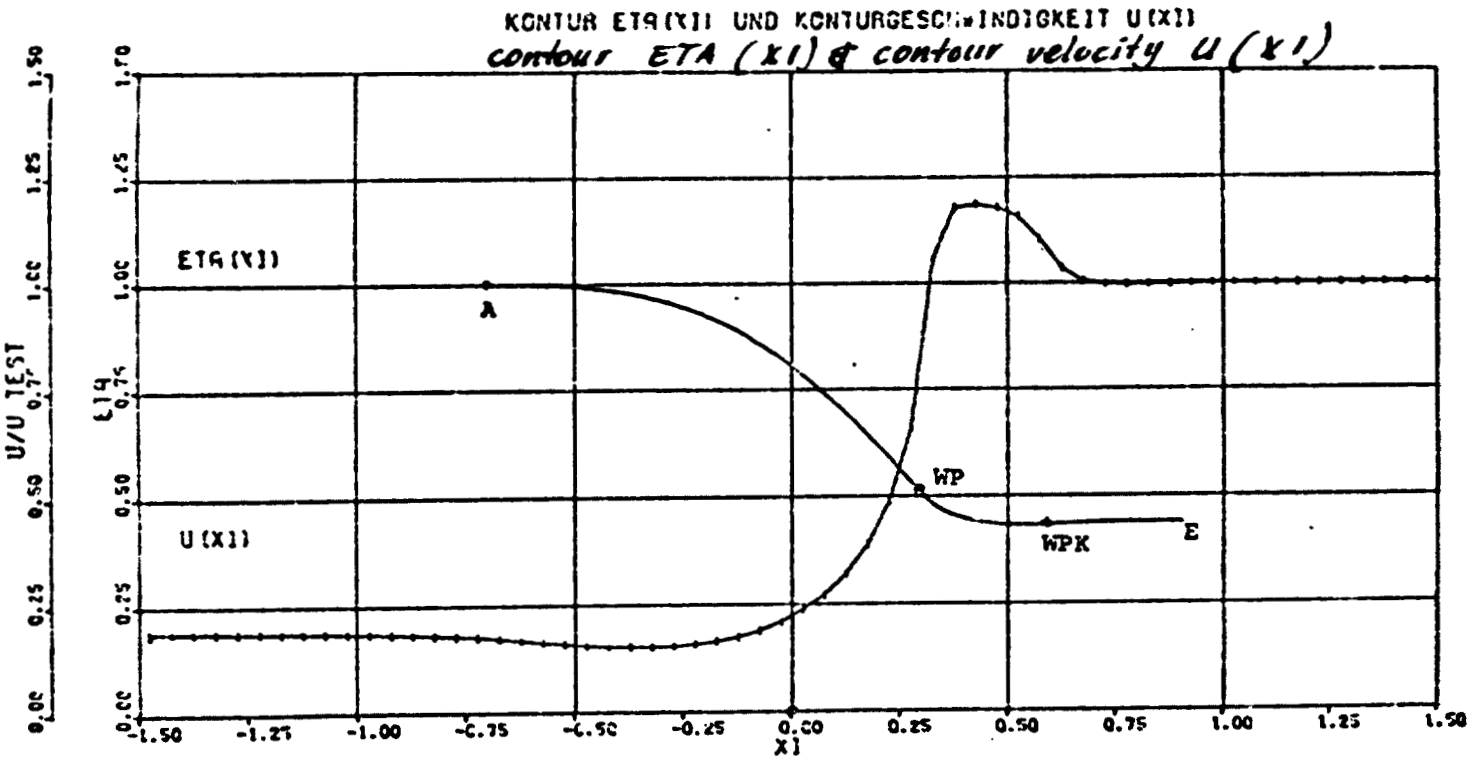

Fig.29 Optimal axi-symmetrical wind tunnel contraction with η_E = 0.439 (compare Fig.28)

exit (XI = 0.91)

Austritt (XI = 0.91):